DEVELOPMENT OF HYDROXYAPATITE GLASS COMPOSITES FOR BIOMEDICAL APPLICATIONS

JOSÉ DOMINGOS DA SILVA SANTOS

1993

DEVELOPMENT OF HYDROXYAPATITE-GLASS COMPOSITES FOR BIOMEDICAL APPLICATIONS

por

José Domingos da Silva Santos

Tese submetida à Universidade do Porto para Candidatura ao Doutoramento em Engenharia Metalúrgica

Faculdade de Engenharia

1993

à Guida e ao Filipe

ACKNOWLEDGEMENTS

I wish to express my most sincere thanks to my supervisor, Prof. F. J. Monteiro, for the supervision, help and encouragement he has always given to me.

I am also grateful to Prof. G. W. Hastings, sub-Director of the Interdisciplinary Research Centre in Biomedical Materials-IRC, University of London, for his valuable advice, stimulating discussions and the provision of research facilities.

I would like to thank Prof. M. A. Barbosa for giving me the opportunity to develop this work for the Brite-Euram Programme 'Surface Coatings for Biomaterials' and Prof. W. Bonfield, Director of the IRC, where this research was carried out, for the provision of laboratory facilities.

I am grateful to Dr. J. C. Knowles, Dr. S. Best and Dr. S. Morrey for their useful discussions and help.

I wish to acknowledge Commission of the European Communities for the provision of a fellowship, and the University of Porto for granting me leave of absence while undertaking this work.

I would like to thank my relatives, friends and colleagues for their help and encouragement.

CONTENTS

EXPERIMENTAL SECTION

Introduction

Recent developments in the design of bone replacement materials have been directed towards the use of materials which allow bone to grow and attach onto their surface. Hydroxyapatite (HA) shows this characteristic and has been extensively used in biomedical applications. However, HA is a fairly inert material when compared to Bioglasses, and is limited to low load applications due to its inadequate mechanical properties. Therefore, there is a need to improve the mechanical properties of HA, and to develop composites which can behave between a fairly inert to a totally degradable biomaterial. According to K. De Groot et al *'the aim is to produce a composite material out of HA+Bioactive glass, via a simple sintering process in a dense form'* (1).

This thesis describes the reinforcement of HA by soluble phosphate glasses chemically related to its composition, and Bioglass®, through a sintering process. Three phosphate based glasses were fabricated, based on J. Burnie's work (2). These glasses differ fundamentally from conventional glasses in that they are not based on silicates but instead have a network forming structure composed of phosphates into which can be incorporated almost any inorganic element. Their chemical composition can be closely approximated to the inorganic constituent of bone. Bioglass® was obtained from Bioglass® Research Centre, University of Florida.

Dense HA-phosphate glass composites could be fabricated, showing a large improvement in mechanical properties relatively to those of

HA. A brief literature survey is initially presented, concerning chemical, physical and mechanical characteristics of natural and synthetic materials with a summary of the conventional techniques to produce and mechanically test dense HA. In the experimental part, HA starting powder and dense HA samples are firstly characterised, with the final part being focused on the glass and HA-composites fabrication techniques. Discussion and conclusions are oriented towards the biomedical applications of these materials.

These composites have shown to be of great interest, and a British Patent was claimed under the control of 'Interdisciplinary Research Centre (IRC) in Biomedical Materials', Queen Mary & Westfield College, University of London, where all the experimetal work was developed: '**Densified Hydroxyapatite**', by the authors, J. D. Santos, J. C. Knowles, G. W. Hastings, W. Bonfield, British Patent Nº 9213774.4 filed on 29th June 1992. Publications were also made based on parts of this work and are enclosed as annexes.

I NATURAL MATERIALS

I.1 Introduction

In order to understand why synthetic HA is currently used in biomedical applications it is useful to consider the characteristics of bone and tooth in their different organisational levels. In this chapter, macroscopic and microscopic structure and mechanical properties will be presented.

I.2 Bone

Bone is one of the hardest tissues of the human body and second only to cartilage in its ability to withstand stress (3). As the main constituent of the skeleton, it supports fleshy structures, protects vital organs such as those contained in the cranial and thoracic cavities, and it encloses the blood forming elements of the bone marrow (3,4).

Besides these functions, bones form a system of levers which multiply the forces generated during skeletal muscle contraction, transforming them into body movements. In addition to these mechanical functions, they also play an important metabolic role as a mobilizable store of calcium (5).

The bone construction ensures the greatest strength with large economy of materials and minimal weight, and it is a dynamic living material, constantly being renewed and reconstructed throughout the

lifetime of the individual. Owing to its continual internal reconstruction and its responsiveness to external mechanical *stimuli*, it can be modified by the surgical procedures and appliances of the orthopaedic surgeon or the orthodontist.

I.2.1 Macroscopic structure

While all bone consists of cells, collagen fibres, ground substance and minerals, different types of bone may be formed depending on the arrangement of fibres and cells. Therefore, upon inspection with the naked eye or hand lens, two forms of bone are distinguishable: compact (*substantia compacta*) and spongy (*substantia spongiosa*) also called cancellous bone (4,6).

In the compact bone the fibre bundles are fine and run in parallel sheets, different sheets having different fibre directions and so giving the whole a stratified appearance. The compact bone usually replaces pre-existing cartilage or spongy bone in the growing skeleton.

The spongy bone consists of a three-dimensional lattice of branching bony trabeculae delimiting a system of intercommunicating spaces that are occupied by bone marrow.

These two forms of bone grade into one another without a sharp boundary. In typical bones such as the femur or the humerus, the shaft (called diaphysis) consists of a thick-walled hollow cylinder of compact bone with a voluminous central medullary cavity (marrow cavity) occupied by the bone marrow. The ends of long bones (epiphysis) consist mainly of spongy bone covered by a thin

peripheral cortex of compact bone. On the articular surfaces at the ends of long bones, the thin cortical layer of compact bone is covered by a layer of hyaline cartilage (the articular cartilage). All bones are protected at both internal and external surfaces by specialised connective tissues, called endosteum and periosteum, respectively.

I.2.2 Microscopic structure

Compact bone is largely composed of the mineralised interstitial substance, bone matrix, deposited in layers or lamellae 3 to 7μm thick. Figure I.1 presents a schematic diagram of the shaft of a long bone (4). Rather uniformly spaced throughout the interstitial substance are lenticular cavities called lacunae, each completely filled by a bone cell or osteocyte. Radiating in all directions from each lacuna are the canaliculi that penetrate the interstitial substance of the lamellae, communicating with the canaliculi of neighbouring lacunae (4,7). The great majority of the lamellae are arranged concentrically around longitudinal vascular channels within the bone to form cylindrical units of structure called osteons or haversian systems. In cross section, the haversian systems appear as concentric rings around a circular opening. The blood vessels from the endosteum and periosteum communicate with those of the haversian systems through the Volkmann's canals.

I.2.3 Composition

The exact composition and relative proportions of collagen fibres, crystals and ground substance depends on the locations and loading requirements of bone. However, the approximate percentages of its

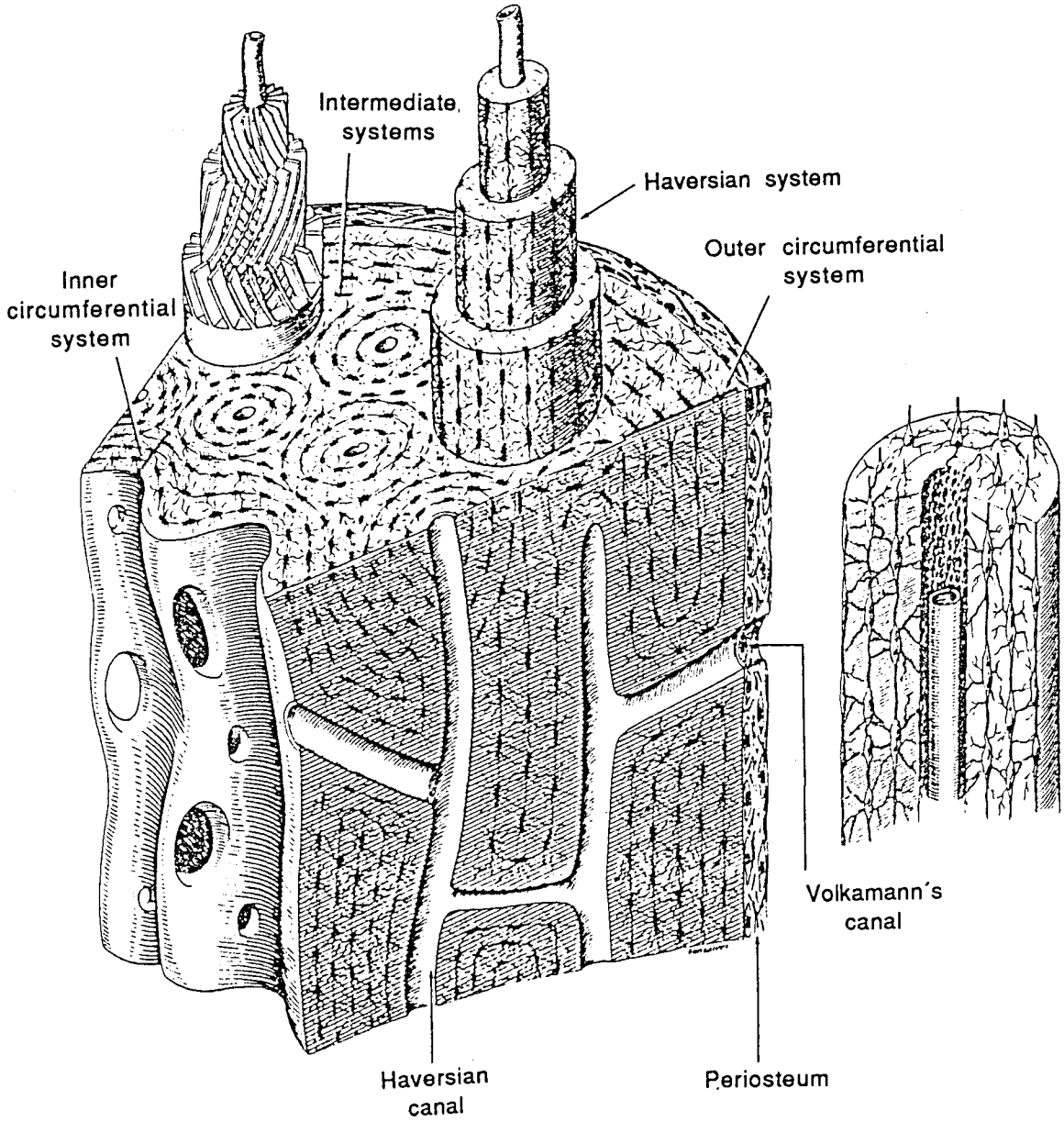

Figure I.1 Schematic diagram of the wall of a long bone diaphysis

components are: collagen-15.5%, mineral-59%, ground substance-2.8% and water-22.7%. The mineral part is mainly composed of Ca and P although other ions are also present (8), as can be seen in Table I.1.

Table I.1 Composition of mature bone mineral (wt%)

Component	%
Ca	34.0
P	15.0
CO_3	8.0
Na	0.8
Mg	0.45
K	0.2
F	0.08
Residuals†	41.47

†Composed of oxygen and other minor elements

Bone mineral is probably deposited initially as amorphous calcium phosphate and subsequently reordered to form crystalline hydroxyapatite, $Ca_{10}(PO_4)_6(OH)_2$ (9). However, Bloom (4) proposed that calcium phosphates can exist in bone mineral with different mineralogical phases, as it is shown in Table I.2.

Table I.2 Phase composition of mature bone mineral

Constituent	Formula	%
Magnesium whitlockite	$Ca_9Mg(HPO_4)(PO_4)_6$	18
Sodium and carbonate-containing apatite	$Ca_{8.5}Na_{1.5}(PO_4)_{4.5}(CO_3)_{2.5}$	13
Carbonate apatite	$Ca_9(PO_4)_{4.5}(CO_3)_{1.5}(OH)_{1.5}$	69

I.2.4 Mechanical properties

Studies about mechanical properties of bone have faced many problems due to the wide range of variables which affect bone such as its microstructure, density, degree of mineralisation, sex and age of the individual (10,11,12). These variables are often inter-related, for example: mineral content increases up to a maximum in middle age and density is higher at early age. Hence, it is difficult to fix all other variables when studying one in particular. Cortical bone is anisotropic and as such, the mechanical properties measured are also affected by specimen orientation. Table I.3 shows representative values of mechanical properties of bone (3,13,14,15,16,17,18).

Table I.3 Mechanical properties of bone

Property	Parallel	Normal
Young's modulus (GPa)	24.0	11.5
Poisson's ratio	0.46	0.58
Tensile strength (MPa)	148	49
Compressive strength (MPa)	193	133
Fracture toughness (MPa $m^{1/2}$)	6.2	3.0

These properties may be tested in a range of orientations with respect to the long axis of bone. Two orthogonal directions may be defined: longitudinal orientation, running parallel to the predominant osteon alignment and the transverse orientation, through the osteon cross section.

I.3 Tooth

There are several types of teeth which are adapted to their specific function. All are similar in structure with a non-mineralised portion called the pulp and three mineralised portions called the enamel, the dentine and the cement. The bulk of the tooth is formed by the dentine, which is thickest in the crown and gradually tapers as it reaches the apex of the root. It is covered by enamel at the tooth's crown, which is thinnest in the cervical region, and by cement at its roots. Figure II.2 shows a diagram of a section of an adult incisor (7).

Enamel is the hardest structure of the body and richest in calcium in the form of large apatite crystals. Dentine is a calcified tissue harder than bone and with higher hydroxyapatite crystals content. Table I.4 shows the amounts of inorganic materials of dental tissues (8,19).

Table I.4 Mineral constitution of tooth (wt%)

Component	Enamel	Dentine	Cement
Ca	37	35	35.5
P	17	16	17.1
C	0.8	1.1	1.17
Mg	0.4	1.0	0.9
Na	0.6	0.4	1.1
K	0.2	0.1	0.1
Cl	0.3	trace	0.1
F	0.01	0.03	0.01
Residuals†	43.69	46.37	44.02

†Composed of oxygen and other minor elements

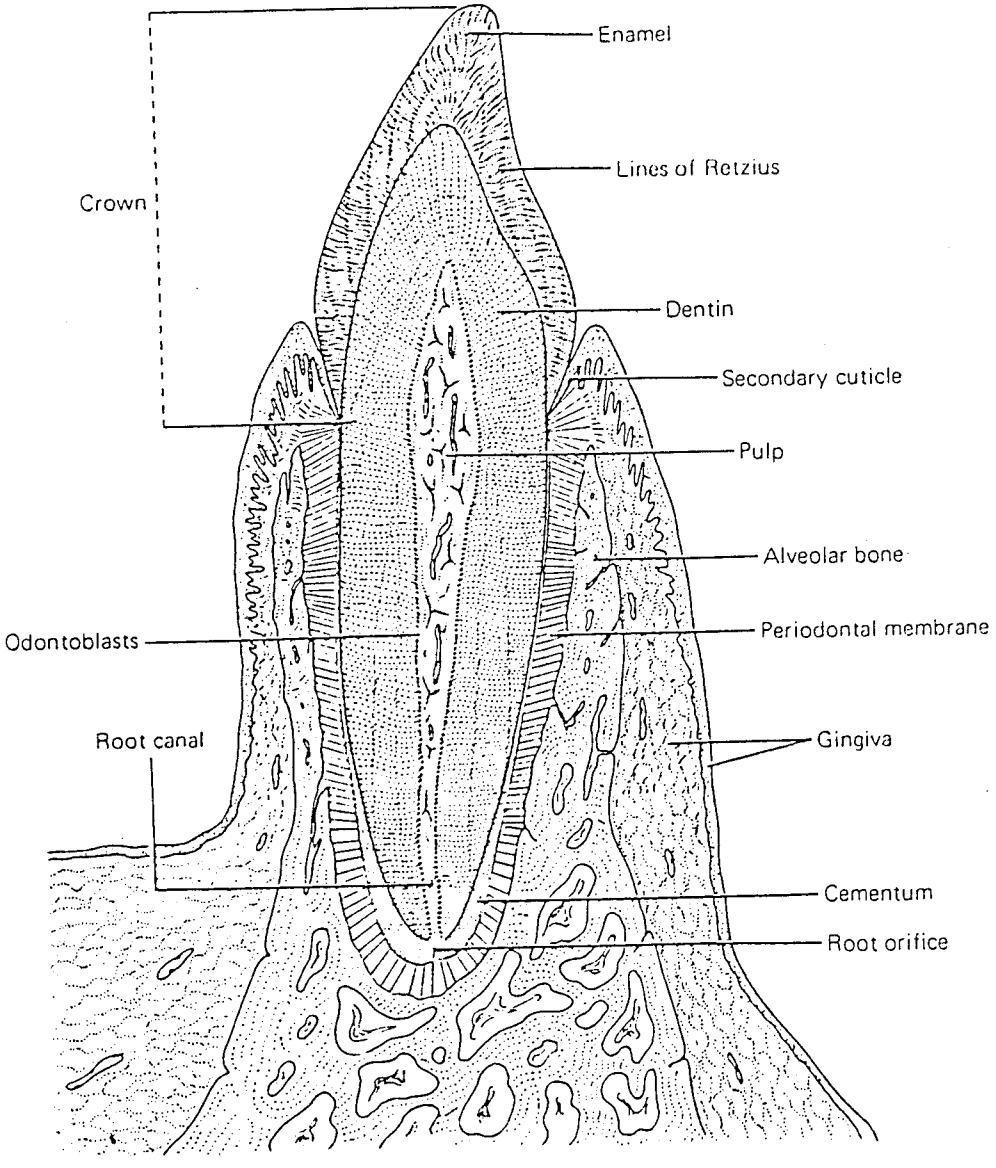

Figure I.2 Diagram of a sagittal section from an incisor tooth

II SYNTHETIC MATERIALS

II.1 Introduction

HA and bioactive glasses have attracted much attention as biomaterials because of their bioactivity (8,20,21,22,23,24,25,26,27). When designing such materials, the aim has been to promote an intimate contact with the surrounding tissues and enhance tissue formation. In this chapter, a general outline of HA is described with a brief summary of the current techniques concerning the production of dense ceramics. A succinct presentation of glasses used on biomaterials is also provided.

II.2 Hydroxyapatite

Calcium phosphate-based bioceramics have been used in medicine and dentistry for nearly 20 years, as reviewed by Aoki (8), Raemdonck (19), Hench (21) and Ducheyne (20). Different phases of calcium phosphate are used depending upon whether a resorbable or bioactive material is desired. Because of its crystallographic similarity to inorganic constituent of osseous and dental tissues, HA has attracted much attention as a substitute material for tooth or bone. Its biocompatibility with the surrounding tissue has been proved to be excellent allowing direct attachment to bone by chemical bonding, usually termed 'bioactive fixation'. The growing importance of HA in biological applications has led to the progress of its fabrication process. Various techniques have been suggested

to produce dense and porous HA materials. Macro-porous implants (with a level of porosity of the order of 50%) were initially produced, however poor mechanical properties severely limited the scope of their application. Manufacturing of HA dense materials has been studied although further progress should be obtained, particularly through a more precise chemical and structural characterisation of both the starting powder and the sintered product.

II.2.1 Preparation

A great variety of methods has been proposed to synthesise HA powders and their characteristics, such as morphology, particle size distribution, Ca/P ratio, etc., are directly related to the process used (8,28). Generally speaking, there are two methods: dry and wet. The most widely used is the wet method, which is well-adapted for mass production. The wet chemical method utilises either precipitation from aqueous solutions or the hydrolysis of calcium phosphates.

Precipitation

The precipitation process is based on the reaction of phosphate salts and calcium salts from aqueous solutions. The technique was firstly introduced by Collin (29). A modified version introduced by Newsley (30) is the most widely technique used today. The precipitation reaction can be described as:

$$5Ca(NO_3)_2 + 3(NH_4)_2HPO_4 + 4NH_4OH \rightarrow Ca_5(PO_4)_3(OH) + 10NH_4NO_3 + 3H_2O \quad (II.1)$$

It is performed at room temperature and uses $4NH_4OH$ to control the pH of the solutions. Similar methods have been introduced since then:

Jarcho (31), Kijima (32), Hirano (33), Xingdong (34), Denissen (35) and Puajindanetr (36). Calcium can also be supplied as $CaCO_3$ (22,37) or $CaCl_2$ (8). Phosphorus sources can also include H_3PO_4 (8). Jarcho (31) stressed the importance of careful control of the Ca/P ratio to obtain a stoichiometric HA, which depends on the time of maturation and stirring, pH and concentration of the starting materials, and to avoid contamination by contact with metal containers. Nitrogen gas flow must be also maintained through the solutions in order to avoid CO_3^{-2} ion formation.

Hydrolysis

This technique involves usually the hydrolysis of either tretracalcium phosphate or tricalcium phosphate (8,28). H_2O can be supplied as a vapour. Using this method the morphology of the powders is very influenced by the pH value (28). pH control is usually performed by HNO_3 or NH_4OH.

Solid-state reaction

The dry method uses solid-state reaction between calcium and phosphorus compounds. Brushite and tricalcium phosphate are frequently used according to the following reactions (8,28):

$$6CaHPO_4\,2H_2O + 4CaCO_3 \rightarrow Ca_{10}(PO_4)_6(OH)_2 + 4CO_2 + 14H_2O \qquad (II.2)$$

at temperatures above 900°C, or

$$3Ca_3(PO_4)_2 + 5CaCO_3 \rightarrow Ca_{10}(PO_4)_6(OH)_2 + 4CaO + 5CO_2 \qquad (II.3)$$

at 1200°C-1300°C.

As synthesis by these methods is carried out at high temperatures, water should be supplied continuously during treatment as source of OH^-. The HA produced is very fine and crystalline.

Hydrothermal synthesis

HA synthesised by the wet method consists of very small crystals. In order to obtain large, perfect single crystal it is common to use a hydrothermal technique. The method is carried out in an autoclave at ≈300°C and 8.6 Pa H_2O vapour pressure for 10 days, approximately (8,28). The new HA crystals are usually grown on sintered HA. The process is usually described by:

$$14CaHPO_4 + 2H_2O \rightarrow Ca_{10}(PO_4)_6(OH)_2 + 4Ca^{2+} + 8H_2PO_4^- \qquad (II.4)$$

Synthesis with zirconia dispersion is also possible (38,39). Large single crystals of HA, 7X3X3 and 2X0.3X0.3 mm in size (28) and 10 mm length (8), have been reported.

II.2.2 Chemical composition

To obtain a clear understanding of the chemical composition of synthetic HA, it is useful to describe the composition of the general apatite group. Apatite is a common term of a family of crystalline solids represented under the general formula $M_{10}^{2+}(ZO_4^{3-})_6X_2^-$. These apatites are frequently non-stoichiometric. However, the number of moles at the ZO_4 position always remains the same (19). Although the M^{2+} ions might usually be double charged ions like Ca^{2+}, Sr^{2+}, Ba^{2+}, Pb^{2+}, the ZO_4^{3-} anions such as AsO_4^{3-}, CrO_4^{3-}, MnO_4^{3-}, HPO_4^{2-} and the monovalent X^- ions, F^-, OH^-, Br^- and C_2^-, more complex structures are

also possible. Instead of the monovalent anions, bivalent anions like O^{2-} and CO_3^{2-} can occupy the X positions. When this occurs, the electrical neutrality is preserved but one anionic position becomes vacant. Examples are the oxyapatite $Ca_{10}(PO_4)_6O\emptyset$ and $Ca_{10}(PO_4)_6CO_3\emptyset$ the so-called A-type carbonated apatite (19,40). The symbol $\emptyset$ represents a vacant position. The M positions may also partially consist of vacancies. An usual feature is the substitution of some of the PO_4^{3-} ions by bivalent groups like CO_3^{2-}, the B-type carbonated apatite. The Ca/P ratio of this apatite is always higher than 1.67 and its chemical composition is, in the limit: $Ca_8(PO_4)_4(CO_3)_2$ (40). Alternatively, the Ca/P ratio is lower than 1.67 in the case of calcium deficient apatite in which substitution for PO_4^{3-} by HPO_4^{2-} ions occurs simultaneously with the loss of Ca^{2+} ion and OH^-, leading to: $Ca_{10-x}(HPO_4)_x(PO_4)_{6-x}(OH)_{2-x}$, $0 \leq x \leq 2$. CO_3^{2-} and HPO_4^{2-} ions play quite similar roles but have opposite effects on the Ca/P ratio (40,41).

II.2.3 Crystal structure

The crystal structure of HA belongs to the space group $P6_3/m$ in the hexagonal system with cell dimensions of a=b=9.418 Å and c=6.884 Å (42). A simplified unit cell is presented in Figure II.1 (8).

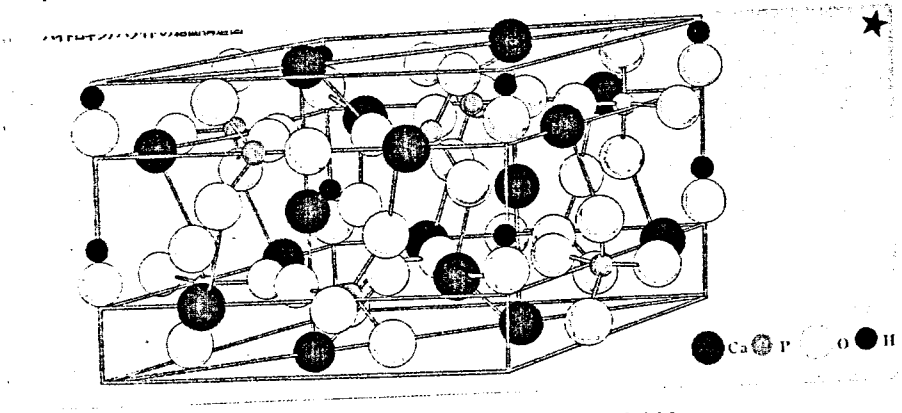

Figure II.1 Crystal structure of HA

HA consists of a skeleton of PO_4 tetrahedra: two oxygen atoms are at an horizontal plane; the other two are on an axis parallel to the c-axis. In one unit cell the PO_4 tetrahedra are divided in two layers, respectively at a crystal height of 1/4 and 3/4. Calcium ions occupy two different sites (19,28). A column, Ca_I, at 0 and 1/2 of the c axis and Ca_{II} at 1/4 and 3/4. Three of these Ca^{2+} form a triangle on a mirror plane. The arrangement of OH^- ions surrounded by a Ca^{2+} triangle along the c axis is also a characteristic of the HA structure.

II.2.4 Thermal stability

Although HA obtained by wet methods is usually nonstoichiometric (HPO_4^{2-} and CO_3^{2-} are the most common) general statements should be made when studying its thermal behaviour. Two ranges of temperatures can be distinguished: (a) between 0-1000°C, where intracrystalline reactions and irreversible decomposition of nonstoichiometric apatites occur and (b) above 1000°C, which corresponds to reversible decomposition of stoichiometric HA (19,41).

(a) Thermogravimetric and IR spectroscopy analysis show the presence of two types of water in precipitated apatites: adsorbed and crystallisation water. Adsorbed water is responsible for a reversible weight loss from room temperature to 200°C, approximately. Lattice water is irreversibly lost between 200-600°C. A possible source responsible for this water is HPO_4^{2-}, according to the reaction:

$$2HPO_4^{2-} \rightarrow P_2O_7^{4-} + H_2O \qquad (II.5)$$

Between 650 and 750°C the $P_2O_7^{4-}$ reacts with OH^- ions of the apatite:

$$P_2O_7^{4-} + 2OH^- \rightarrow 2PO_4^{3-} + H_2O \qquad (II.6)$$

This reaction can lead to presence of β-tricalcium phosphate (β-TCP) depending on the quantity of PO_4^{3-} formed. Thus a mixture of HA and β-TCP may co-exist in the microstructure. A Ca/P<<1.67 in the initial precipitate encourages the formation of β-TCP. For Ca/P=1.67 pure HA is obtained. When the Ca/P>>1.67 the final product is constituted by a mixture of CaO and stoichiometric HA. Carbonate ions, when present, begin to decompose at 600°C (41).

Above 850°C, in an atmosphere free of water vapour, HA decomposes according to the reaction (19):

$$Ca_{10}(PO_4)_6(OH)_2 \leftrightarrow Ca_{10}(PO_4)_6(OH)_{2-2x}O_x\,\acute{O}_x + xH_2O \qquad (II.7)$$

where x<1. This is an equilibrium reaction and the final product (oxyhydroxyapatite) is influenced by the partial H_2O pressure. The substitution of OH^- by O^{2-} ion and one vacancy induces a slight decrease of the unit cell 'a' and a slight increase of 'c' (32). This highly reactive apatite interacts with water on cooling and HA can be regenerated.

(b) At temperatures above 1050°C HA may decompose into two compounds, β–TCP and tetracalcium phosphate (32):

$$Ca_{10}(PO_4)_6(OH)_2 \rightarrow 2Ca_3(PO_4)_2 + Ca_4P_2O_9 + H_2O \qquad (II.8)$$

Above 1200°C, β–TCP transforms to α–TCP. This phase is the high temperature phase which is maintained upon cooling (19). Rey (41) states, however, that the reaction (II.8) is reversible and HA can be regenerated.

II.2.5 Related calcium phosphates

A useful way of classifying calcium phosphate compounds is through its Ca/P ratio. Various types of calcium phosphate, with a Ca/P ratio between 0.5 and 2.0, can be synthesised by mixing calcium and phosphate solutions under acid or alkaline conditions (8). Table II.1 summarises various types of calcium phosphates (40).

Table II.1 Calcium phosphates of biological interest

Name	Chemical Formula	Ca/P
Dicalcium phosphate dihydrate	$CaHPO_4\,2H_2O$	1.00
Dicalcium phosphate anhydrous	$CaHPO_4$	1.00
Octacalcium phosphate	$Ca_4H(PO_4)_3\,2.5H_2O$	1.33
Tricalcium phosphate	$Ca_3(PO_4)_2$	1.50
Hydroxyapatite	$Ca_{10}(PO_4)_6(OH)_2$	1.67
Tetracalcium phosphate	$Ca_4(PO_4)_2O$	2.00

The first three are very soluble and their use as biomaterials are limited, the last one being difficult to synthesise (40). Consequently, calcium phosphate biomaterials are usually constituted of HA and TCP. Two forms of TCP exist (β and α) and the rate of bioactivity follows the order: α-TCP > β-TCP > HA. However, De Groot (43) stated that TCP decomposes into HA when in contact with water and some time after implantation no biological differences should be expected.

II.2.6 Processing bulk hydroxyapatite

Most traditional and technical ceramics are manufactured by compacting powders into shapes which are subsequently heated to a high-enough temperature to bond the particles together. The basic steps in the process are: 1) material preparation 2) forming 3) drying and 4) firing by heating at the desired temperature to obtain a bulk ceramic (44).

II.2.6.1 Material preparation

Ceramic powders must have a controlled particle size to obtain a bulk ceramic with microstructural reproducibility. The size, arrangement and packing of particles have a significant effect on the time and temperature required for sintering. The basic precursor of bulk ceramic is the 'green compact', composed by a great number of particles (more than 10^{12}). According to Barringer (45) heterogeneity in green bodies and hence difficulty in the sintering process is the main reason for material rejection. This author indicated that when processing single phase ceramics two requirements should be met: a) the use of unagglomerated powder of monosized particles of 1μm in size or less (providing sufficient surface free energy for sintering but avoiding the adsorption/desorption of gases usually associated with very high surface areas) and b) as many particle/particle contacts as possible.

As it will be discussed later, the most important process for shrinkage is the material transport from grain boundaries to pores. Regardless of whether this occurs by bulk or grain boundary diffusion, the smaller the particle size is, the higher the sintering

rate will be. The presence of agglomerates constituted by small particles with other larger particles should be avoided. Small particles tend to sinter very rapidly and the higher shrinkage rate in this areas will promote an increase in the distance between agglomerates and the development of pores with very high coordination numbers and very stable. Coble (46) also indicated that a monodispersed powder was a desirable starting point for the attainment of high density in the microstructure after sintering.

II.2.6.2 Forming

Ceramic products may be formed by a variety of shaping techniques. Cold-forming processes are predominant but hot-forming techniques are also used. Dry-pressing, isostatic pressing, hot-pressing and slip casting have been applied to HA.

Dry-pressing (47,48) and isostatic-pressing processes (32,37,49) have been predominant in the fabrication of HA materials for biomedical applications. In some cases, dry-pressing followed by isostatic pressing has been used (35,50). Isostatic pressing has been used for larger specimens, with one elongated dimension and more complex shapes. Hot-pressing process, combining the pressing and firing operations has also been applied to HA by Denissen (35). According to that author, sintering temperature could be lowered to 900°C and therefore the decomposition of HA into TCP structures would be avoided. Slip casting of HA has been developed to obtain materials with differential porosity (51) or to improve mechanical properties (52). The process is advantageous for forming thin-walled materials of uniform thickness (53).

However, the green compact is of low density and strength since particles are joined together only by frictional/mechanical interlocking and low energy physical bonds (54).

II.2.6.3 Drying

After the ceramic bodies are formed, they are usually dried. The purpose of drying ceramics is to remove water before firing at high temperatures, allowing an easier particle/particle contact.

II.2.6.4 Sintering

The densification of a particulate compact to form a solid (usually polycrystalline) where the particles are bonded together, is referred to as sintering. The process causes shrinkage of the material since the pore size between particles is reduced (54,55,56). Sintering involves the replacement of high energy solid-gas interfaces by lower solid-solid interfaces in the form of grain boundaries. It is the reduction in the total interface energy that is the driving force for the sintering process. Since the grain boundary formation results in a increase in the free energy of a system, there is also a driving force for grain growth, which results in their elimination. Thermodynamically, the ideal post-sintering state would be a pore-free single crystal (46,55). These theoretical considerations are applied to the solid state sintering, where the solid phase is the unique present and the number of variables to consider is lower. Three steps of the solid state sintering process are possible to be distinguished: initial, intermediate and final (46,55,56,57,58,59).

Initial

The initial stage of sintering is concerned with first stages of neck formation between particles, before any grain growth has occurred and total shrinkage is only a few per cent. Most studies have been confined to geometrically simple systems, usually the joining of a pair of spheres (46), as it is shown in Figure II.2.

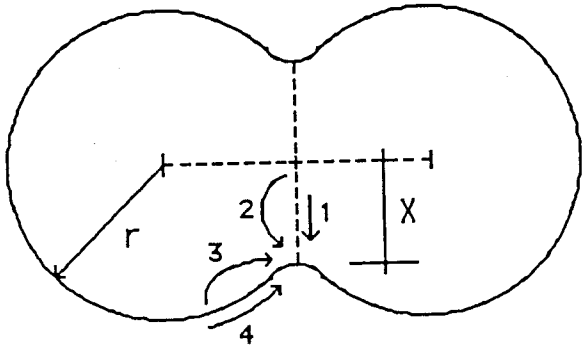

Figure II.2 Schematic diagram of mass transport mechanisms

In order that two particles in contact bond together, material transport must occur. Two classes of material transport can operate: those which can produce densification (reduction in the separation of the centres of the particles) and those which cannot (57). If the neck grows from material transported from the grain boundary source, through grain boundary diffusion (1) or bulk diffusion (2), there is shrinkage and densification of the compact. On the other hand, if the neck grows from material that comes from a surface source, through surface diffusion (4) or bulk diffusion (3), there is no overall densification. Various systems were established to model the initial stage of sintering. Equations have been derived for each of the transport mechanism which indicate how the neck changes as a function of important variables such as sintering time and temperature. According to Coble (46) a general equation for the neck

growth, x/r, can be written, establishing that $(x/r)^n$ is proportional to a factor that includes the sintering time, t.

$$\left(\frac{x}{r}\right)^n \alpha \frac{D t}{r^m} \qquad (II.1)$$

where x is the size of the neck, r is the radius of the particle, D diffusion coefficient and m and n are constants dependent upon the mass transport mechanism (n=4 and m=3 for bulk diffusion, for example). Further details can be found in Vieira (57).

Intermediate

This stage is associated with a group of structures in which the pore phase forms an essentially continuous cylindrical channel along all three-grains edges of the polygonal grains. Coble (46,60,61) developed a model for the progress of densification where he considered that the grains were regular, truncated to form 14-sided polyhedra (tetrakaidecahedra), as can be seen in Figure II.3.

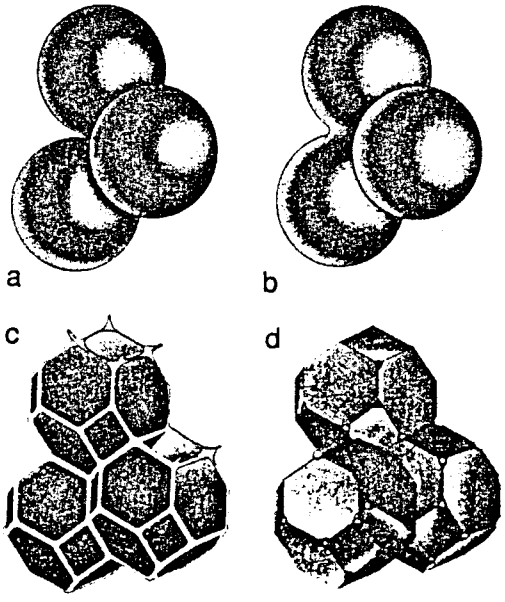

Figure II.3 Sintering stages: (a) particles are in contact (b) necks have been formed between spheres (c) necks have grown and pores form a continuous channel along 3 grain edges (d) pores closed at 4 grain corners

For grain boundary diffusion, the author found that the densification rate can be generally expressed by:

$$p - p_o = A\ D\ [\ln (t - t_o)]^{2/3} \qquad (II.2)$$

where p_o and t_o are the porosity and time at the beginning of the intermediate stage, A is a constant and D is the diffusion coefficient. Assuming a bulk diffusion model the decrease of porosity is linear with time (46,57).

Final

Stage three starts when interconnected pore channels break down into isolated pores. Pores are now spheroidal at four grain corners. In non-ideally packed compacts, interconnected porosity and isolated pores may co-exist. Similar equations to intermediate stage have been developed, with the sintering rate being defined by the rate of densification (46). In the final stage other complications appear such as grain growth and gas pressure.

A closed pore is able to shrink if it is attached to a grain boundary. If it becomes detached, its source of matter for densification eventually disappears (10,46,60). For a detached pore to shrink, matter must be transported through greater distances from the grain boundary to the pore situated inside the grain. However, other effects may operate. When grain growth occurs with attached porosity, pore coalescence and pore growth may occur simultaneously with grain growth (46). The initial pores on the edges or grain boundary of a grain that is disappearing will converge to the centre of that grain and will coalesce when it disappears. Discontinuous grain growth can

also occur. In the later stages of sintering the porosity decreases and many of the small pores may disappear locally allowing some grain boundaries to move. The grains that grow will consume their neighbours and add more sides. Having more sides, they will no longer be prevented from growing. The grain boundaries will move on across pores and reform on the other side with the pores left inside the grains.

The pressure of the gas trapped inside the pores increases and this may inhibit pore closure, leading to a reduction in the rate of densification which may slow down or even stop.

Solid state sintering is the best understood form of sintering. Even for this case there is a complexity of steps through which the powder progress as it is heated. Most theories assume a monosized spherical powder, while most sintering processes involve particles in a range of sizes and a shape far from spherical.

II.2.6.5 Liquid phase sintering

Liquid phase sintering can be defined as a sintering process involving a coexisting liquid and particulate solid during some part of the thermal cycle. The liquid phase usually enhances the rate of interparticle bonding during sintering because the atomic diffusion is accelerated. This process is very complex as many variables are involved: material characteristics, such as solubility of the solid in the liquid, wetting properties of the liquid, spreading and penetration through the grain boundaries, segregation effects, etc. and processing conditions, particle size, particle size distribution, density of the green compact, and atmosphere, for example. The interaction of all

these characteristics contributes to the difficulty in studying and understanding the process.

Generally speaking, the presence of a liquid phase provides very interesting advantages in comparison with the solid state process: (1) faster sintering mechanism associated with faster atomic diffusion, (2) a wetting liquid develops capillary attraction and the solid particles are forced to bond together, (3) the surface tension of the liquid also acts to bond the solid particles, (4) the liquid allows a rapid particle arrangement by reducing interparticle friction and providing some dissolution of the sharp edges and finally (5) grain size control of the material can be achieved.

These advantages are emphasised specially when a) the liquid wets the solid b) it has a low liquidus temperature compared to the sintering temperature and 3) the solid is soluble in the liquid.

The rapid rate of liquid phase sintering results in a less predictable process than solid state sintering and qualitative treatment is usually employed rather than quantitative. This sintering process densifies in three overlapping steps (62,63,64): 1) rearrangement 2) solution-reprecipitation and 3) solid state, as shown in Figure II.4.

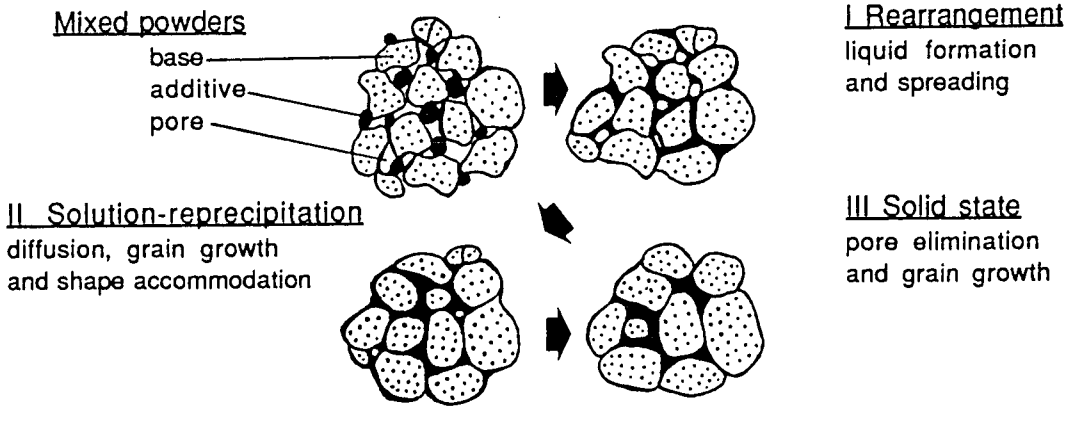

Figure II.4 Stages of liquid phase sintering

Rearrangement

It is the shortest step with a rapid densification as a result of liquid formation and spreading, which lead to a rearrangement and sliding of the solid particles. The capillary force and the surface tension of the liquid develop an attraction force between particles and a rapid densification occurs. The elimination of the porosity takes place as the system tends to minimise its surface energy. This step is conditioned by several variables: the volume percentage of liquid (it is estimated that 30-35% can lead to full densification), contact angle liquid-solid (the lower the better), particle shape (an irregular shape causes higher friction between particles and less rearrangement and densification (62).

Solution-reprecipitation

In this step the solubility of the solid in the liquid becomes an essential factor. The rate of densification depends on the rate of mass transfer through the liquid. Microstructural coarsening is observed because there is dissolution of small grains and the material is transported to the large grains. This process also contributes to densification. Grain accommodation (edges tend to disappear by dissolution) enhances pore elimination. Several variables are important at this step, particularly the solubility of the solid in the liquid and the amount of liquid present (46).

Solid state

The presence of a solid skeleton slows down further particle rearrangement. Grain contacts are promoted if there is no liquid

phase between particles allowing for solid state sintering. Microstructural coarsening continues by diffusion (solid state diffusion or solution-precipitation) and grain growth is observed.

II.2.7 Biomedical applications

Although calcium phosphate-based bioceramics have been used in medicine and dentistry for nearly 20 years, it is only in the past decade that the use of HA for implantation has been widely developed. Several dental, orthopaedic and other medical applications use HA materials (8,20,65,66,67,68,69,70,71).

Dental applications

Probably the two more important dental applications of HA is as bone filler and tooth root (8,72). Reconstruction of a defective bone absorbed by alveolar pyorrhoea is very important for keeping teeth standing above the bone. HA granules and porous materials have been successfully used for reconstruction of bone defect (8), as it is shown in Figure II.5

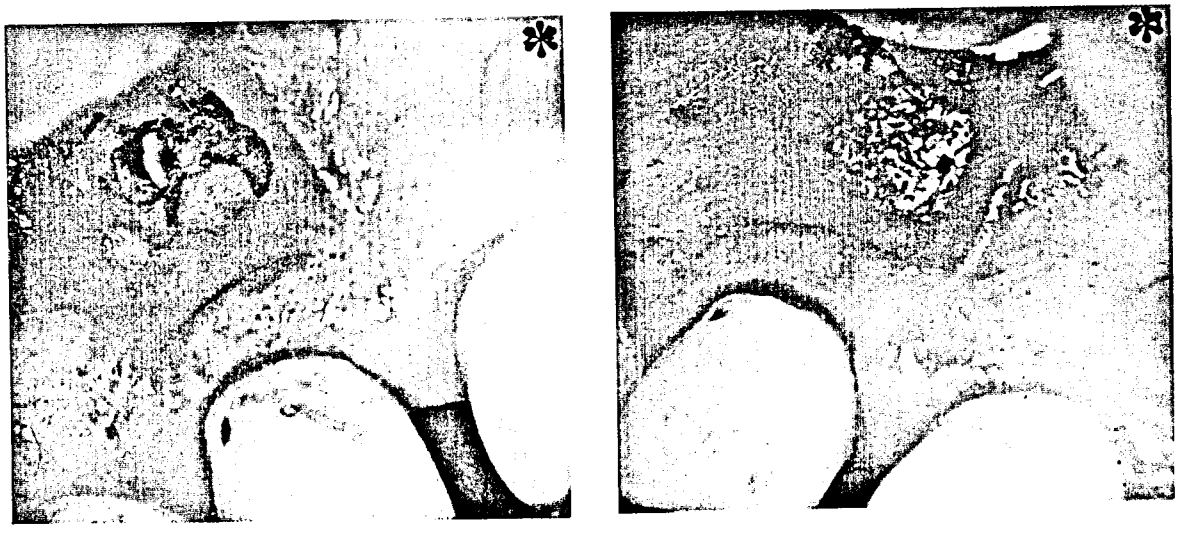

Figure II.5 Cyst (left) and porous HA implanted into bone defect (right)

HA artificial tooth roots have been applied in jawbones where no natural teeth are present and after few months of implantation dentures are attached above the tooth roots (8), as may be seen in Figure II.6.

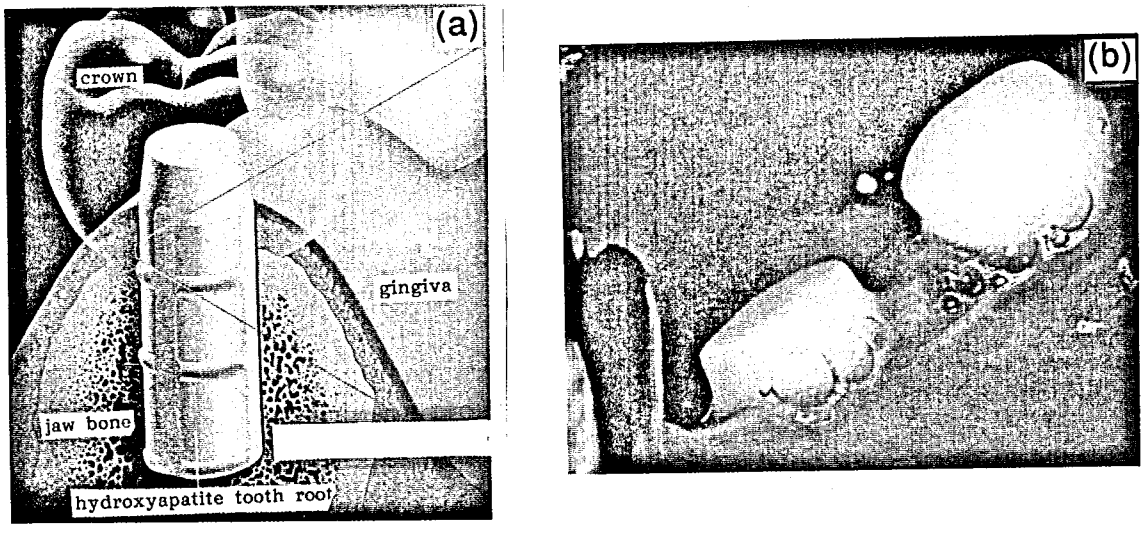

Figure II.6 Scheme of HA tooth root (a) Oral cavity after 8 years' implantation (b)

Very good biocompatibility with bone and gingival tissues has been achieved. Other dental applications include toothpast (dentifrice) and dental cements (8,19,21).

Orthopaedic applications

Orthopaedic applications of HA include bone fillers as well as artificial bones and joints. They are already being clinically used worldwide. As a bone filler in non-bearing applications, HA has been used when bone defects occur due to tumours and accidents (8). When iliac bones are usually used as autografts, HA is inserted into the defected zone. As the iliac spacer bonds physicochemically to the bone, the loosening of the filler does not occur and the patient does not complains of motor pains (65).

As sintered HA is mechanically weak, artificial joints made of HA coatings on metallic materials have been extensively used (73,74,75,76,77,78,79,80) in order to prevent corrosion and loosening, as it is shown in Figure II.7 (8).

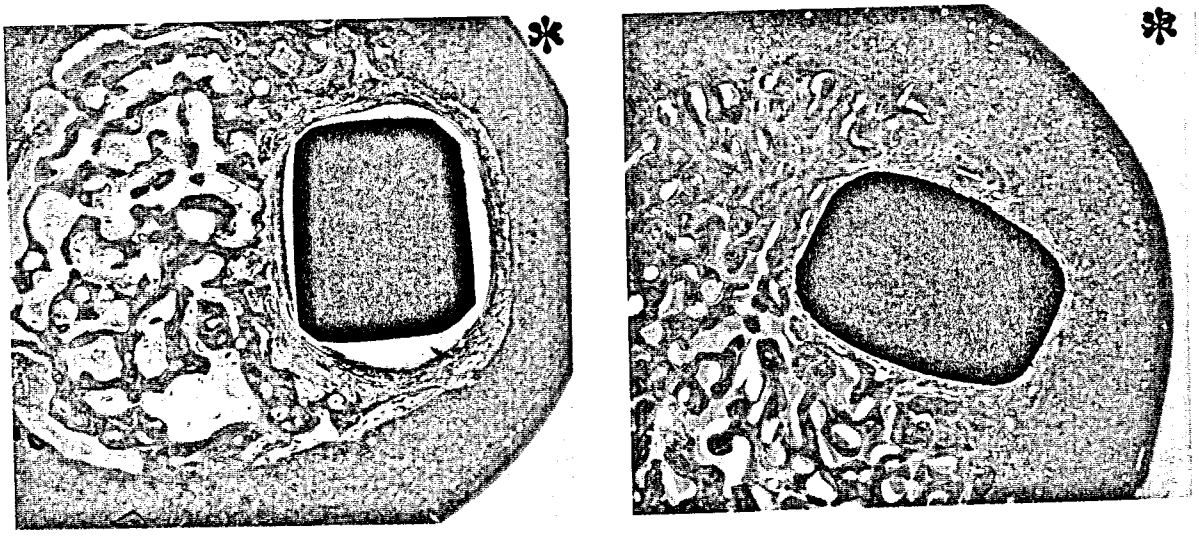

Figure II.7 Decalcified cross-sections of hip joints. 316L stainless steel (left). 316L coated with HA (right)

After 3 months implantation, thick connective tissue and gaps appeared around the hip 316L joint, causing the loosening phenomenon. With the HA-coated hip joint, neither connective tissue nor gaps surrounding the implant were found. Other orthopaedic applications include, for example, artificial blood vessels, artificial trachea and drug delivery carrier (8).

II.3 Bioglasses

II.3.1 Glass transition temperature

Most inorganic materials melt to form liquids which on cooling will crystallise rapidly. However there exists a range of materials which

when cooled even at a high rate, from a temperature above the freezing point, will not crystallise. Thus, a glass can be defined as an inorganic solid product of fusion which has cooled to rigid condition without crystallisation (53,55). The solidification behaviour of a glass is different from that of a crystalline solid, as illustrated in Figure II.8.

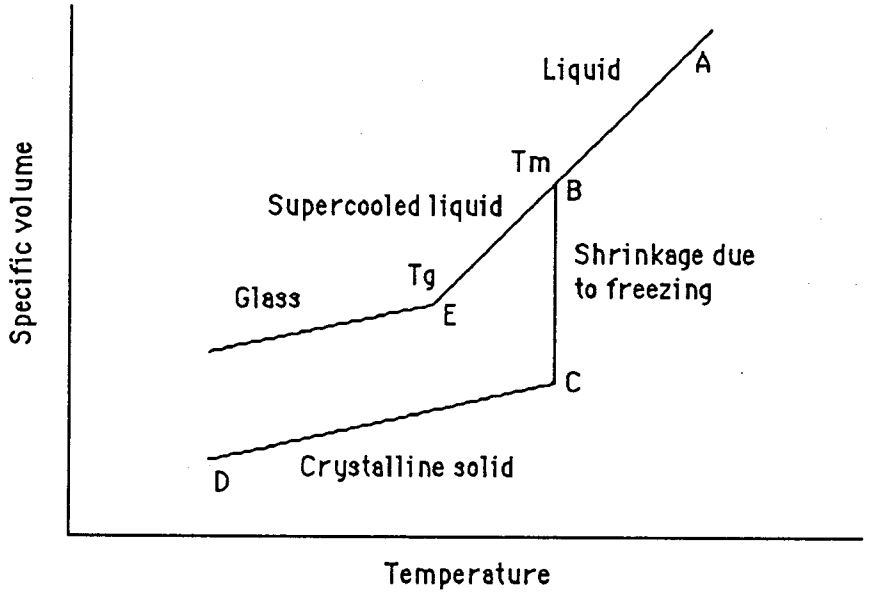

Figure II.8 Solidification of crystalline and glassy materials

When a liquid is cooled from an initial state, A, a continuous decrease in its temperature will cause a reduction in its specific volume along the line AB. Providing this temperature decrease is sufficiently slow and the required nuclei exist in the melt, crystallisation will occur at Tm, its melting temperature, with a volume decrease along BC. This liquid-crystalline transition is accompanied by an abrupt change as the atoms and molecules go from their random state to their well-ordered regular structure. This change is associated with the evolution of the latent heat. Continued

cooling below Tm will be accompanied by further contraction along CD. Alternatively when a rapid cooling is applied and crystallisation does not occur at Tm the volumetric contraction continues along BE and the material is now referred as a supercooled liquid and BE is a smooth continuation of AB. As the temperature decreases the liquid becomes more viscous and transforms to a rigid, brittle glassy phase in a narrow temperature where the slope of the specific volume vs. temperature is markedly decreased. This temperature defines the glass transition temperature, Tg. It is only below Tg that it is correct to refer to the highly viscous material as a glass (10^{13} poises, 10 poises=1 Pa.s).

It is useful to have in mind typical viscosity values at these various states (53,81).

Melting temperature: viscosity $\approx 10^2$ poises.

Working range: at this temperature glass fabrication operations can be carried out. Viscosity $\approx 10^{4.5}$-10^7 poises.

Softening point: At this temperature the glass will flow at an appreciable rate under its own weight. Viscosity $\approx 10^8$ poises.

Annealing point: Atoms can move sufficiently so that residual stresses can be relieved. Viscosity $\approx 10^{13}$ poises.

Transition temperature: Viscosity $\approx 10^{13}$ poises.

Strain point: Below this temperature the glass is rigid so that it may be handled without deformation. Viscosity $\approx 10^{14.5}$ poises.

II.3.2 Silicate glasses

The chemical composition is an important factor in determining whether a compound will or not form a glass. Oxides which will easily form glasses include SiO_2, GeO_2, B_2O_3 and P_2O_5 (81). Silicate glasses are the most widely used in biomaterials. The primary structural unit of silicates is the SiO_4^{4-} tetrahedron in which one silicon atom is coordinated interstitially among four oxygen atoms. These oxides have a high bond strength and behave as glass formers (54). However, each oxygen of the tetrahedra has only seven electrons rather than eight in its outer shell. This deficiency can be overcome by (1) an electron obtained from metal oxides, which tend to be oxides involving electro-positive ions of a low charge (network modifiers), Na^+, K^+, Ca^{2+}, Ba^{2+}, etc or (2) each oxygen atom sharing an electron pair with a second silicon. The shared oxygen is the bridging oxygen.

With pure silica there are no metal ions and every oxygen is a bridging atom between two silicons which gives a networklike structure and the glass is very rigid and viscous even when it gets around its liquid state. This high viscosity makes it very difficult to shape. Most silicate glasses have network modifiers which are unable to build a continuous network on their own and disrupt the glass network in that they do not form an integral part of it but occupy its interstitial spaces. As shown in Figure II.9 the addition of Na_2O introduces two Na^+ ions and produces two nonbridging oxygens, each with a single negative charge. Likewisé, the introduction of one Ca^{2+} ion also leads to two nonbridging oxygens.

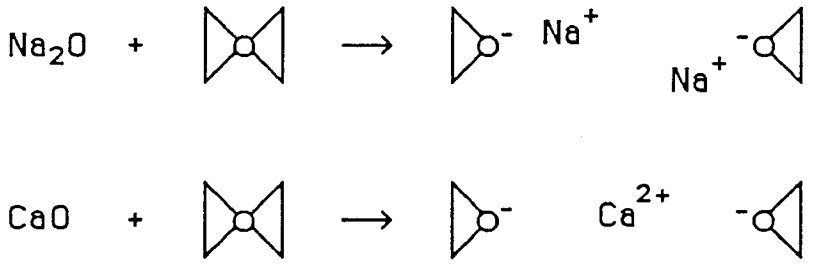

Figure II.9 Modifiers ions disrupt the network structure

The presence of network modifiers affects the properties of the material i. e. the softening point is lowered, the viscosity is reduced and generally the activation energy for atom movements in molten state is reduced. Mechanical properties are also reduced (82). The glass has a thermoplastic behaviour at high temperatures and can be shaped into products. There are also other oxides referred to as intermediate oxides (Al, Ti oxides, for example) that are incapable of forming a glass on their own, but can become part of a network structure and help to preserve the structure.

Silicate based bioglasses have been developed by Hench (21,24,83,84). Their composition is based on the SiO_2-Na_2O-CaO- P_2O_5 system with some compositional conditions. Other authors have also been working on silicate bioglasses with slight modifications: Moroni (85), Andersson (86,87) and Ebisawa (88), for example. Glass-ceramics based on a SiO_2 system and containing a crystalline apatite phase have been developed as biomaterials,. which show higher bending strength and fracture toughness than HA and bioglasses (89,90,91,92).

II.3.3 Phosphate glasses

Phosphorous has three oxide forms, P_2O_3, P_3O_4 and P_2O_5 but only phosphorous pentoxide is capable of forming a glass on its own. Phosphate glasses are similar to silicate glasses and have a three dimensional network of PO_4 tetrahedra (2). However, while each one of the four oxygen ions in the SiO_4 tetrahedra is shared between two silicon atoms, only three of the four oxygens are shared between two phosphorous atoms, with the remaining oxygen being bonded to only one phosphorous. The oxygen atoms in the tetrahedra are thus shared only at three corners. Consequently vitreous silica is more difficult to melt and chemically more stable when compared with phosphate glasses which are readily fusible and chemically unstable (93). The fact that phosphorous has five positive charges opposed to the four of silicon induces certain anomalies in its study.

Na_2O additions acts as a modifier and weakens the structure. This effect is produced by the fact that the monovalent Na^+ occupies interstitial positions of the network and disrupts the structural continuity. However, it should be noted that in a glass with one sodium atom to one phosphorous atom there will be no PO_4 groups sharing three oxygens and its structure must then differ from a glass with a mole ratio of Na_2O/P_2O_5 ≤ 1. Conversely, the addition of an alkaline earth oxide such as CaO increases the stability of the glass by its incorporation as an integral part of the network (94). Al_2O_3 promotes heterogeneous nucleation and glass-ceramic formation (95).

Phosphate based glasses have been recently used as biomaterials. Phosphorus-calcium-sodium compositions chemically related to the

inorganic part of bone have been developed (23,94). They differ from the former because they contain no silica. Silica is sometimes referred to as having caused harmful effects when implanted (96).

III MECHANICAL TESTING OF CERAMICS

III.1 Introduction

Ceramics have a great number of notable properties including high resistance to wear and corrosion, low thermal and electrical conductivity. However, they are very brittle (low toughness) and tend to fracture in an unpredictable manner without prior plastic deformation. The phenomenon is known as 'fast fracture' and is caused by the growth of a crack that suddenly becomes unstable. The lattice resistance of ceramics makes slip very difficult, even at the crack tip where the stress is intensified. It is the plastic deformation at the crack tip that gives metals their high toughness: energy is absorbed in the plastic zone, making the propagation of the crack very difficult.

A variety of techniques were introduced to characterise the mechanical properties of ceramics and some of these were applied to HA. This chapter is designed to give a general overview of the aspects related to the mechanical behaviour of ceramics, emphasising those related to HA and its biomedical applications. Some theoretical treatments are discussed, and methods to measure the mechanical properties of HA are presented.

A large number of tests have been conducted to characterise the strength of HA. However, the results obtained seem to be specifically related to the test used and comparisons between them are always difficult, particularly when different stress

concentration states are applied to the specimen and different volumes of material are submitted to the maximum stress. On the other hand, the high hardness and brittleness of HA lead to difficult and expensive sample preparation. Simple sample shapes are often used and results are sometimes difficult to interpret, as it is the case of indentation methods and bending tests on bars to characterise fracture toughness and bending strength, respectively. In this work, fracture toughness was determined by two standard processes apart from indentation, and bending strength was measured using a concentric-ring test. These tests are recognisably more accurate but involve difficult and time-consuming sample preparation, and the manufacture of complicated jigs, as it will be discussed later in the experimental part.

III.2 Fracture mechanics

Inglis model

The first quantitative approach for the stress concentration effect of flaws was provided by Inglis (97,98,99). He proposed a model which takes into account the presence of existing cracks in an elastic material and showed that the stress which exists at the tip could rise to a level several times that of the applied stress, according to the equation (III.1) and Figure III.1:

$$\sigma_m = 2\sigma \left(a/\rho\right)^{1/2} \qquad \text{(III.1)}$$

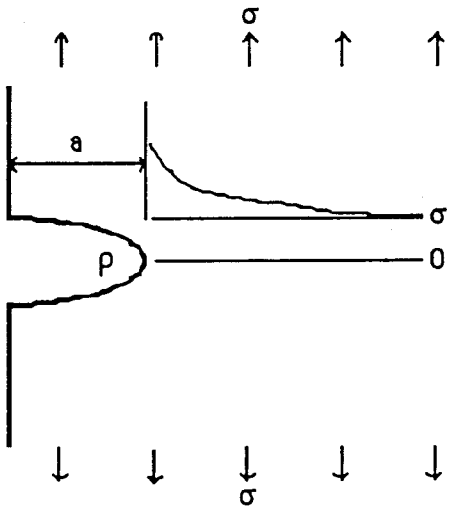

Figure III.1 Stress concentration under tensile stress

where σ_m and ρ are the stress and the radius of curvature at the tip of the crack, respectively, and a is half the crack length. Equation (III.1) predicts an infinite stress at the tip of an infinitely sharp crack, where $\rho=0$. Although this model showed that the stress at the tip is much larger it does not indicate the conditions under which a crack will propagate until failure.

Griffith energy-balance concept

Griffith used a thermodynamic approach to establish the critical conditions for fracture to occur (100,101,102,103): an existing crack can grow only if such a process causes the total energy of the material to decrease. A brief consideration of the Griffth approach now follows: suppose a crack of length a in an ideally brittle material of thickness t advances by δa, then it is required that: work done by loads is higher than the change of elastic energy plus the energy absorbed at the crack tip, i.e.

$$\delta w \geq \delta U^{el} + G_c\, t\delta a \qquad \text{(III.2)}$$

where G_c is the energy absorbed in making unit area of crack and $t\delta a$ is the crack area. Consider a plate clamped under tension so that its upper and lower ends are fixed as it is shown in Figure III.2.

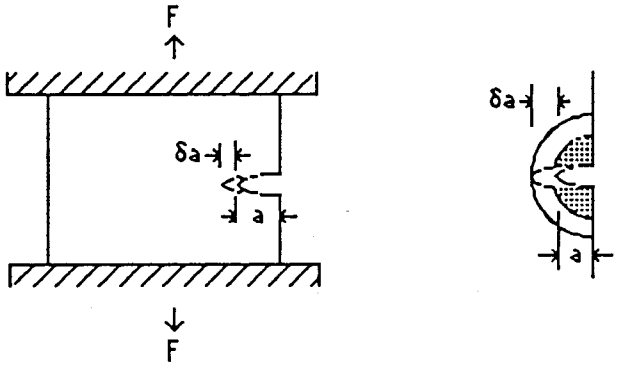

Figure III.2 Fast fracture in a fixed plate. Release of strain energy as the crack grows

Since the ends cannot move, the forces acting on them can do no work, so the equation takes the form:

$$-\delta U^{el} = G_c\, t\, \delta a \qquad (III.3)$$

As the crack grows it allows the material near it to relax so that it becomes less highly stressed and loses energy, δU^{el} is therefore negative. δU^{el} can be approximately estimated: a strain ε is produced in a cube subjected to a stress σ. Each unit cube has strain energy $U^{el} = \frac{1}{2}\,\sigma\varepsilon$ or $\sigma^2/2E$. If the crack of length a is introduced, the dotted material relaxes to zero stress so it loses all its strain energy. The energy change is (100):

$$U^{el} = -\frac{\sigma^2}{2E}\,\frac{\pi a^2 t}{2}. \qquad (III.4)$$

Considering that the crack spreads by its length of increment δa, δU^{el} becomes:

$$\delta U^{el} = \frac{dU^{el}}{da}\,\delta a = -\frac{\sigma^2}{2E}\,\frac{2\pi a t}{2}\,\delta a \qquad (III.5)$$

The assumption made about the way in which the plate material relaxes gives an approximate result, and a more rigorous calculation of the elastic strain energy released around the crack showed that this value is doubled (100,101). The critical condition for fast fracture is then:

$$\sigma\sqrt{\pi a} = \sqrt{EG_c} \qquad (III.6)$$

Because E and Gc are material properties the left side of the equation indicates that fast fracture will occur when, in a material subjected to a stress σ, a crack reaches some critical size a or, alternatively, when a material containing cracks of size a is subjected to some critical stress σ. Consequently, crack extension occurs when the product $\sigma\sqrt{\pi a}$ attains a certain value. The term is usually abbreviated to Kc (critical stress intensity factor) and often called fracture toughness with usual units: MN $m^{-3/2}$. Kc can be determined experimentally for any material by inserting a crack of known length and loading until fast fracture occurs (100).

Stress intensity approach

The term $\sigma\sqrt{\pi a}$ is usually abbreviated to the symbol K and is called the stress intensity factor. It is a constant that gives the magnitude of the elastic stress field (101). The achievement of a critical stress intensity factor is then the critical condition for fast fracture to occur. The equation (III.6) is only valid for a thin, semi-infinite plate. Other specimen geometries have some correction factor and a more general approach can be made if a

dimensionless parameter is introduced, as it was demonstrated by Irwin (101):

$$K = \sigma\sqrt{\pi a}\ f\left(\frac{a}{w}\right) \qquad \text{(III.7)}$$

where $f\left(a/w\right)$ is a parameter that depends on the geometries of specimen and crack. K values for different specimen geometries can now be determined from conventional elastic stress analysis.

III.3 Microstructural effects

The mechanical properties of ceramic materials are mainly governed by structural defects. The principal sources of fracture in ceramic polycrystals have been identified to include surface cracks created during surface finishing, porosity, inclusions and large grains produced during processing. When interpreting the data one should be aware of these factors.

Porosity

Pores in brittle materials are regions where stress concentrates and, if a critical value is achieved, a crack can form and propagate. Pores are also detrimental to strength, because they reduce the cross-sectional area over which a load is applied and lower the stress the material can withstand. The size and volume fraction of pores are important factors in determining the strength of ceramic materials.

Grain size

The fracture process for a polycrystal is more complicated than for a single crystal. The most obvious effect is that the fractured

surface of a polycrystal is much rougher than that of a single crystal. This rough surface is associated with the necessary changes in orientation of the crack as it passes from one grain to another. Typically, ceramics with small grain size have improved mechanical properties compared to those with larger grain size. A larger grain size is associated with higher residual stress (more strain energy) due to anisotropic thermal contractions in different crystallographic orientations on cooling after fabrication (104). In fully dense ceramics in which there are no large pores the flaws size are usually related to the grain size. Even small amounts of impurities present will be concentrated at the grain boundaries and their chemical and physical nature may also be an important factor in determining fracture behaviour (97).

III.4 Measurement techniques

Unfortunately the simple tensile test so widely used to characterise the mechanical behaviour of metals is difficult to carry out on brittle materials. The main difficulty is the avoidance of premature failure associated with stress increases due to misalignment of the specimen in the loading attachments or to contact effects at the attachments (105,106,107). On the other hand it is difficult to prepare ceramic samples with complicated shapes without increasing the preparation cost to a prohibitive level. An essential feature of ceramic specimens is that geometry and loading must be such that a calculable stress state prevails at the section where fracture occurs so that the fracture stress can be readily calculated from the fracture load.

III.4.1 Tensile and compression

The mechanisms which lead to the fracture of brittle materials subjected to tensile and compressive stresses are significantly different (105,108). While under tension, failure occurs by fast and unstable propagation of the critical flaw, situated on a normal plane to the load direction, and the calculated value represents the maximum load to propagate that flaw. Under compression, several flaws can simultaneously propagate showing a tendency to adopt a parallel direction in comparison to the compressive load until general crushing occurs (108), as it may be seen in Figure III.3.

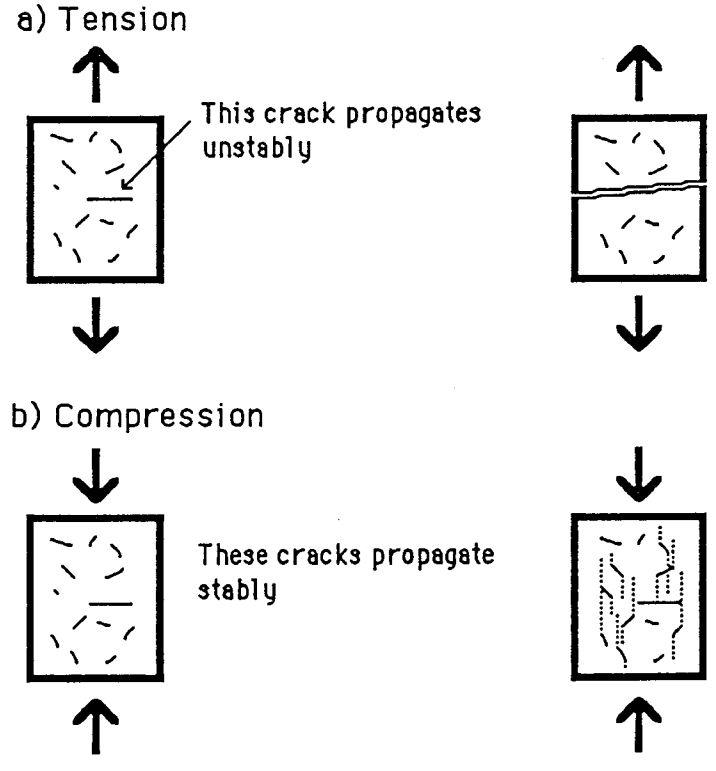

Figure III.3 Fracture mechanisms in tension (a) and compression (b)

The tensile strength of a brittle material is then substantially lower, on average about 15 times, than its compressive strength (108). The compressive strength of HA is indicated by some authors. For example, Rootare (109) has determined 376±13 MPa, Denissen

(35) 390±40 and 430±95 MPa for two HA powders, and Akao (110) 308±46 and 509±47 MPa.

III.4.2 Diametral compression

Simple disc specimens subjected to two diametrically opposed compressive loads are widely used for the determination of the tensile fracture stresses of brittle compacts (108,111). The test is usually referred to as 'indirect' tensile test, the term 'indirect' arising presumably to cover the apparent anomaly of deriving the tensile fracture from compressive loading (111), as can be seen in Figure III.4.

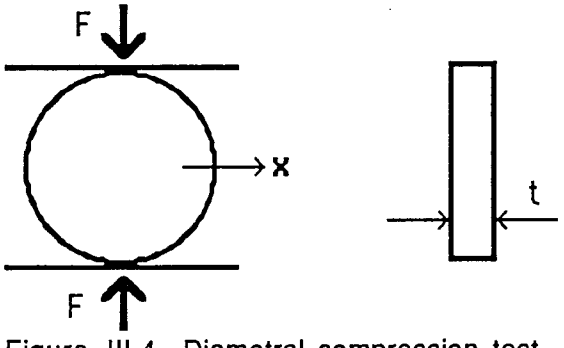

Figure III.4 Diametral compression test

A transverse tensile strength is developed across the diameter and is equal to:

$$\sigma_t = \frac{2F}{\pi D t} \qquad (III.8)$$

Where F is the load and D and t are the diameter and thickness of the specimen, respectively.

III.4.3 Bending

III.4.3.1 Uniaxial

Because the conventional tensile test is unsuitable for ceramics, the bending strength is the alternative way to test these materials

when subjected to tensile stress. Load alignment problems are eliminated by the use of a simple fixture or jig in which the beam is supported on and loaded through cylindrical rollers. 3-point or 4-point systems can be used and the maximum tensile stress is obtained on the surface of the specimen opposed to the load application. The maximum tensile stress is called modulus of rupture, σ_r, and it is related to the maximum moment in the elastic beam, M, by (105):

$$\sigma_r = \frac{M\,t}{2\,I} \qquad \text{(III.9)}$$

where t is the thickness of the specimen, M is the maximum moment applied and I the moment of inertia. Both testing procedures have been used on HA but the 4-point bending has significant advantages (106,111,112), as it is shown in Figure III.5.

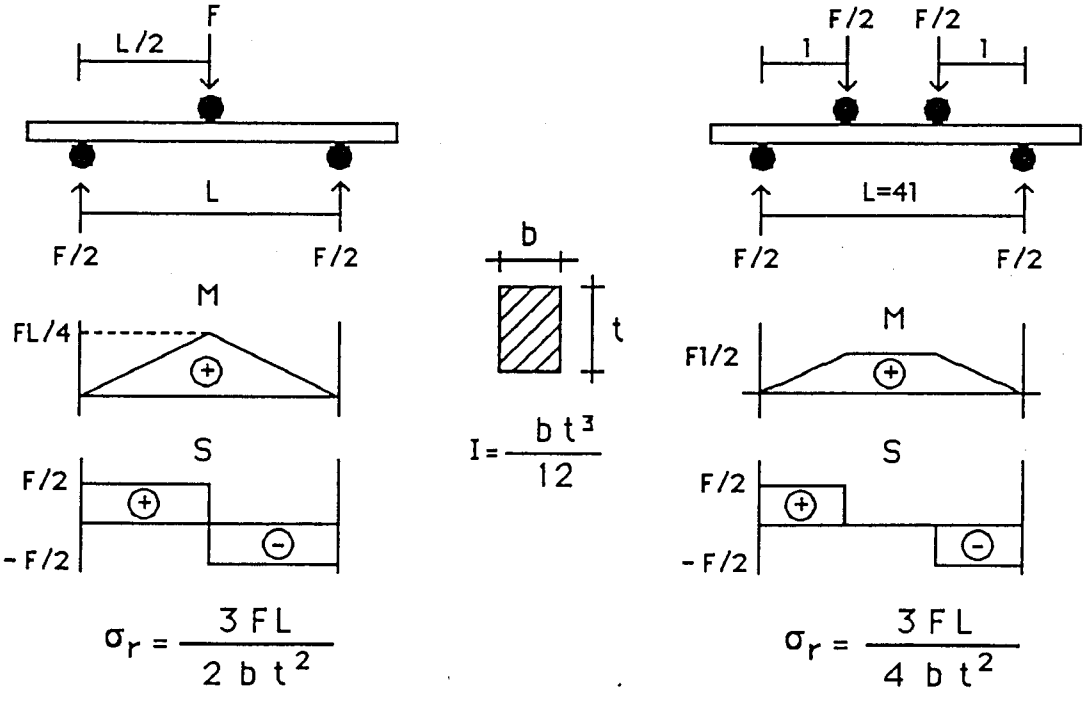

Figure III.5 Bending moment (M) and shearing force (S) diagrams

b and t are the depth and thickness of the specimen, respectively, L is the long span and l the distance from the support to the load

applicator. In the 3-point bending system only a small portion of the material is subjected to maximum stress while in the 4-point bending the volume of material is much larger. Therefore the probability of the critical flaw being submitted to maximum stress increases and the calculated value, σ_r, decreases. On the other hand a pure bending state is obtained on that area for the 4-point bending arrangement. The elasticity modulus (Young's modulus) in 3-point bending is obtained as follows (113):

$$E = \frac{FL^3}{4 w t^3 \delta} \qquad (III.10)$$

and for 4-point bending:

$$E = \frac{\left[FI\left(3L^2 - 4I^2\right) \right]}{4 w t^3 \delta} \qquad (III.11)$$

where E is the elasticity modulus, F the load, w and t the width and thickness of the specimen, respectively, L the supporting span, I the distance from the support to the load applicator and δ the deflection at midspan. The bending strength of HA has been determined by several authors, namely: Jarcho (31), Akao (110), Best (114) and With (115).

III.4.3.2 Biaxial

A circular plate is supported on circular ring and the load is applied by a second ring which is positioned concentrically on the opposite side of the specimen. This arrangement can be regarded as an extension of the 4-point bending test in two dimensions by rotating the specimen around the vertical axis of symmetry. The biaxial

strength of a brittle material with randomly oriented and uniformly distributed flaws should be lower than its uniaxial strength because in a biaxial stress field the probability of the critical flaw being highly stressed is higher. The mathematical solution to calculate the biaxial stress field within the loading ring and between the two rings can be found in Kirstein (116) and Soltesz (117). The method has been used to investigate pure surface effects on the bending strength, avoiding the influence of edge effects. Attempts have been made to apply this test to biomaterials (117). Some variations of concentric-ring test have been introduced to determine the biaxial strength (118,119,120,121,122):

Ball-on-ring test

In this test the specimen is supported on a ring and centrally loaded by a ball. This test jig has the advantage of minimising the frictional stresses between the loading device and sample (123). In this case the biaxial strength is calculated by:

$$\sigma_r = \frac{3F(1+\nu)}{4\pi t^2}\left[1+\ln\frac{r_2}{r_1}+\frac{1-\nu}{1+\nu}\left(1-\frac{r_1^2}{2r_2^2}\right)\frac{r_2^2}{r^2}\right] \qquad \text{(III.12)}$$

where F is the load, t the sample thickness, r_1 the radius of the region of uniform loading at the centre, r_2 the radius of support, r the radius of the disk and ν the Poisson's ratio.

Piston-on-3 ball

This method has the advantage in that the support of the disk on 3 balls allows the use of a slightly warped specimen. The load is

applied by a cylindrical piston. The modulus of rupture in bending is calculated by (119):

$$\sigma_r = -\frac{3F}{4\pi t^2}(X-Y) \qquad \text{(III.13)}$$

where:

$$X = (1+\nu)\ln\left(\frac{r_1}{r}\right)^2 + \left[\frac{(1-\nu)}{2}\right]\left(\frac{r_1}{r}\right)^2 \qquad \text{(III.14)}$$

$$Y = (1+\nu)\left[1+\ln\left(\frac{r_2}{r}\right)^2\right] + (1+\nu)\left(\frac{r_2}{r}\right)^2 \qquad \text{(III.15)}$$

and F is the load, t sample thickness, r_1 radius of the region of uniform loading at the centre, r_2 radius of support, r radius of the disk and ν Poisson's ratio.

III.4.4 Weibull statistics

Within a brittle material there is a multitude of microscopic structural and material defects in the form of cavities, fractured zones, porosity etc. These defects act as minute stress concentrators in the material and, as the applied load is increased, fracture will initiate and propagate from one of them. Since the defects are randomly distributed throughout the material and are of random severity, there is a inherent variability in the strength of nominally identical brittle specimens. It is difficult to predict a single ineherent tensile strength for the material, there is only a certain probability that a given sample may have a given strength. The distribution of cracks length has other consequences. A larger

sample will fail at a lower stress than a smaller one, on average, because it is likely that it will contain one of the larger flaws. So there is a volume dependence of the strength (97,108). This variability requires that strength test results for brittle materials should be treated statistically. The Weibull probability distribution is usually used for this purpose (97,124,125,126). Weibull defined the survival probability $P_s(V_o)$ as the fraction of identical samples each of volume V_o, which survive loading to a tensile stress σ. Experimentally the following equation is verified (124):

$$P_s(V_o) = \exp\left[-\left(\frac{\sigma}{\sigma_o}\right)^m\right] \qquad \text{(III.16)}$$

where σ_o and m are constants. When $\sigma=0$ all the samples survive and $P_s(V_o)=1$. As σ increases more and more samples fail and $P_s(V_o)$ decreases. In the limit $P_s(V_o) \rightarrow 0$ as $\sigma \rightarrow \infty$. If one sets $\sigma = \sigma_o$, one finds that $P_s(V_o)=1/e$. So σ_o is the tensile stress that allows 37% of the samples to survive. The constant m indicates how rapidly the strength falls as σ_o is approached and it is called the Weibull modulus. The lower m value the greater the variability of the strength. Taking logs twice in equation (III.16):

$$\ln\left[\ln\left(\frac{1}{P_s(V_o)}\right)\right] = m \ln\left(\frac{\sigma}{\sigma_o}\right) \qquad \text{(III.17)}$$

The slope of the straight is m. The P_s values can be calculated by equation (III.18) for a batch of N samples (97):

$$P_{s_i} = 1 - \frac{(i - 0.3)}{N + 0.4} \qquad \text{(III.18)}$$

The larger the specimen the more likely it is that it will contain a flaw of a given severity, and consequently the smaller will be the mean fracture stress of a batch of such specimens. The predicted relationship is (97):

$$\frac{\sigma_{V_1}}{\sigma_{V_2}} = \left(\frac{V_2}{V_1}\right)^{1/m} \qquad \text{(III.19)}$$

Which shows that the survival probability depends on both the stress and the volume of the sample.

III.4.5 Fracture toughness

There is a wide range of specimen geometries available for fracture toughness measurements (127,128,129,130,131,132,133). The techniques have been standardised in order to determine a mathematical solution for the stress intensity factor. These techniques will now be summarised very briefly:

Single-edge-notched (Sen)

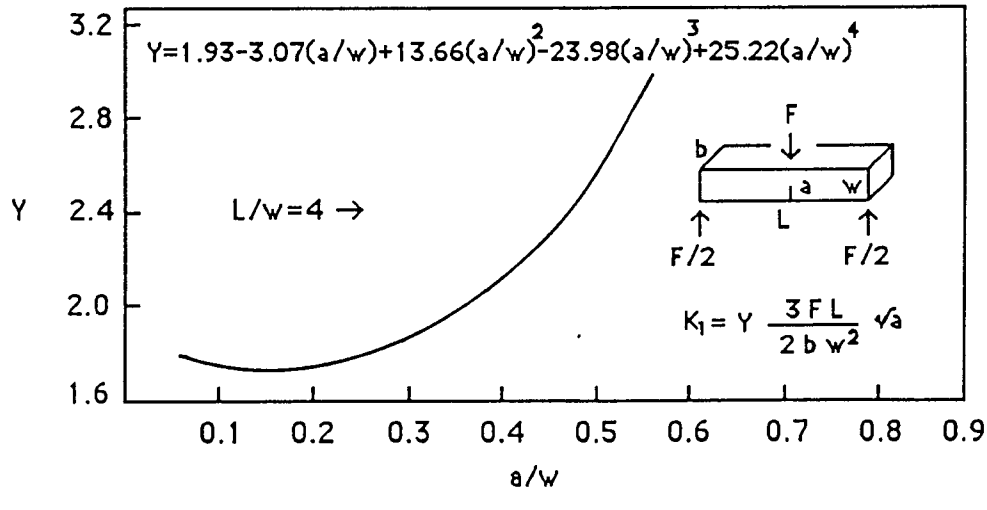

Figure III.6 3-point bend specimen

This technique was used on HA by With (115) who found values of K_{1c}=1 MPa $m^{1/2}$. Under wet conditions the K_{1c} was roughly 25% lower.

Compact-tension (Ct)

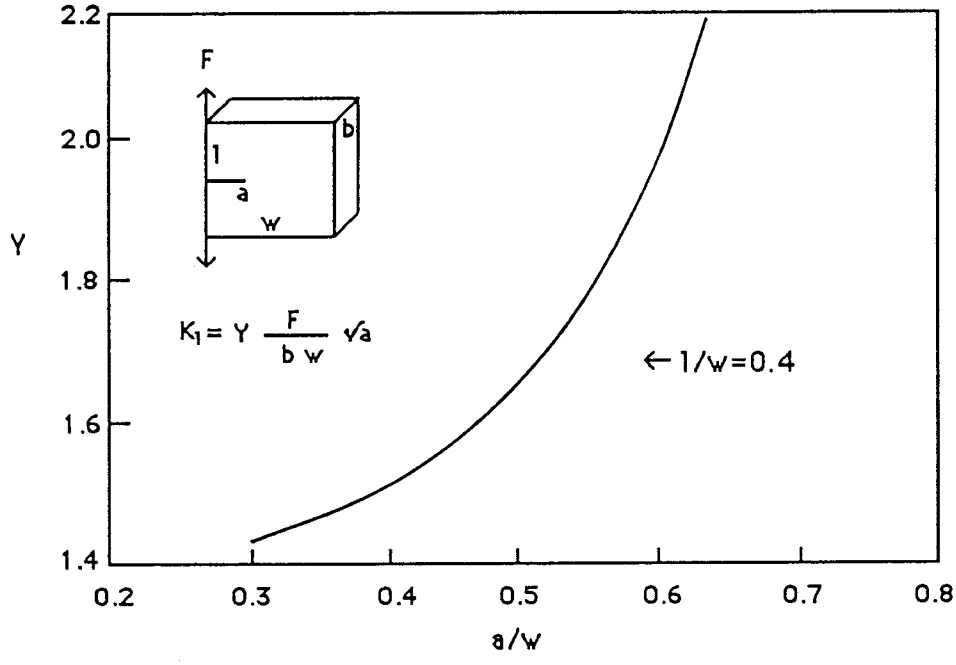

Figure III.7 Compact-tension specimen

Double-cantilever-beam (Dcb)

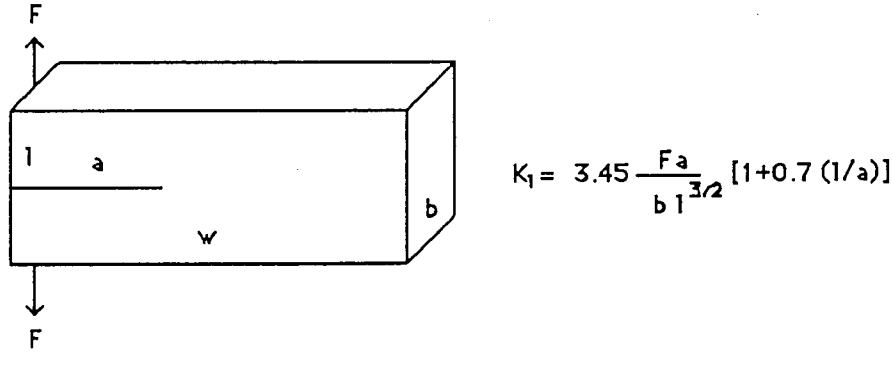

Figure III.8 Double cantilever beam

The bend specimen is the most efficient and easiest to test. The difficulties involved in the complex gripping system, necessary to

give adequate alignment, makes the tension specimens the least satisfactory. Any of these specimens can be used for measurements however an accurate crack measurement is required. Specimen configurations which result in crack length independent values for K 'constant K specimens' have extensive application in ceramics. Two specimens in particularly are used (97,101,131,134,135).

Tapered double cantilever

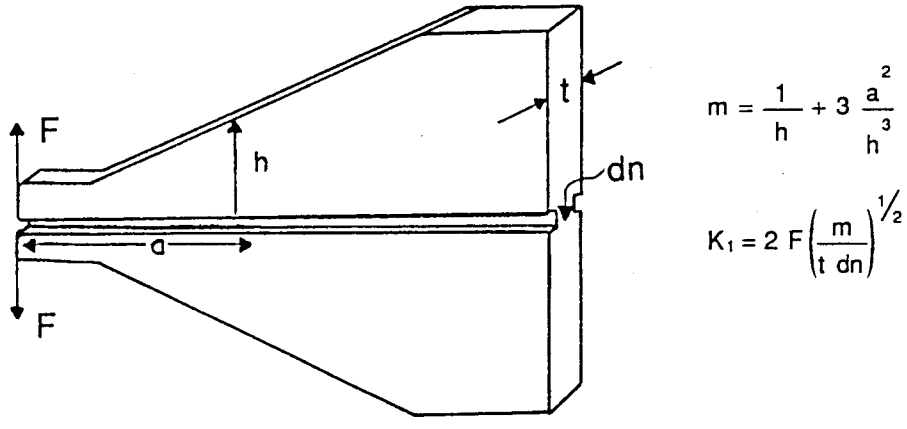

Figure III.9 Tapered double cantilever. Constant K conditions are obtained by shaping the specimen to give constant m.

Double torsion

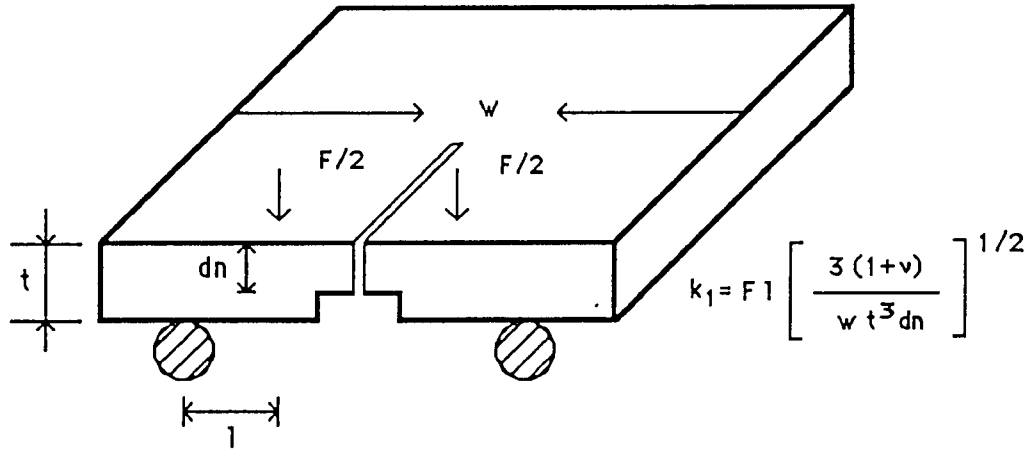

Figure III.10 Double torsion test

Experimental requirements

Two general features associated to fracture mechanics are required to carry out these tests:

i) The thickness of the specimen, t, should be 2.5 $t>(K_{1c}/\sigma_r)^2$. This condition is usually satisfied because σ_r is high and K_{1c} low in ceramic materials.

ii) The specimen dimensions under test should be large enough to be microstructurally representative of the material.

iii) Fracture in ceramics usually occurs from small sharp cracks; to correlate the data with this aspect it is necessary that the cracks in the specimens are similarly sharp.

Indentation method

Indentation techniques are finding increasing application in the study of the fracture toughness of brittle materials. The particular attraction of these techniques lies in their simplicity as a non-destructive method for producing regions with high stress intensity in a specimen. The test uses a hard, sharp indenter and loads the specimen surface with a normal force. When the indenter penetrates a brittle material the first event is the formation of a inelastic zone, the size of which increases with the load according to equation (III.20):

$$H = \frac{F}{\alpha_o d^2} \qquad \text{(III.20)}$$

where H is the hardness, F is the force, α_o is a constant dependent on the geometry of the indenter and d is the radius of the deformation zone. With the Vickers indenter the stress concentrates on median planes containing the diagonals of the square-shaped surface impression producing the radial star pattern shown in Figure III.11:

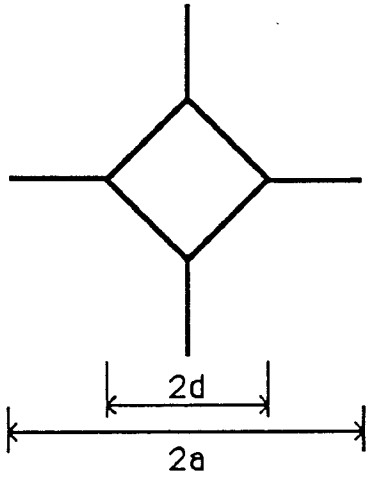

Figure III.11 Penny shaped cracks

where a is the crack dimension. Several authors have shown that the length of the cracks could be related to toughness, although some discrepancies in the establishment of calculations have occurred (136,137,138,139). The most successful results have probably come from Lawn (136) and Laugier (138).

One further set of cracks referred to as 'lateral cracks' may be formed with sharp indenters and these originate below the surface of the specimen and extend outwards the deformation zone, running parallel to the surface (136,140). Because these cracks are not taken into account in the formulas, the results obtained from these methods are usually overestimated (140). To overcome this problem a routine bend test has been introduced to measure the strength of

the Vickers-indented test pieces (141). The resulting indentation/strength data was analysed and an appropriate calibration factor has been obtained with very good correlation with conventional techniques.

I V HYDROXYAPATITE POWDER CHARACTERISATION

IV.1 Introduction

A wide variety of techniques were used to characterise the HA powder, as its chemical and physical nature strongly influences the characteristics of the final product, HA dense ceramic. Complete powder characterisation is usually absent in the literature. Some techniques were also applied to the sintered compacts in order to follow the sintering behaviour of HA, namely mineralogical transformation to TCP structures by OH^- loss by heating at high temperatures.

IV.2 X-ray diffraction

The mineral composition of the HA powder was analysed using Philips-1710 diffractometer with the help of the Phillips P-1877 software, using Cu-Kα radiation at 35mA and 50KV. Scans were obtained at a rate of 0.5^0/min. Lattice parameters were calculated by square minima, using the Latcon software facility. Full width half maximum and integral width values were determined for the three main HA standard peaks, using a fitting procedure in the software.

IV.3 Chemical composition

A chemical route for the determination of the Ca/P ratio was used, as specified by Plasma Biotal. The method is based upon the production of a precipitate of magnesium pyrophosphate using 5g of

HA and solutions of ammonia (2%), citric acid with ammonia solution, and ammonium chloride. The product was ignited and weighed to give a percentage yield of P_2O_5. The percentage yield of CaO was calculated from the mass of the ignited product (a calcium oxalate precipitate) when 0.5g of HA was dissolved in 36% hydrochloric acid and 50% ammonia solution. Further details can be found in Neuerburg (142). Calcium was also determined by atomic absorption spectroscopy using an Instrumental Lab-357 equipment. Residual elements were analysed by the same process. A complete description of the method used can be found in the literature (143). Phosphorous was determined by a photocolourimetric by ascorbic acid method (144), using a Shimadzu UV-1201 spectrophotometer.

IV.4 Infra-red spectroscopy

The frequency of most molecular vibrations corresponds to that of the infra-red spectrum region, 625-4000cm^{-1}. The molecular groups have vibration frequencies characteristic of their own functional group and within well-defined areas of spectrum range. Table IV.1 summarizes the frequency ranges absorbed by each molecule (145,146,147).

Table IV.1-Absorption bands characteristics

Group	Range (cm^{-1})	Remarks
OH-	3590-3650	Sharp peak
	630	Peak
CO_3^{-2}	1410-1450	Broad band
	879	Peak
PO_4^{-3}	1000-1100	Broad band
	550-600	Band
H_2O	3100-3600	Broad band

Thin transparent discs were prepared by mixing HA and potassium bromide in the proportion of 1/50 and pressing at 10 T/cm^2 in a steel die using an hydraulic press. The analysis was performed in a Perkin Elmer Series FTIR equipment. Fifty scans were averaged in order to obtain each spectrum.

IV.5 Water content

Water content analysis was performed with a Brainweigh MB-301 equipment. 10.16 g of powder were heated at 167°C for 15 min, as fixed by the machine. The process is based on the weight loss by water liberation at high temperature. The result was directly read in the instrument.

IV.6 Scanning electron microscopy

The morphology of the powder particles was observed using a Jeol 35 JSM microscope. Small amounts of powder were attached to adhesive aluminium tape and placed on an aluminium stub. Before observation the powder was sieved to -75 μm and sputter coated with gold for 3 min.

IV.7 Surface area analysis

A Rapid Surface Area Analyser Micromeritcs was used to determine particle surface area by a BET method (148,149). The samples were previously sieved at -75μm and heated at 250°C for 60 min to allow drying and degassing to occur. Liquid nitrogen was employed to form a monolayer around particles at -196°C. The process was repeated three times to check the reproducibility.of the values obtained.

IV.8 Particle size analysis

Particle size distribution profiles were obtained by laser diffraction (148,150) using a Malvern Mastersizer MS-20 equipment with an He-Ne laser. 2.0g of -75 μm sieved powder were suspended in 50 ml of distilled water using Tween 81 from Shell company, as a dispersant. The samples were immersed in an ultrasonic bath for 3 min to break up any agglomerate. Distribution profiles and values of the median particle size ($D_{0.5}$) and particle values at 10% and 90% ($D_{0.1}$ and $D_{0.9}$) on the cumulative frequency curve were also recorded.

IV.9 Thermogravimetric analysis

Thermogravimetric analysis was carried out with a Stanton Redcroft apparatus, from room temperature to the maximum temperature allowed by the equipment, 1260°C, at a 6°C/min heating rate followed by natural cooling inside the furnace. 2.0000g of HA powder were used in the test, as fixed by the apparatus.

V SINTERED HYDROXYAPATITE

V.1 Introduction

In this research project, conventional ceramic techniques were used for the production of a dense HA ceramic. Sintering cycles were studied and highly dense HA could be obtained with short sintering times. Dense materials were microstructurally characterised and their mechanical properties determined by a large number of techniques, aiming at biomedical applications. Dies and test jigs were designed and manufactured for this purpose.

V.2 Specimen preparation

V.2.1 Sieving

Before pressing the HA powder was sieved to -75 μm (2000, 212 and 75μm stainless steel sieves) in order to destroy the agglomerates, using a Fritsch Vibratory Sieve Shaker.

V.2.2 Pressing

Two types of pressing were used to produce dense HA ceramics: uniaxial pressing and isostatic pressing.

V.2.2.1 Uniaxial pressing

Disc specimens with 30mm diameter and 2mm thickness approximately, were uniaxially pressed using a 20T CAM press. The

die was designed and made cylindrical with the aim to test strength using a biaxial bending method. 4.0g of material were weighed to produce each sample and an initial 3MPa pre-load was applied to obtain a perfect alignment of the cylinder with the steel die. The load was then increased to its maximum value, 19MPa. In each pressing operation, the die was cleaned with water. Figure V.1 shows the die employed and a typical sample geometry.

Beam specimens, 60 mm in length and 6x3 mm^2 in section, were also fabricated. This shape was abandoned because a biaxial bending test (ring-on-ring) was intended to be used to test the strength of HA, which has many advantages in relation to the conventional 3 and 4-point bending tests on beams. These specimens tended also to warp after sintering which was another difficulty to overcome.

V.2.2.2 Isostatic pressing

HA samples were isostatically pressed to 100MPa using a Breack Block machine by the 'wet-bag' process. 12.0g of powder per specimen were put in polyethylene bags. Shell-Dromus B fluid was utilised to promote the isostatic pressing. Cylindrical samples, approximately 25 mm in diameter and 25 mm in height, were obtained after pressing.

V.2.3 Drying

As the HA powder had 1.2% water content (see chapter VIII) which was also used to clean the die, the samples were dried overnight in an oven at 110°C before sintering.

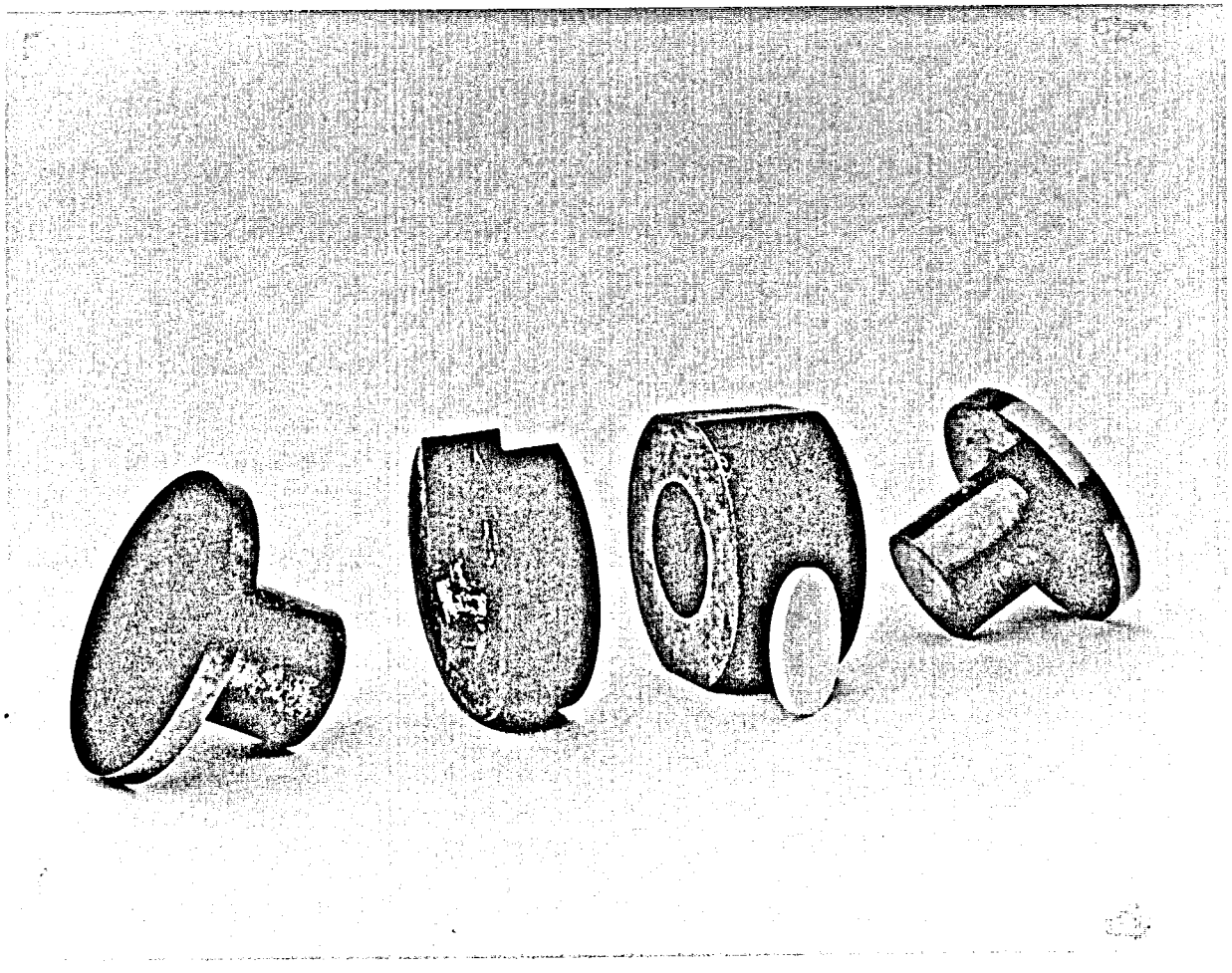

Figure V.1 Single action die used to press disc specimens

V.2.4 Sintering

Samples were sintered using a Carbolite RHF 16/3B muffle furnace with a Eurotherm type 812 controller. The samples were put on Al_2O_3 plates to avoid the contact with furnace floor. A 4°C/min heating rate, 1200, 1250, 1300 and 1350°C sintering temperatures and 1h and 3h dwell times were employed, followed by natural cooling inside the furnace. 10 uniaxially and 1 isostatically pressed samples were sintered under each sintering condition. With this vast scheme the sintering behaviour of HA powder was established.

V.3 Specimen characterisation

V.3.1 Macroscopic observation

Macroscopic observations were made by eye concerning the blue coloration that the samples showed after sintering. The starting powder was white.

V.3.2 Shrinkage

The linear percentage shrinkage of the samples after sintering, relative to their initial size in the green compact, was determined by measuring the diameter of each sample and using the following equation (V.I):

$$\text{Shrinkage} = \frac{D_{green} - D_{sintered}}{D_{green}} \times 100 \qquad (V.1)$$

The diameter was measured using a vernier calliper with an accuracy of 00.1 mm.

V.3.3 Density

The density of the sintered compacts was measured by Archimedes principle using mercury and the percentage of densification calculated assuming the theoretical density of 3.156g/cm^3 for HA. Samples were weighed with an accuracy of 0.01g and the temperature of the mercury was measured to determine its density. Each density result corresponds to the average of the density of 10 uniaxially pressed samples. The test was performed in a Bulk Density Measuring apparatus.

V.3.4 X-ray diffraction

X-ray diffraction analysis was direct performed on specimens fired at all sintering conditions to see whether any phase transformations had occurred during sintering. Lattice parameters were calculated for specimens sintered for 1h. Full width half maximum and integral width values were measured on samples sintered at all sintering temperatures for 1h. The same test conditions were used as those described in section IV.2.

V.3.5 Infra-red spectroscopy

Sintered samples were reduced to powder in a ball mill for infra-red analysis. Zirconia balls were employed in order to minimise contamination. All sintering conditions were analysed and the evolution of the spectrum with temperature was followed. Test conditions were kept the same as in section IV.4.

V.3.6 Microstructure

Before scanning electron microscopy analysis, sintered samples were cut, polished and chemically etched to reveal grain boundaries, according to the following process:

(a) Cut with a diamond saw

(b) Grinding, 100μm, 50μm and 20μm discs

(c) Rinsing with water, ultra-sonic bath for 5 min.

(f) Polishing, 6μm, 3μm, 1μm diamond discs and colloidal silica

Grinding and polishing operations were carried out in a Struers-Petrodisc equipment. Between each grinding and polishing operation the samples were rinsed in water to avoid contamination. The grain boundaries were revealed by etching with a 10% citric acid solution for 3-4 min at room temperature. Samples were gold coated using a sputtering process for scanning electron microscopy analysis. Grain size was determined using a linear intercept method proposed by Jarcho (31). In this method, circles 4 and 5 cm in diameter are drawn on the photograph and grain size is determined by the equation (V.2):

$$G = \frac{c}{N M} \qquad (V.2)$$

where G is the grain size, c is the circle diameter, N is the number of intersections with grain boundaries and M the magnification of the photograph.

V.3.7 Mechanical properties

V.3.7.1 Hardness

As-received sintered samples were hardness tested using a

Schimadzu microhardness machine with a 9.8 N load for 10 sec. To obtain a given hardness value for each sintering condition 30 indents were measured. Vickers hardness values were calculated using equation (V.3):

$$HV = \frac{1854.4 \times F}{(2d)^2} \qquad (V.3)$$

where F is the load, 2d is the averaged mean of the two diagonals of the indent.

V.3.7.2 Biaxial bending strength

Bending strength was obtained from concentric ring-on-ring test in a concentric-ring jig with 20 mm supporting span and 10 mm loading span at a cross head speed of 5 mm/min. The test was carried out in an Instron 6025 Universal Machine with a 5KN load cell. The modulus of rupture (within the loading ring) in biaxial bending concentric-ring test is calculated using (117,120):

$$\sigma_r = \frac{3F(1+\nu)}{4\pi t^2}\left(1 + \ln\frac{r_2}{r_1} + \frac{1-\nu}{1+\nu}\frac{r_2^2 - r_1^2}{r^2}\right) \qquad (V.4)$$

where F is the load, t is the thickness of the sample, r_1 the radius of the loading ring, r_2 the radius of the supporting ring, r the radius of the disc and ν the Poisson's ratio. A value of 2.8 was assumed for the Poisson's ratio of HA as found in the literature (115,151).

This jig was particularly designed and made for these disc samples and knife circular edges were carefully created at the contact points

on the loading and supporting spans. A perfect alignment of the loading ring was obtained by the perpendicular pins where the ball fits. Figure V.2 shows the jig that was prepared.

The concentric-ring test has the advantages of eliminating many problems associated with the fracture induced by the edges of the samples, so that the strength determined is much more representative of the true strength of the material. Bar-shaped specimens exhibit additional flaws at the edges which are generated by the particular shaping process. These flaws cannot be avoided, nor can their influence on the strength value be determined. 10 specimens were tested to calculate the strength for a given set of sintering conditions, as stated by the JIS R 1601 standard (152). Weibull modulus was determined to characterise the variability of the strength results. As an example, Appendix 1 shows the method applied to samples sintered at 1300°C.

Young's modulus was also calculated using equation (V.5) (153,154):

$$E = \frac{0.17\, L^3 \left(1 - \nu^2\right) F}{10\, \delta\, t^3} \qquad (V.5)$$

where E is the Young's modulus, L is the supporting span, t is the thickness of the sample, ν is the Poisson's ratio, F is the load and δ is the deflection at mid-span. The deflection at mid-span was measured through the speed of the recording system and the cross-head speed and the slope of the tangent to the straight-line portion of the load deflection curve according to ASTM D 790M-82 standard (112).

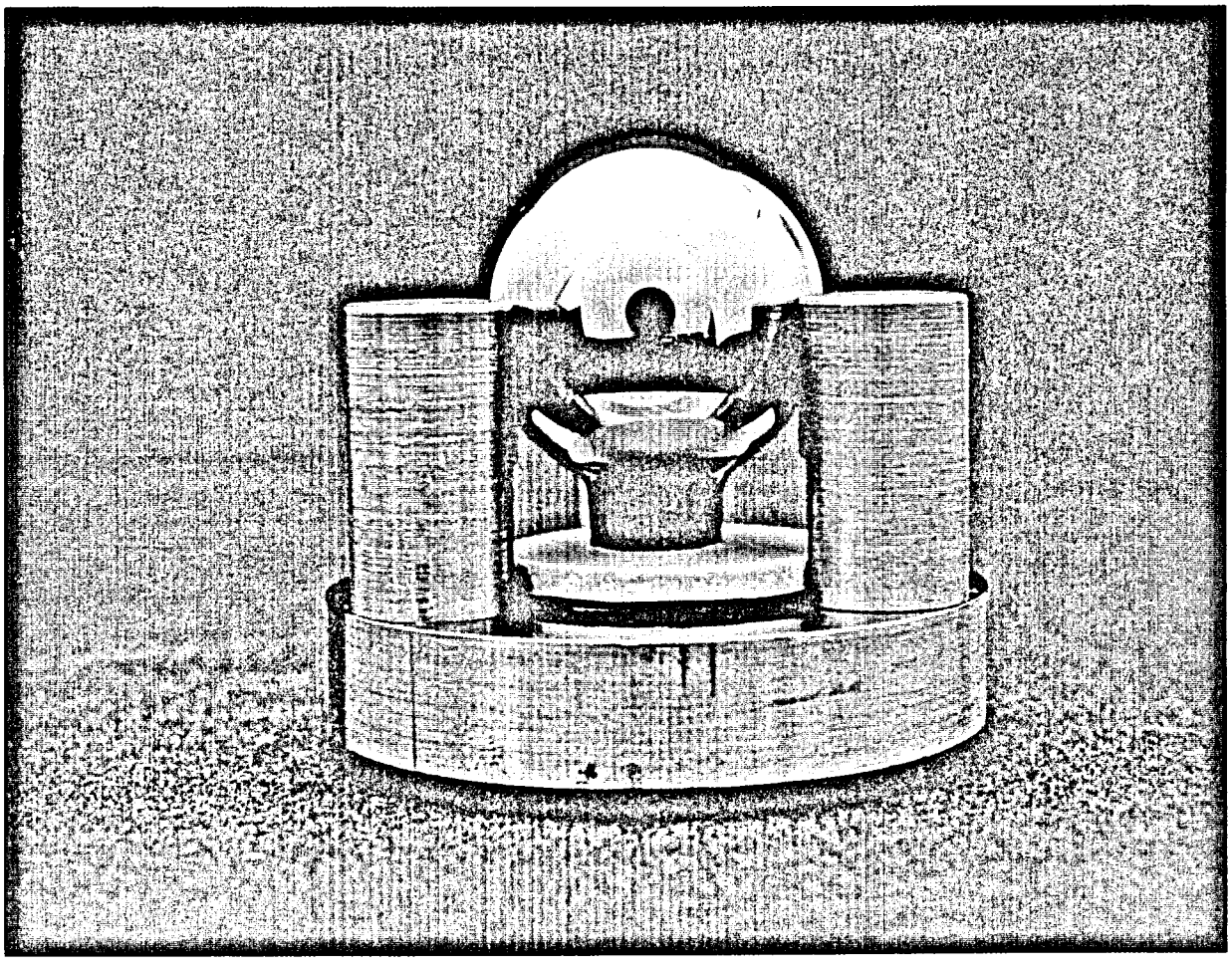

Figure V.2 Concentric ring test jig

V.3.7.3 Fracture toughness

V.3.7.3.1 Indentation

Fracture toughness was calculated using an indentation technique proposed by Laugier (138) and given by equation V.6:

$$K_{1c} = 0.015 \left(\frac{a - d}{d}\right)^{-\frac{1}{2}} \left(\frac{E}{H}\right)^{\frac{2}{3}} \frac{F}{a^{3/2}} \qquad (V.6)$$

where a is the crack length, d is the half indent diagonal, F is the load, E is the Young's modulus and H is the hardness. A 9.8 N load was applied to the surface of the as-sintered samples for 10 sec., using a pyramidal diamond indenter. A calibration trial was performed on soda glass to ensure compatibility of results with those reported in the literature (138). The mean of the dimensions of 40 indents were measured for a given set of sintering conditions. A result was considered valid when no chipping of the material occurred around the indent. Crack lengths for samples sintered at 1200°C for 1h could not be measured because of their relative high porosity and the results were not considered.

V.3.7.3.2 Strength-indentation

Strength-indentation test has special application to those materials for which their sample preparation for the conventional fracture toughness methods is difficult, as it is the case of HA. At the same time, it gives a much more accurate result than the indentation processes, which tend to overestimate the results, because the formulas to calculate K_{1c} do not take into account the 'lateral cracks'

that develop during the indentation, as it was referred in section III.4.5. However, a conventional method was used to characterise the fracture toughness of HA, the double torsion test, but this test could not be used for HA-glass composites as it will be discussed in chapter VI.

A Vickers indentation was made at the centre of the face submitted to a tensile effort, which was then tested under biaxial bending using the same jig mentioned before for the strength test. The same operating conditions were used as those for the hardness and strength test and above indicated. 10 samples were tested, sintered at 1250°C, 1300°C and 1350°C for 1h. The fracture toughness was determined by the following equation proposed by Chantikul (141):

$$K_{1c} = A \left(E/H \right)^{1/8} \left(\sigma F^{1/3} \right)^{3/4} \qquad (V.7)$$

where, K_{1c} is the fracture toughness, A is a geometric constant, σ is the strength of the pre-cracked sample, E is the Young's modulus, H is the hardness and F is the load.

V.3.7.3.3 Double torsion

Sample preparation for conventional methods to determine fracture toughness is very difficult to perform on HA, particularly grooving and machining operations. HA is very brittle and samples tend to fracture very easily. This is probably one of the main reasons why only very few authors have carried out these tests on HA. In this work a double torsion process was used, but the method presented many difficulties which will be succinctly described.

A steel die was designed and made to produce slab compacts, 100mm in length and 32x3 mm^2 in section, using a pressure of 19MPa, according to the usual procedure used throughout this work. Samples were then cut to three of 30mm in length each, using a diamond saw. Firstly, a direct sintering process at 1300°C was applied at a 4°C/min heating rate and 1h soaking time, followed by natural cooling inside the furnace. A theoretical relative sample density of 97% was achieved, but at this density and hardness level almost all samples fractured when the groove was made. Therefore, direct heating to full sintering temperature was abandoned and another method was tried. A pre-sintering stage at 900°C for 1h was used to give some consistency to the material for the machining operations (relative sample density of 69±4%). Grooving was then carried out and samples were fully sintered at 1300°C, applying the same sintering cycle as before. This method was successful and ≈80% of the samples could be available. Finally, a notch of ≈5mm length was sawn. A double torsion sample prepared in this way is shown in Figure V.3.

Conventional techniques were then applied to pre-crack these samples, namely (135) wedge loading at a sawn notch, using a compressive stress ahead of the sawn notch and thermal shock. These methods are usually well-adapted to ceramics but very little success was achieved on HA. The crack extended to fracture without stopping which was attributed to the fragility of HA. The only technique found suitable to pre-crack the HA samples was by making an indent at the crack notch tip using a Vickers indenter. This technique has been used by With (115) and Aoki (8).

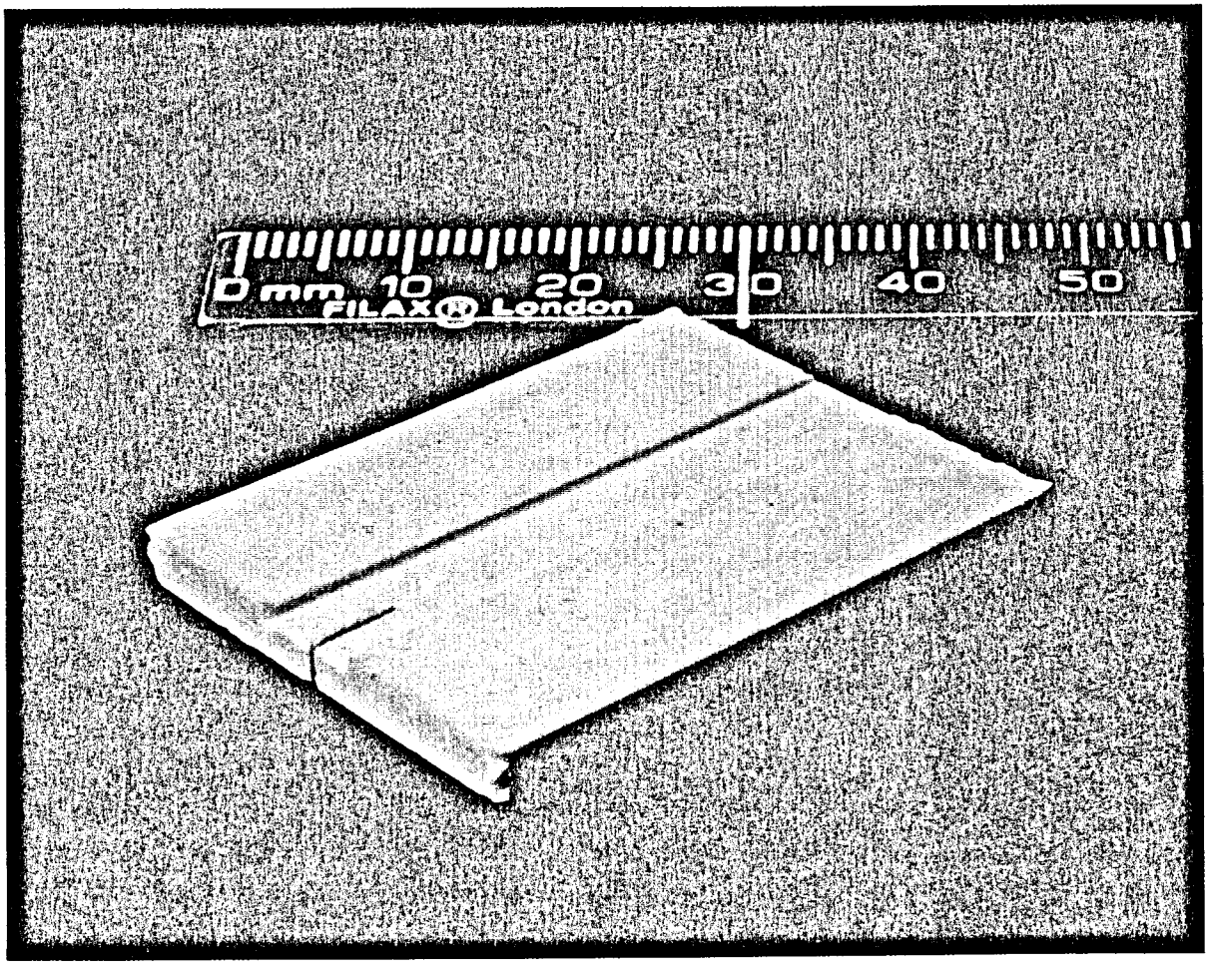

Figure V.3 HA specimens for double torsion test

A 4-point bending jig test was also designed and made with 22mm supporting span and 12mm loading span. Steel balls were the contact points. The test was carried out on 7 samples using an Instron 6025 Universal Machine with a 5KN load cell. K_{1c} was determined according to the process and equation presented in section III.4.5 for double torsion test.

V I HYDROXYAPATITE-GLASS COMPOSITES

VI.1 Introduction

HA is currently of great interest to biomedical applications due to its well-established bioactivity. However, the material is limited to low load applications owing to its inadequate mechanical properties when compared with mature bone (8). Enhancement of the mechanical properties of HA has been centred around the development of compaction methods and also choice/control of grain size (10). Whilst optimising the fabrication processes of HA, they do not give significant increases in the mechanical properties. More recently glass-ceramic materials have been developed which show higher mechanical properties but have a different microstructure (89,90,155,156,157,158,159), based on a silica network glassy phase and a crystalline apatite structure. Most times the apatite phase is not even HA. Although these materials seem to show bioactivity when implanted, with their different microstructure a difference in biological behaviour should be expected. This chapter describes a new approach to the enhancement of the mechanical properties of HA by using a sintering liquid phase mechanism. Glasses closely related to HA, i.e., soluble phosphate based glasses (P_2O_5-CaO system) and Bioglass® were added to the sintering process of HA. The phosphate glasses were prepared and Bioglass® was obtained from the Bioglass® Research Center, University of Florida, USA. The method has shown great success and a British Patent was made under the control of the Interdisciplinary Research Centre (IRC) in Biomedical

Materials, Queen Mary & Westfield College, University of London, where all this work was developed, under the title: 'Densified Hydroxyapatite' by the authors, J. D. Santos, J. C. Knowles, G. W. Hastings and W. Bonfield, British Patent Nº 9213774.4, filed on 29th June 1992.

VI.2 Glass preparation

Three phosphate based glasses were produced with the following chemical composition, in mol%: 54.5CaO-45.5P_2O_5, 28CaO-45P_2O_5-27Na_2O and 10.1CaO-62.9P_2O_5-10.1Na_2O-16.9Al_2O_3. Starting from a P-Ca oxide base, therefore chemically related to the Ca-P base of HA, additions of sodium oxide and aluminium oxide were made to alter both the physical and chemical properties of the glasses. These aspects will be discussed later in the discussion chapter where the sintering process of HA and the properties of the glasses are interrelated. 45S5-Bioglass® was also added to HA to compare the effect of a silica network glass on HA with that of the phosphate. Very low percentages were added to HA, 2.5 and 5 wt%, to avoid problems of altered biocompatilibity and minimise phase changes.

VI.2.1 Chemical calculations

All chemicals used in the production of phosphate glasses are A.R. grade and were bought in BDH Chemicals Ltd. The following chemical calculations were performed to fabricate the glasses, assuming 1 mol of glass for calculation basis:

a) 2 oxide glass: 54.5CaO-45.5P_2O_5 mol%

	$CaCO_3$	→	CaO +	CO_2
Mw	100		56	44
%			0.56	

Require 0.545 moles of CaO 0.545 x 56/0.56 = 54.5g of $CaCO_3$

Mw of P_2O_5 is 142g, then: 142gx0.455 = 64.6g of P_2O_5

b) 3 oxide glass: 28CaO-45P_2O_5-27Na_2O mol%

$2NaH_2PO_4$	→	Na_2O +	$2H_2O$ +	P_2O_5
240		62	36	142
		0.26	0.15	0.59

Require 0.27 moles of Na_2O, then: 0.27x62/0.26 = 64.4g of NaH_2PO_4

64.4g of NaH_2PO_4 produces: 64.4x0.59 = 38g of P_2O_5

$CaCO_3$	→	CaO +	CO_2
100		56	44
		0.56	

Require 0.28 moles of CaO, then 0.28 x 56/0.56 = 28g of $CaCO_3$

P_2O_5 needed: 0.45x142 = 63.9g

added: 63.9-38 = 25.9g of P_2O_5

c) 4 oxide glass: 10.1CaO-62.9P_2O_5-10.1Na_2O-16.9Al_2O_3 mol%

$$2NaH_2PO_4 \rightarrow Na_2O + 2H_2O + P_2O_5$$

240 — 62 — 36 — 142

0.26 — 0.15 — 0.59

Require 0.101 moles of Na_2O, then: 0.101x62/0.26 = 24.1g of NaH_2PO_4

24.1g of NaH_2PO_4 produces: 24.1x0.59 = 14.2g of P_2O_5

$$2CaHPO_4 \rightarrow 2CaO + H_2O + P_2O_5$$

272 — 112 — 18 — 142

0.41 — 0.066 — 0.52

Require 0.101 moles of CaO, then: 0.101x56/0.41 = 13.8g of CaH_2PO_4

13.8g of CaH_2PO_4 produces: 13.8x0.52 = 7.2g of P_2O_5

$$2AlPO_4 \rightarrow Al_2O_3 + P_2O_5$$

244 — 102 — 142

0.42 — 0.58

Require 0.169 moles of Al_2O_3, then: 0.169x102/0.42 = 41g of $AlPO_4$

41g of $AlPO_4$ produces: 41x0.58 = 23.8g of P_2O_5

P_2O_5 needed: 0.629x142 = 89.32g

added: 89.32-(14.2+7.2+23.8) = 44.12g of P_2O_5

VI.2.2 Fabrication method

Chemicals were weighed according to the above calculations and then mixed in a vibratory mixer for 10 min. As the P_2O_5 absorbs water, long periods of contact with air were avoided. Chemicals were then placed in a Pt crucible and heated at 1250°C for 1h. A 2h heating time was used and the molten glass was poured into a pre-heated steel mould. This process allowed the chemicals to react together and unwanted gaseous bubbles to escape from the melt. The chemical reactions assumed a complete decomposition of reagents. To avoid glass contamination Pt crucible was carefully cleaned with 50% hydrochloric acid solution at 80°C between each glass fabrication.

Once the glass was poured, it was coarsely reduced to a sand type particle and milled in a porcelain ball mill pot for 24h. A fixed proportion number of balls/amount of material was maintained. The same milling process was applied to Bioglass®.

VI.3 Glass characterisation

VI.3.1 Particle size analysis

After milling, particle distribution was determined using a Malvern Mastersizer according to the process described in section IV.8. The analysis was performed in methanol in order to avoid dissolution, as the glasses are water soluble.

VI.3.2 Chemical composition

Chemical composition was analysed by atomic absorption

spectroscopy using an Instrumental Lab-357 equipment. The following elements were determined: Ca, Na, Si and Al. The photocolourimetric method was applied to analyse P content.

VI.4 Composite preparation

HA-glass composites were prepared by adding phosphate based glasses and Bioglass® to the same HA powder used to fabricate HA dense compacts. At the sintering temperature the glasses produced are liquid so that a sintering mechanism in the presence of a liquid glassy phase will take place. Glasses chemically related to HA were chosen, therefore a strong bond between the two phases would be expected. In simple terms, a crystalline Ca-P structure was sintered in the presence of a Ca-P oxide liquid glassy phase. Bioglass® was also used although a weaker bond was expected as the material was not chemically similar to HA. Anticipating a strong bond between the liquid phosphate phase and HA, glass additions were kept low (2.5 and 5wt%) in order to preserve a Ca-P crystalline structure.

VI.4.1 Mixing

Having milled the glass, HA and methanol were added to wet mix the powders together for a further 24h. A relation of 350ml methanol/200g of material was kept constant. The same ball mill pot was used with the same proportion of number of balls/material used before. 2.5wt% and 5wt% glass additions were made to HA. To verify the influence of the milling process, an HA batch was also milled. It

should be emphasised that some tests were carried out using 7h mixing process and 100 ml of methanol. Samples were pressed and sintered, and inhomogeneous samples were obtained with some glass particles concentrated in some areas. After this experience, it was decided to increase the time for mixing and the quantity of methanol for the values mentioned above.

VI.4.2 Drying

Following milling, the slip was poured to a glass container and oven dried overnight to allow the methanol to evaporate.

VI.4.3 Sieving

The dried materials were then autosieved to -75μm. Particle size analysis was performed to determine particle distribution profiles.

VI.4.4 Pressing

Discs were uniaxially pressed at 19 MPa using the conditions described in section V.2.2.1. HA-2.5wt% glass and HA-5 wt% glass composites (per each glass) were fabricated. 40 HA samples were also pressed and sintered using the milled powder.

VI.4.5 Drying

Before sintering, samples were oven dried overnight at 110°C to remove water.

VI.4.6 Sintering

Specimens were fired at 4°C/min heating rate with 1h soak followed by natural cooling inside the furnace. 1200, 1250, 1300 and 1350°C sintering temperatures were used. 10 samples per composite were sintered at each sintering temperature.

VI.5 Composite characterisation

Chemical and physical analysis were performed on HA-glass composites to characterise their microstructure and mechanical properties. Whenever possible, samples were mechanically tested using the same techniques as before for HA, and results compared. In vitro tests were also conducted to determine their solubility on physiological solutions and its effect on mechanical properties, which will be dealt with in the next chapter.

VI.5.1 Density

Density measurements were performed by the Archimedes principle using mercury. Process details can be seen in section V.3.3.

VI.5.2 X-ray diffraction

X-ray diffraction analysis was performed in a Siemens D5000 diffractometer using Cu-Kα at 35 mA and 50KV. Relative intensities of the three main peaks of each phase (HA, β–TCP and α-TCP) were used to estimate phase contents of HA-phosphate glass composites. Appendix 2 shows an example of the process employed. Due to peak

overlapping caused by much higher proportions of β–TCP and α-TCP, x-ray diffraction quantification proved to be less accurate and therefore was not considered for 5% addition.

VI.5.3 Microstructure

Cutting, grinding and polishing operations were employed to reveal the microstructure of HA-glass composites, which were already described in the section V.3.6. O.1M solution of acetic acid was used to chemically etch the samples. Scanning electron microscopy analysis, equipped with energy dispersive spectroscopy and micro-analysis, was performed to analyse the microstructure and differentiate TCP structures from HA. Optical microscopy was also employed to verify phase distributions. Grain size was determined by the linear intercept method after chemical etching with 10% citric acid solution for 3-4 min at room temperature.

VI.5.4 Mechanical properties

VI.5.4.1 Biaxial bending strength

Biaxial bending strength was determined by the concentric-ring test used before for HA, as it is referred in section V.3.7.2. The same test conditions were used and Young's modulus was also calculated through the deflection at mid-span. 10 samples were tested per HA-glass composite and sintering temperature. HA sintered compacts were also tested using the milled powder to detect any influence of the mixing process on biaxial bending strength.

VI.5.4.2 Fracture toughness

Fracture toughness was calculated by the indentation and strength-indentation processes, as described in sections V.3.7.3.1 and V.3.7.3.2. Double-torsion was not employed because HA-glass samples had to be pre-heated to 900°C and at this level of temperature the reaction between HA and glass would have already begun and the samples would not have been representative of the structure of the HA-glass composites fabricated by only one sintering cycle.

VI.5.4.2.1 Indentation

Using the indentation technique referred to in section V.3.7.3.1, 40 cracks were measured per each HA-glass composite and sintering temperature. The test was also carried out on HA sintered specimens produced from the milled powder.

VI.5.4.2.2 Strength-indentation

The strength-indentation technique was also applied to calculate fracture toughness of HA-glass composites. Initially, a Vickers indentation was made at the centre of the tensile face of each HA-glass composite and HA. Test conditions can be seen in section V.3.7.3.2. 10 samples, sintered for 1h, were tested per composite and sintering temperature.

VII *IN VITRO* TESTS

VII.1 Introduction

Various attempts have been made to increase the mechanical properties and bioactivity of HA by incorporation of a glassy phase (160,161,162). Probably the most successful have been the glass-ceramic materials. Fast bone-implant bonding is an important factor in most biomedical applications. Phosphate glasses are water soluble and their incorporation in the HA could lead to high dissolution in the physiological medium, producing a premature loss of mechanical properties. *In vitro* tests were performed to determine the solubility characteristics of the HA-glass composites. Weight loss tests are usually an indicative parameter of the solubility.

VII.2 Weight loss

Dulbecco-A tablets for 'in vitro diagnostic use', from the Oxoid company, were dissolved in de-ionised water (1 tablet in 100ml of water) to prepare a phosphate buffered saline solution. De-ionised water was also used to determine any effect of the solution on the solubility of the materials. Sterile glass bottles from Sterile company, of the type used to store biochemical specimens, were chosen to ensure chemical inertness. HA and HA-2.5% glass samples were sintered at 1300°C and placed inside these bottles. Fourty samples were sintered for each material and mechanically tested at 28 and 56 days after being immersed in the physiological solution

and in de-ionised water. A jig was designed to allow testing of 10 samples per container, which consisted of perspex supports with 316 stainless steel wires. Therefore, a total of 20 containers and 200 samples were prepared for the tests, using a fixed solid/liquid relation of 10 samples/180ml. Figure VII.1 shows the scheme employed.

The containers were put inside an oven at a temperature of 37°C, which was maintained constant during the tests. Samples were weighed with an ±0.0001g accuracy and measured with an ±0.01 mm accuracy prior to exposure to the solutions. After a period of immersion of 4, 28, 56 and 84 days samples were dried, re-weighed and re-measured.

VII.3 Chemical analysis

As the chemical composition of the initial physiological saline solution used in tests was unknown, Ca and Na concentrations were analysed by atomic absorption spectroscopy and P determined by the photocolourimetric method using ascorbic acid. Chemical analysis of solutions after 28 and 84 days' sample immersion was carried out to determine ion leaching in terms of Ca, Na, Si and Al, from HA-glass composites.

VII.4 Biaxial bending strength

HA-2.5% glass composites and HA were mechanically tested using the concentric-ring test, after 28 and 84 days exposure in the physiological solution and de-ionised water. The tests were performed using the conditions previously reported in section V.3.7.2.

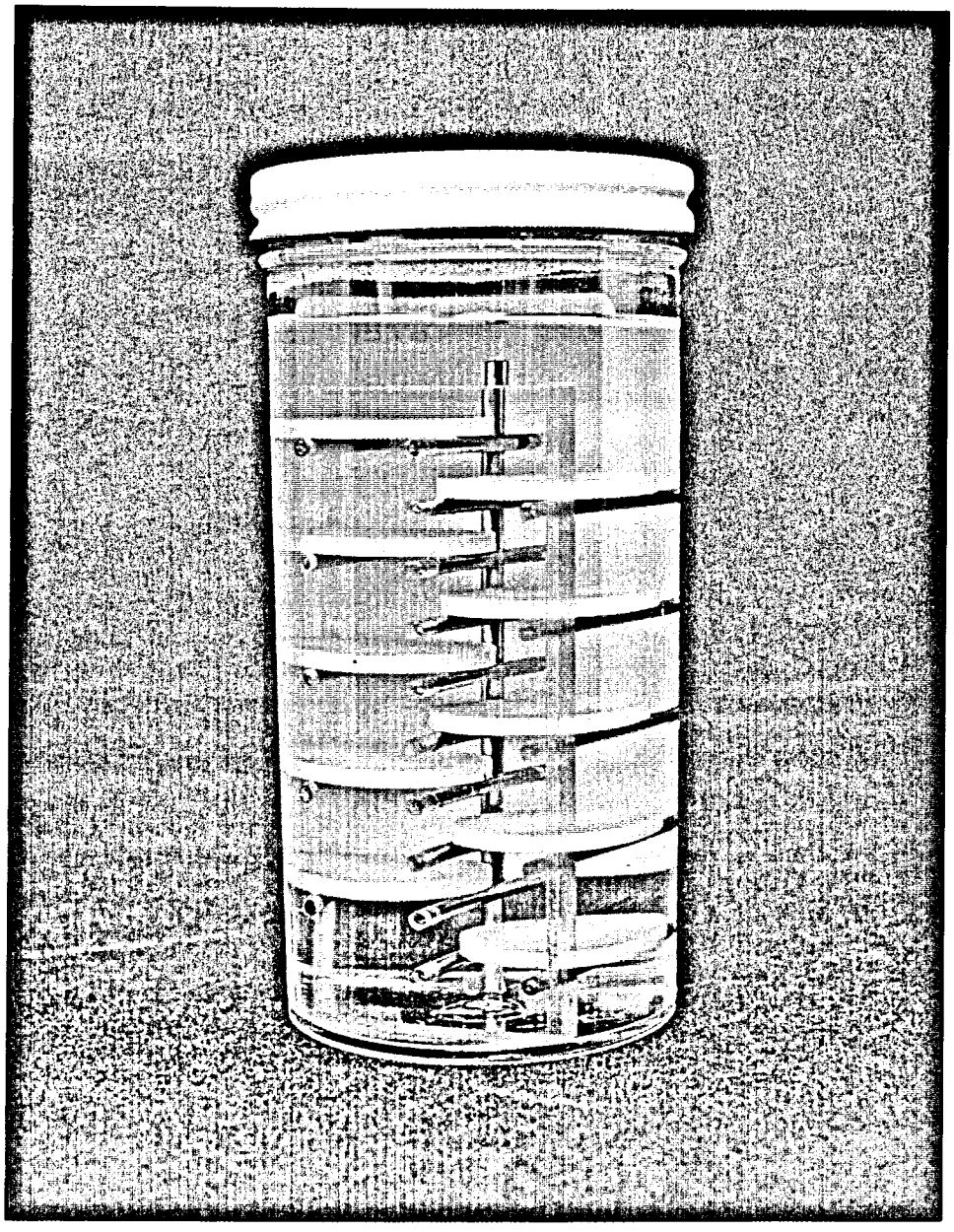

Figure VII.1 Scheme used for 'in vitro' test

VIII RESULTS

VIII.1 Introduction

The experimental results presented in this chapter are divided into the four main investigation areas of this work: a) hydroxyapatite powder characterisation b) sintered hydroxyapatite c) hydroxyapatite-glass composites and d) in vitro tests.

For each area, whenever possible, typical results will be presented in the same order used for the experimental techniques in the previous chapters. In some cases, a preliminary interpretation will be carried out.

VIII.2 Hydroxyapatite powder characterisation

VIII.2.1 X-ray diffraction

Figure VIII.1 shows the x-ray diffraction analysis obtained for the HA powder in the as-received condition. The x-ray traces were automatically run through and compared with the JCPDS-powder diffraction standard files-International Centre for Diffraction Data, installed in the software. No extraneous mineral phases were detected, apart from the peaks that corresponded to HA.

Lattice parameters, full width half maximum (FWHM) and integral width (IW) values are shown in Table VIII.1. FWHM and IW are arbitrary values obtained by using a fitting procedure in the

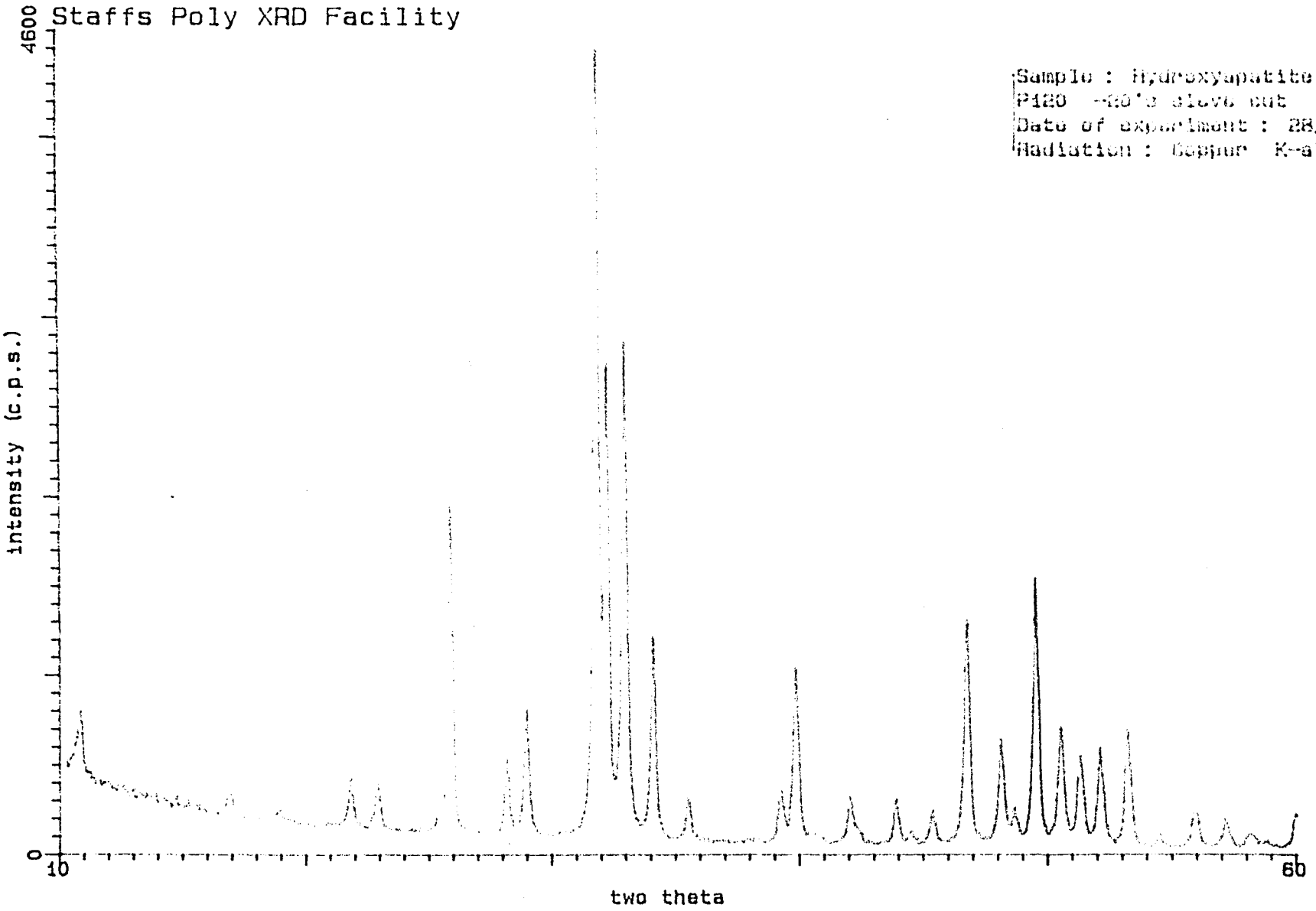

Figure VIII.1 X-ray diffraction analysis for HA powder

software. Comparison with values measured from samples heated at all sintering temperatures will be carried out in section VIII.3.4.

Table VIII.1 Lattice parameters, FWHM and IW values

Compound	Lattice parameters (Å) a	c	FWHM (°)	IW (°)
HA#	9.418	6.884		
HA	9.430	6.890	0.1889 (d=2.81)	0.2087 (d=2.81)
			0.1609 (d=2.78)	0.1569 (d=2.78)
			0.2147 (d=2.72)	0.2351 (d=2.72)

JCPDS standard 9-482

The lattice parameters matched well with the standard values for HA within an error of 0.12%. Peaks were relatively broad as indicated by FWHM and IW values.

VIII.2.2 Chemical composition

Calcium and phosphorous contents in HA powder are presented in Table VIII.2, according to the different methods used.

Table VIII.2 Ca and P analysis

Analysis	%Ca	%P	Ca/P (mol)
Gravimetric*	39.18	17.95	1.687 (±0.002)
Photocolorimetric*	–	18.00	–
Atomic abs. spectroscopy*	39.00	–	–

* mean value of two independent tests

A good agreement among the techniques was achieved and HA showed

a Ca/P ratio higher than its stoichiometric value, 1.67. The concentrations in residual elements were, in ppm: Fe-240, Al-200, Si-1200, Cu-10, Mg-2000, Ni<1 and Cr<1.

VIII.2.3 Infra-red spectroscopy

The infra-red analysis for HA powder is shown in Figure VIII.2. PO_4^{-3}, OH^-, CO_3^{-2} and H_2O groups are all visible in the spectra. CO_3^{-2} was detected as a peak at $\approx 879cm^{-1}$ and as a band at $1410\text{-}1450cm^{-1}$. OH^- peaks were detected at 3590-3650 and $630cm^{-1}$, approximately. A broad H_2O band in the 3200-3600 cm^{-1} range was also found.

VIII.2.4 Water content

HA powder showed a 1.2% water content after heating at 167°C. Although some water may have come from the KBr itself, this result seems to confirm the analysis above. The presence of water is undesirable for the sintering process as it avoids particle-particle contacts and can promote cracking. Therefore, a drying operation was carried out before sintering, as it was referred in section V.2.3.

VIII.2.5 Scanning electron microscopy

The HA powder consisted of 1-3μm particles although some agglomerates bigger than 15 μm could also be observed, as it is shown in Figure VIII.3. At higher magnifications, X4300, a smooth and porous structure was detected and the primary particles were shown to be composed of much smaller ones. Finally, very fine crystallites of 0.05-0.3μm in size were found at X20000 magnification.

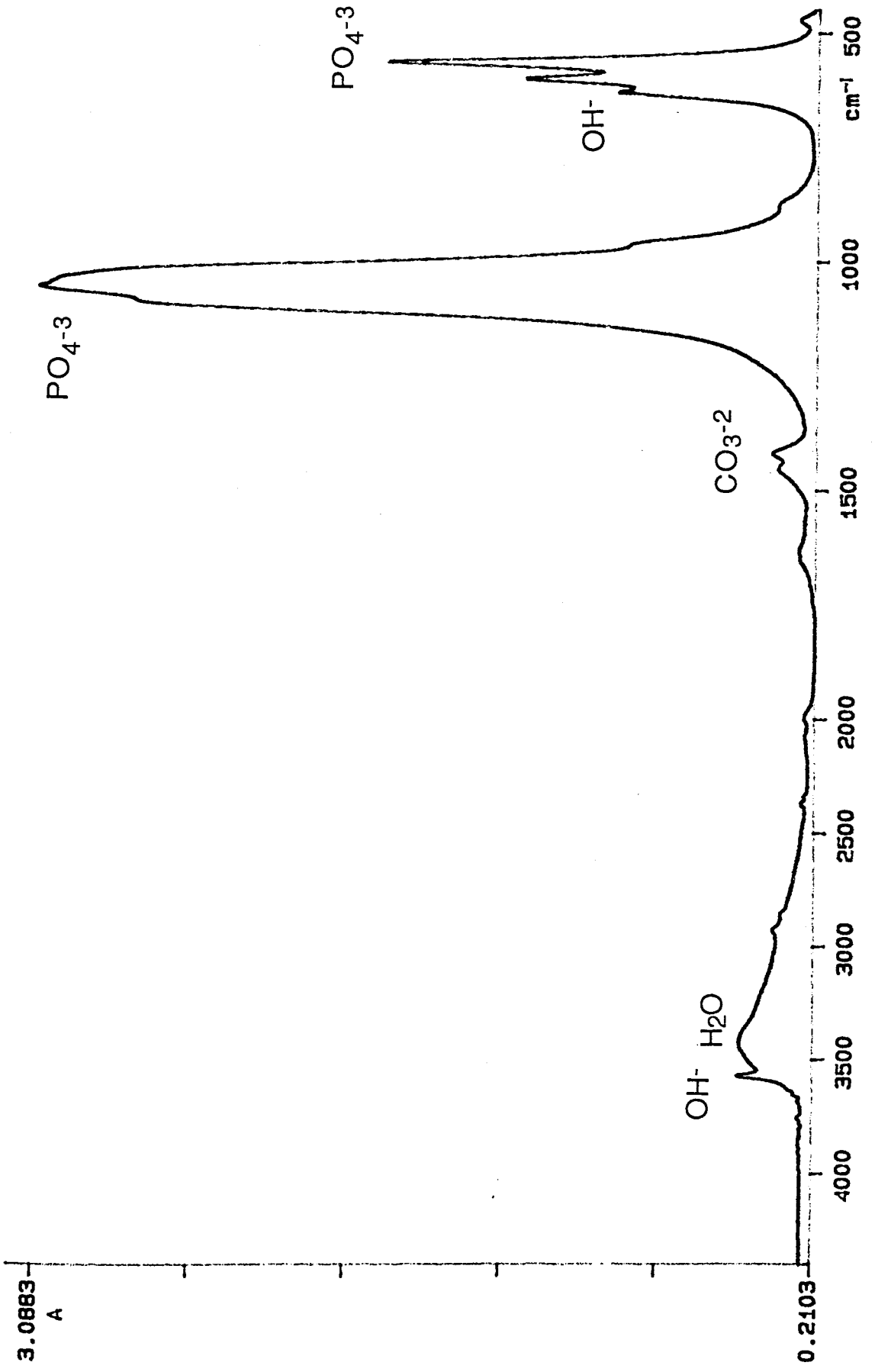

Figure VIII.2 Infra-red analysis for HA powder

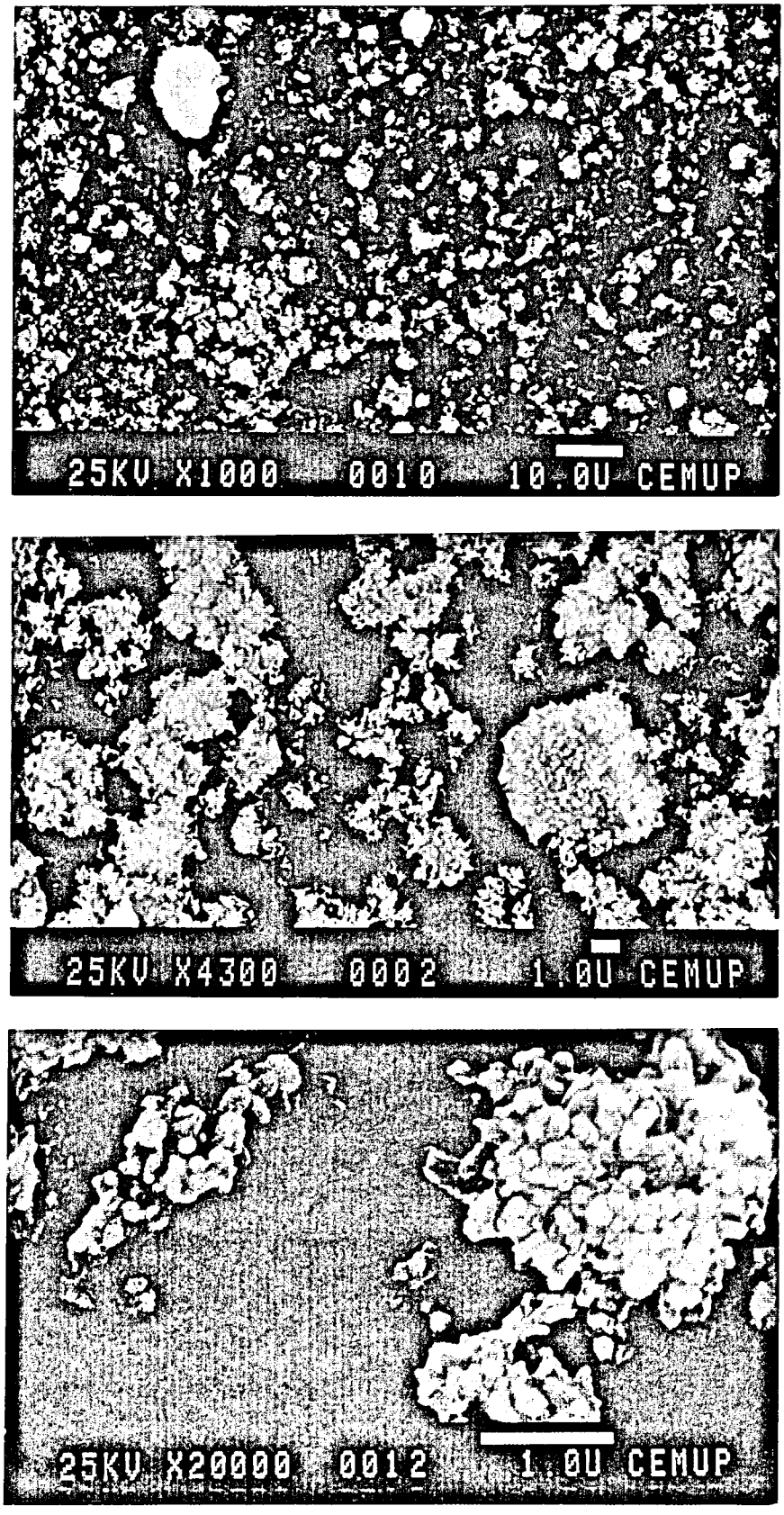

Figure VIII.3 Scanning electron micrographs of HA powder. The primary particles were composed of very small crystallites of ≅0.05-0.3μm in size

VIII.2.6 Surface area analysis

Surface area measurement results are described in Table VIII.3.

Table VIII.3 Surface area analysis

Weight (g)	Total surface area (m^2)	Specific surface area (m^2/g)
2.9300	47.5	16.21
2.5395	46.8	18.43
4.0537	64.6	15.94

A mean value of 16.86±1.36 m^2/g was found. This result will be compared and related to those of scanning electron microscopy and particle size analysis, in the chapter "Discussion'.

VIII.2.7 Particle size analysis

Particle size distribution profile and $D_{0.1}$, $D_{0.5}$ and $D_{0.9}$ values obtained from laser diffraction are shown in Figure VIII.4.

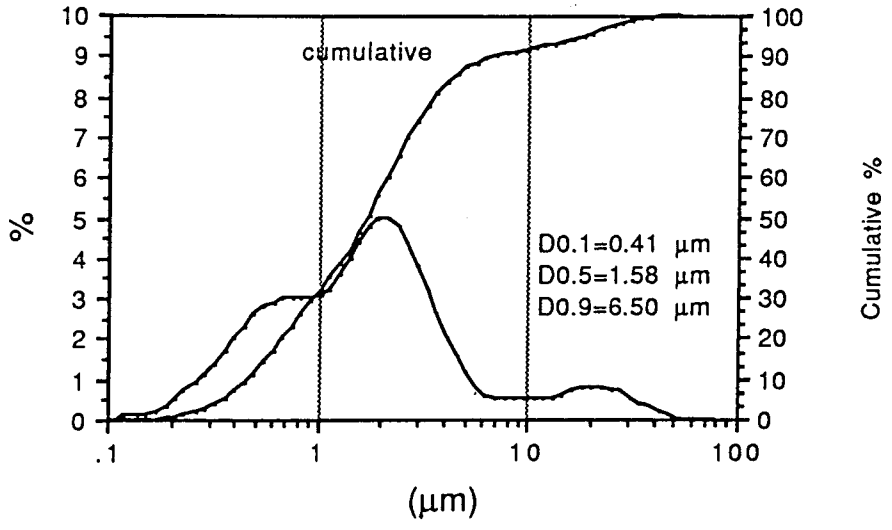

Figure VIII.4 Particle size distribution for HA powder

HA showed an aproximate bimodal distribution. The powder can be considered fine, as 90% of its particles are below 6.50μm after being sieved to -75μm. However, some relatively coarse particles (agglomerates) were found in the 20-50 μm range.

VIII.2.8 Thermogravimetric analysis

Thermogravimetric analysis results of the HA powder, during heating and cooling cycles, are presented in Figure VIII.5.

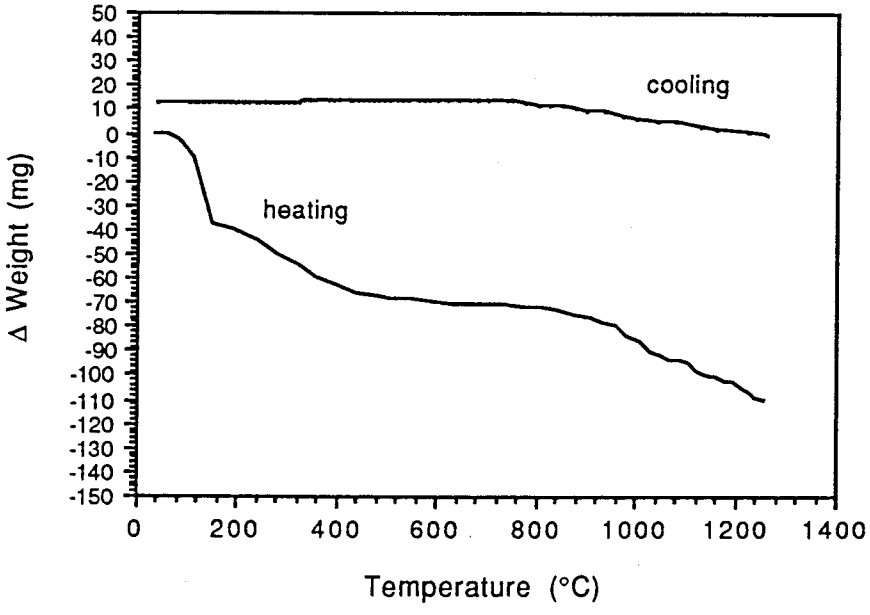

Figure VIII.5 Thermogravimetric analysis

Two zones can be seen on the heating cycle where the weight loss is high: between 100-400°C and above 850°C, approximately. A slight weight increase was detected on the cooling process, between 1260°C and 700°C, without any significant further weight variation until room temperature.

VIII.3 Sintered hydroxyapatite

VIII.3.1 Macroscopic observation

All samples showed a blue colouration after sintering. The blue colour was observed to become more intense with increasing sintering temperature and soaking time. For samples sintered at 1350°C for 3h, a very deep blue colour was found.

VIII.3.2 Shrinkage

Variation of shrinkage results with sintering temperature for both sintering times, is shown in Figure VIII.6.

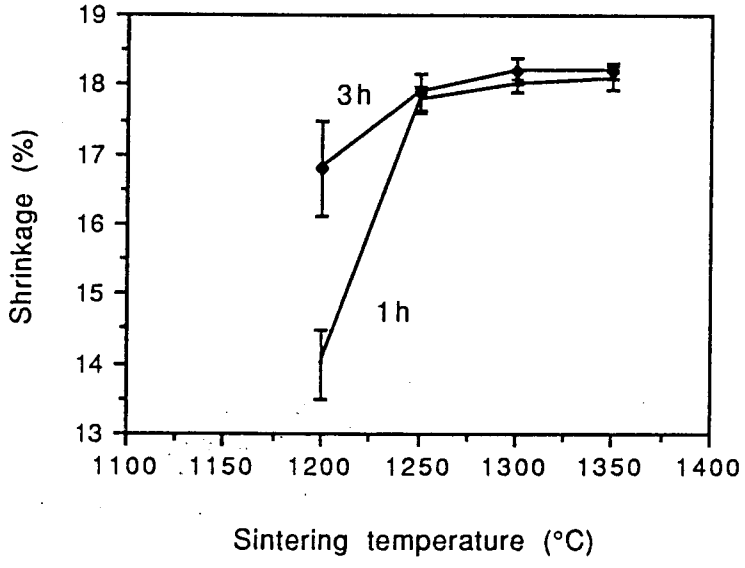

Figure VIII.6 Linear shrinkage of HA sintered compacts

A high shrinkage rate was found from 1200 to 1250°C, specially for samples sintered with 1h soaking time. Above this temperature the rate decreases sharply. A similar behaviour was detected for densification curves presented in the next section.

VIII.3.3 Density

Green compacts showed a theoretical relative density of 52% and 57% for uniaxially and isostatically pressed samples, respectively. Densification curves are shown in Figure VIII.7 for both sintering times.

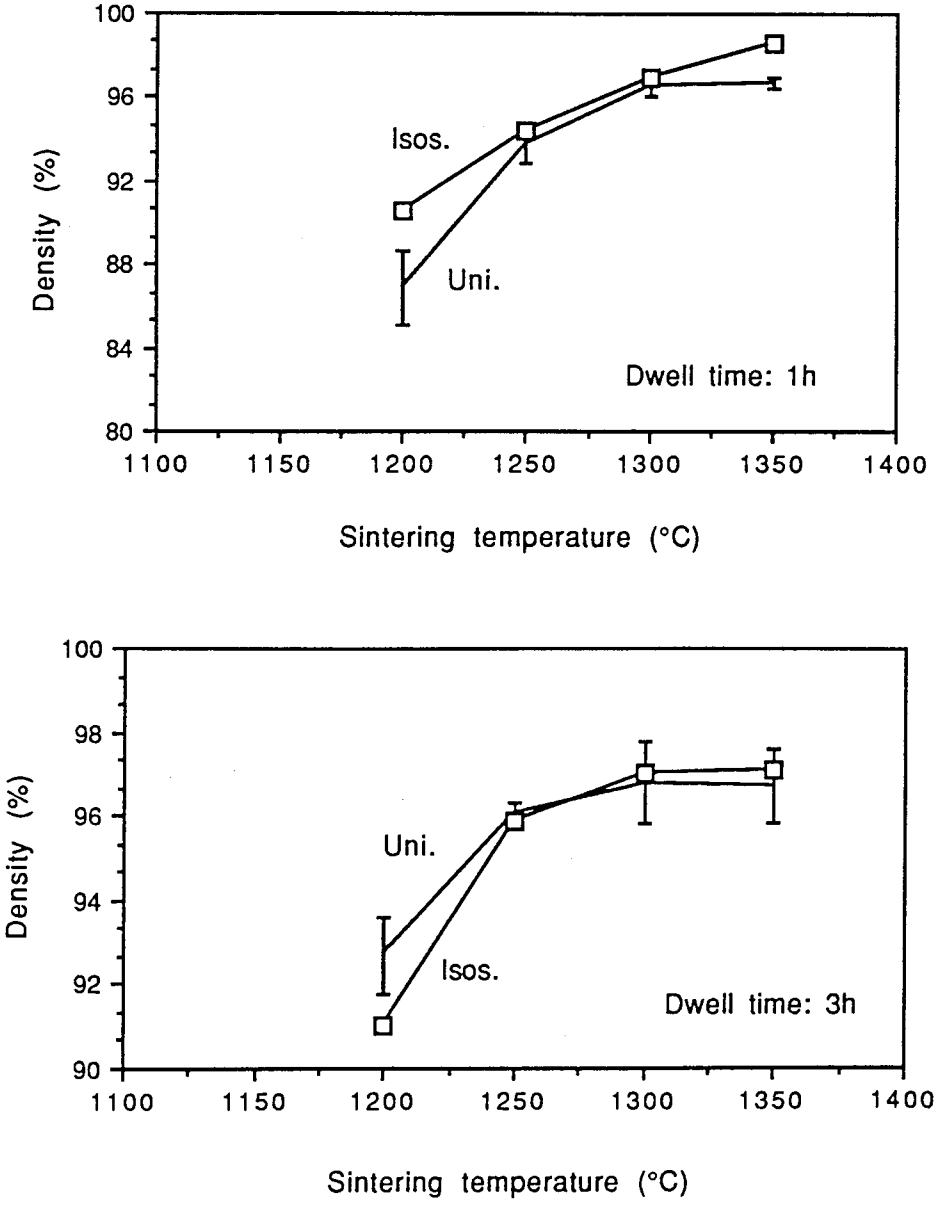

Figure VIII.7 Variation of density with sintering temperature for 1h and 3h dwell times

High density was achieved for samples sintered above 1250°C in both cases. After 1300°C no increase in density was observed for all compacts apart from the isostatically pressed sample, sintered at 1350°C for 1h. In addition to that, samples isostatically pressed showed no signs of improvement in terms of their theoretical relative density, compared with those uniaxially pressed when sintered above 1250°C for both dwell times.

VIII.3.4 X-ray diffraction

No mineralogical transformation was detected by X-ray diffraction, even after HA had been sintered at 1350°C for 3h, as it is shown in Figure VIII.8. Lattice parameter values for samples sintered for 1h are presented in Table VIII.4.

Table VIII.4 Lattice parameters for samples sintered for 1h

Temperature (°C)	Lattice parameters (Å)	
	a	c
1200	9.428	6.894
1250	9.423	6.897
1300	9.421	6.890
1350	9.422	6.898

Comparing these values with those of the starting powder, there was a tendency for lattice parameter 'a' to decrease and parameter 'c' to increase, with increasing sintering temperature, although this trend was not always maintained for two consecutive temperatures. FWHM and IW values are presented in Figures VIII.9 and VIII.10.

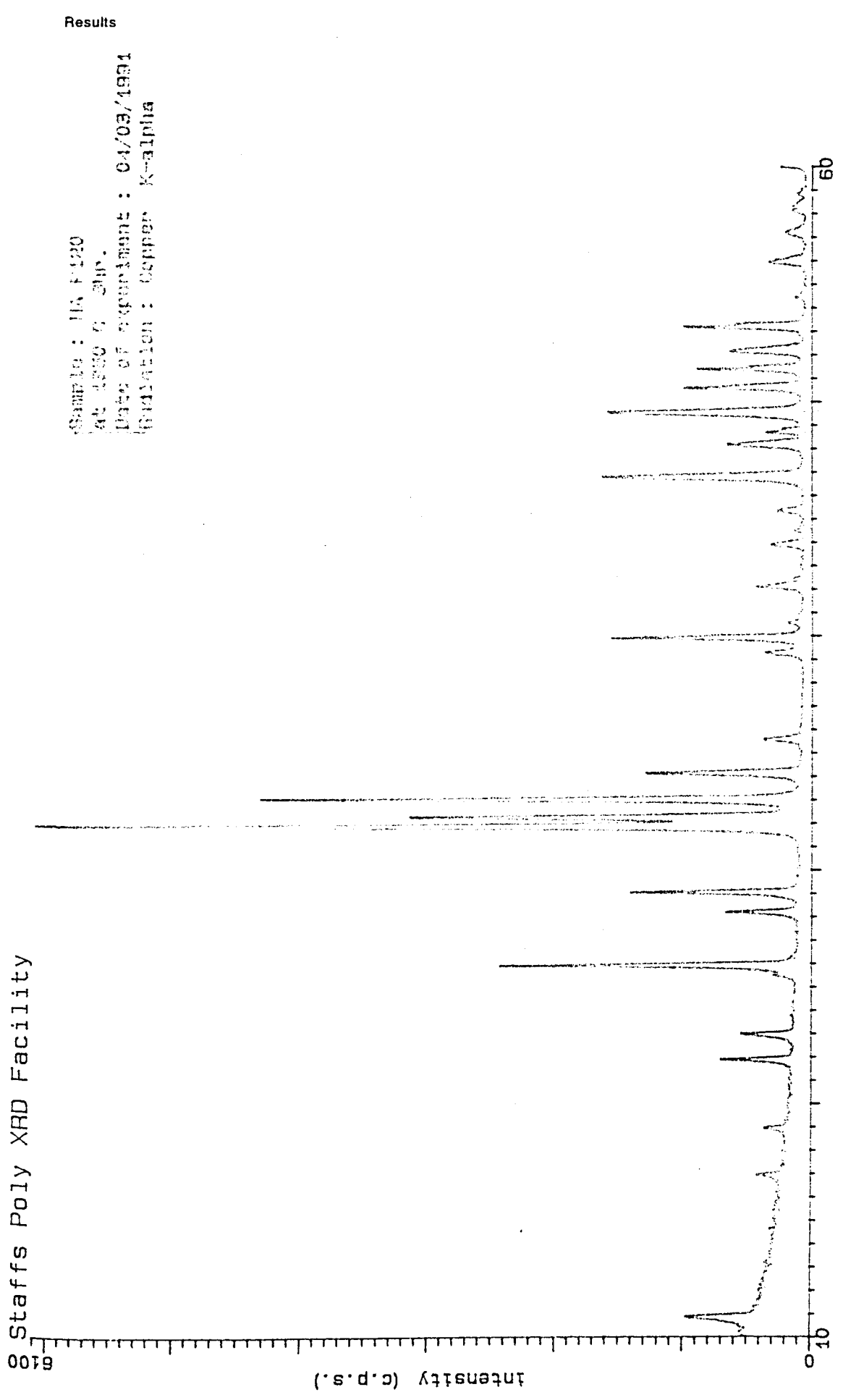

Figure VIII.8 X-ray diffraction for HA sintered at 1350 °C for 3h.

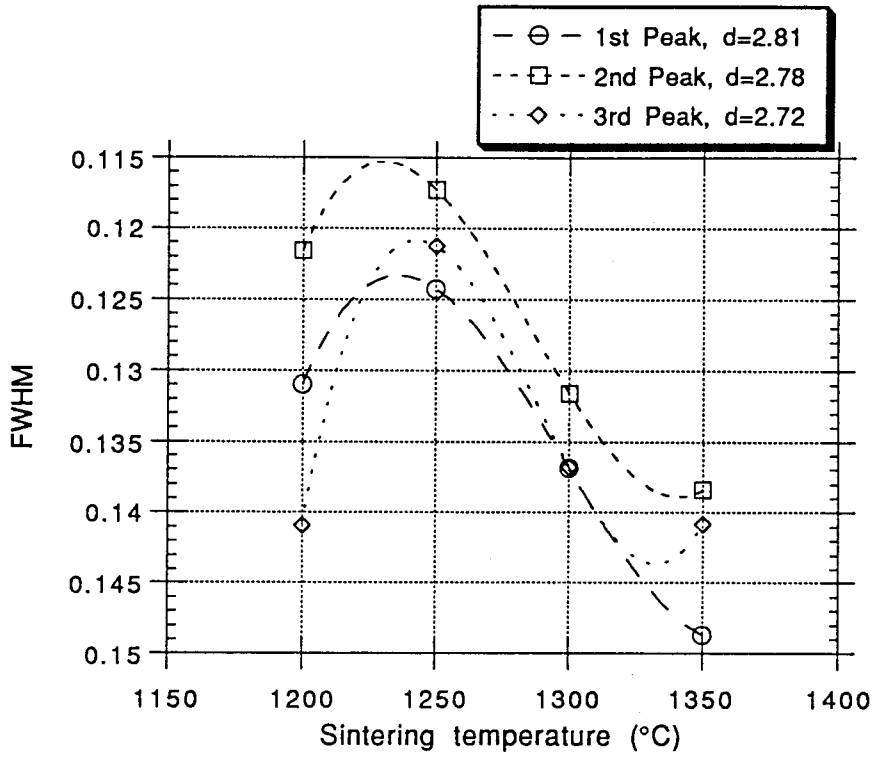

Figure VIII.9 FWHM (arbitrary scale) values for HA sintered compacts

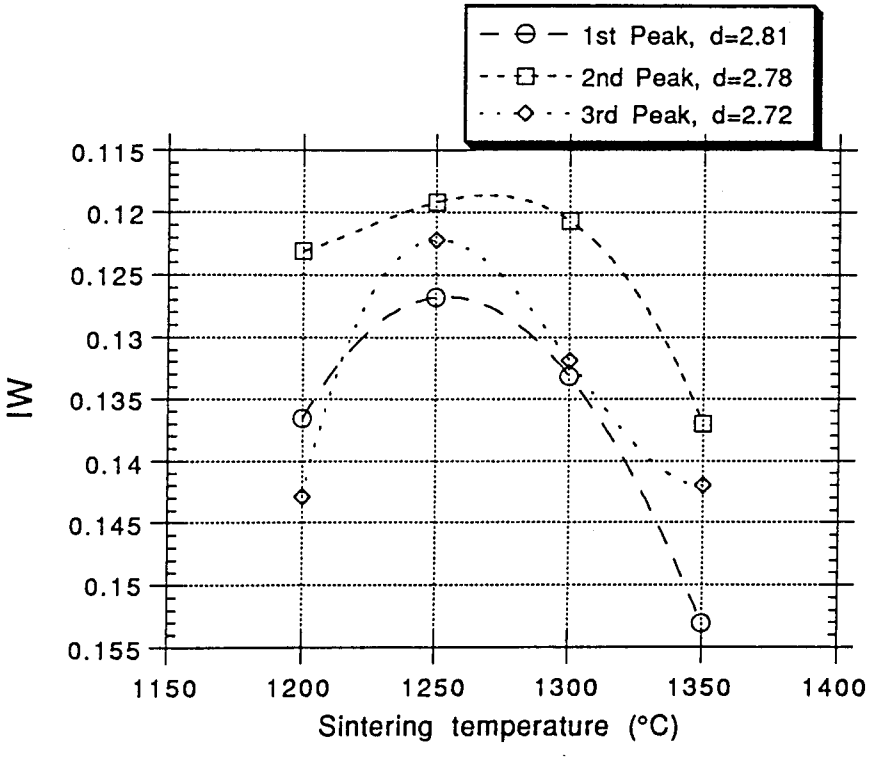

Figure VIII.10 IW values (arbitrary scale) for HA sintered compacts

Both curves exhibit the same behaviour: a decreasing value until 1250°C followed by an increase above that temperature. However, all FWHM and IW values are lower than those of HA, and therefore a significant narrowing of the peaks occurred.

VIII.3.5 Infra-red spectroscopy

The infra-red analysis results are shown in Figure VIII.11. The CO_3^{-2} band disappeared when HA was heated to 1200°C and above that temperature. The OH^- peak at 3590-3650 cm^{-1} was still present in all spectra but the small OH^- peak at 630 cm^{-1} disappeared after heating above 1200°C. The band at 3100-3600 cm^{-1}, associated with the presence of water, was also still present. It should be emphasised that the scan presented at each condition was the averaged mean of fifty scans.

VIII.3.6 Microstructure

HA sintered microstructures for all sintering temperatures used and both dwell times can be seen in Figure VIII.12 and VIII.13. High density was achieved after sintering above 1250°C for both dwell times. Porosity was usually concentrated on grain boundaries although some pores could also be detected inside the grains.

The increase in densification was followed by an increase in grain size and above 1300°C a large increase was detected. Grain size measurements are presented in Figure VIII.14.

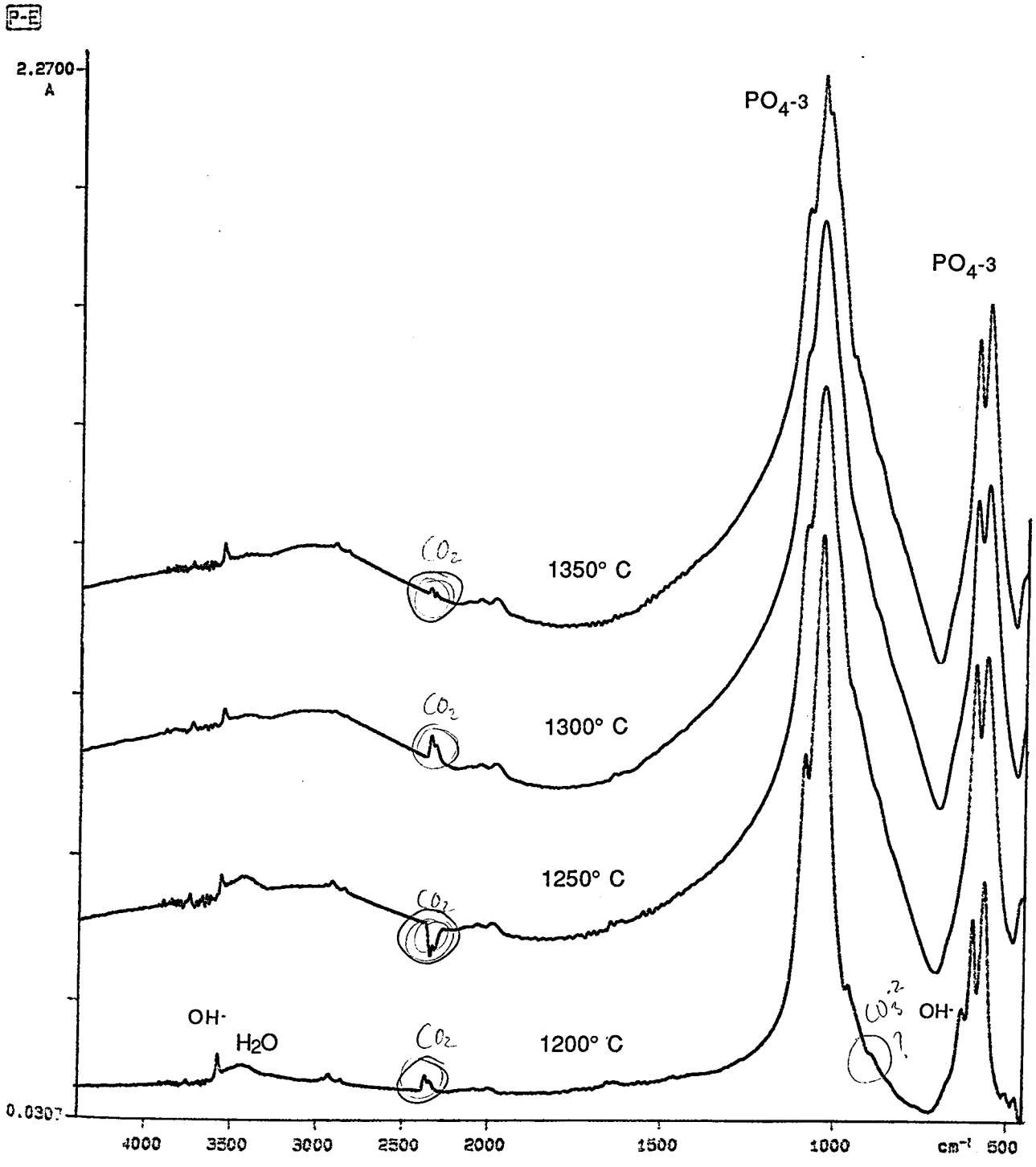

Figure VIII.11 Evolution of infra-red spectra of HA with sintering temperature

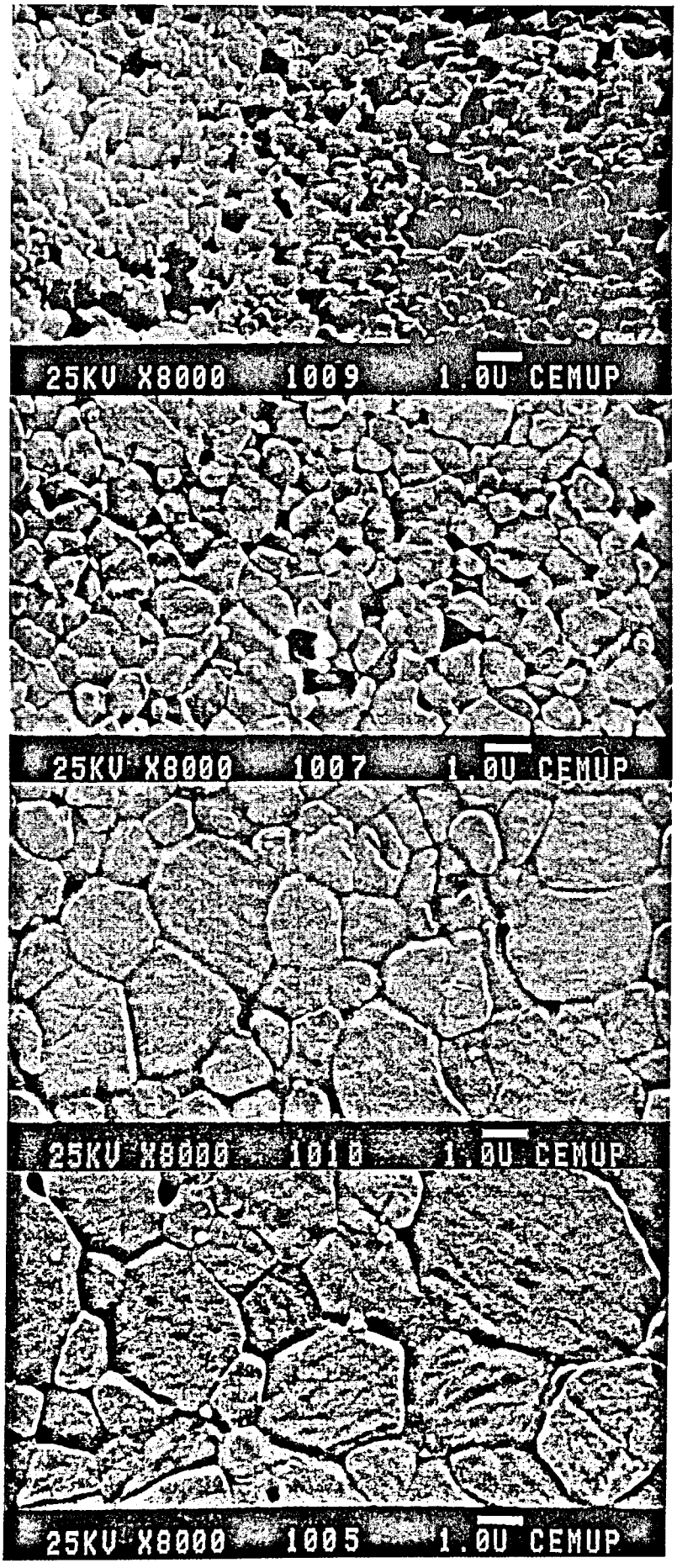

1200° C

1250° C

1300° C

1350° C

Figure VIII.12 Microstructures of HA compacts sintered for 1h

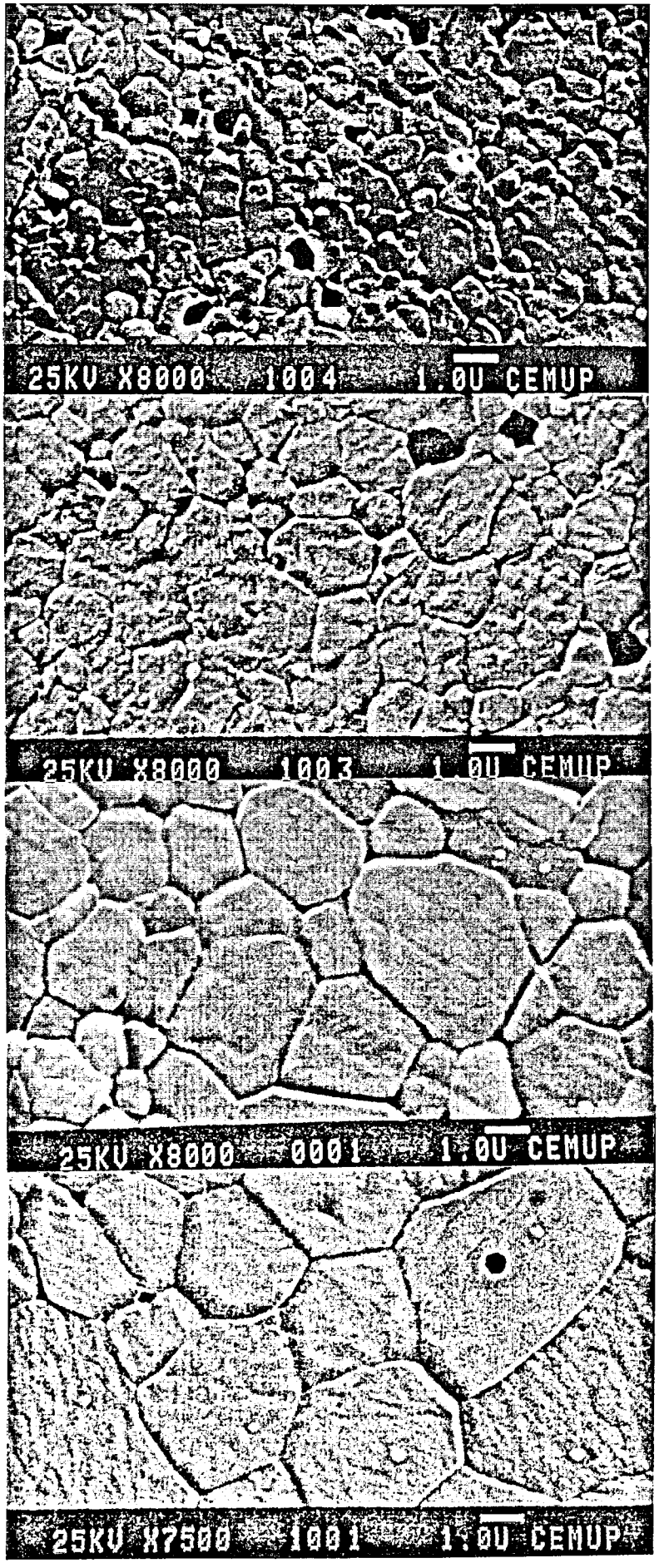

Figure VIII.13 Microstructures of HA compacts sintered for 3h

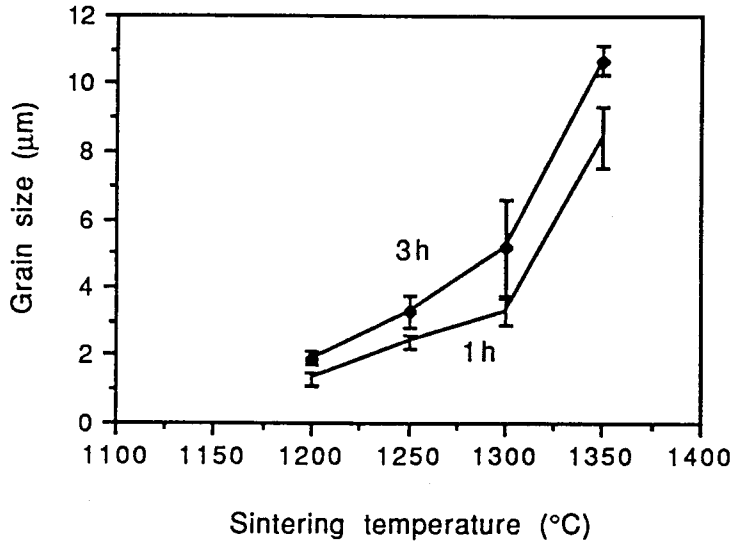

Figure VIII.14 Variation of mean grain size with sintering temperature

As expected, samples sintered for 3h showed a larger grain size than those sintered for 1h. A two stage curve was obtained for both sintering times: a slow increase in grain size below 1300°C followed by a rapid increase above that temperature. Observing Figure VIII.12 and VIII.13, a relatively wide variation in grain size may be noted in some cases, reflecting a different grain growth rate from one area to another.

VIII.3.7 Mechanical properties

VIII.3.7.1 Hardness

As it is presented in Figure VIII.15, hardness values increased with sintering temperature for both dwell times used, and the curves assumed a similar behaviour when compared to those related to the shrinkage and densification results. Likewise, after 1300°C no further significant increase in hardness was observed for both sintering times.

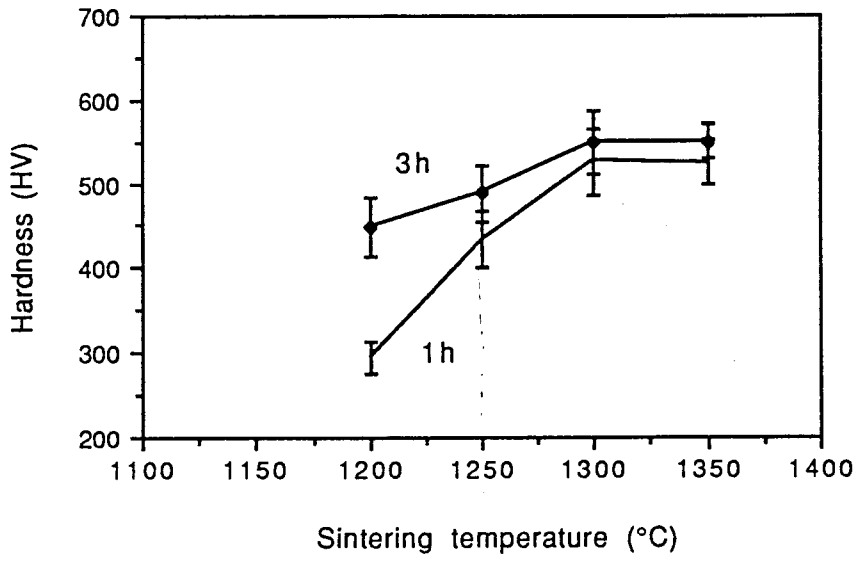

Figure VIII.15 Variation of hardness with sintering temperature

VIII.3.7.2 Biaxial bending strength

As it was previously referred for the densification and hardness curves, the use of a 3h dwell time brought no general improvement in terms of those properties. In fact, the 3h dwell time was even detrimental in terms of fracture toughness results for samples sintered above 1250°C, as it will be shown in the next section. Therefore, it was decided not to use the 3h dwell time. Biaxial bending strength tests were then only applied to HA and HA-glass composites sintered for 1h. On the other hand, the use of a short sintering time would minimise phase changes, when HA was sintered in the presence of a chemically related liquid phosphate phase.

Concentric-ring test results showed a slight increase in biaxial bending strength with sintering temperature. Young's modulus increased from 1200 to 1250°C and then kept constant above that temperature. Both results are presented in Table VIII.5.

Table VIII.5 Variation of biaxial bending strength and Young's modulus with sintering temperature

Temperature (°C)	Strength (MPa)	Young's modulus (GPa)
1200	24±4	59±7
1250	26±5	87±10
1300	28±7	88±8
1350	28±7	89±9

Figure VIII.16 presents the Weibull modulus results.

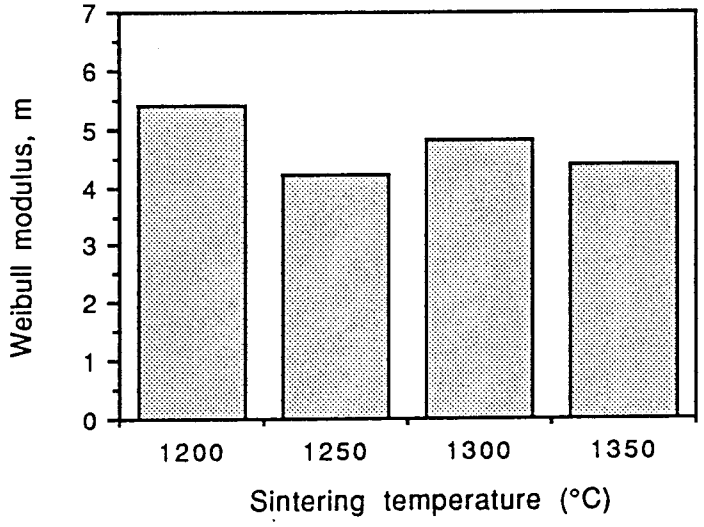

Figure VIII.16 Variation of Weibull modulus with sintering temperature

Low Weibull modulus values were found for sintered HA, 4.2-5.4, indicating a large variability in the strength results (the lower m the higher variability of strength). There was no general trend in Weibull modulus versus sintering temperature.

VIII.3.7.3 Fracture toughness

VIII.3.7.3.1 Indentation

Fracture toughness determinations required the use of the Young's

modulus/hardness parameter, which is a material characteristic. This parameter was calculated according to the values evaluated through the hardness and biaxial bending tests. Samples sintered at 1200°C were not considered because they showed relatively high porosity for this test and the indent produced would not have been representative. Fracture toughness results showed an increase up to a peak at 1300°C for both dwell times, as may be seen in Figure VIII.17.

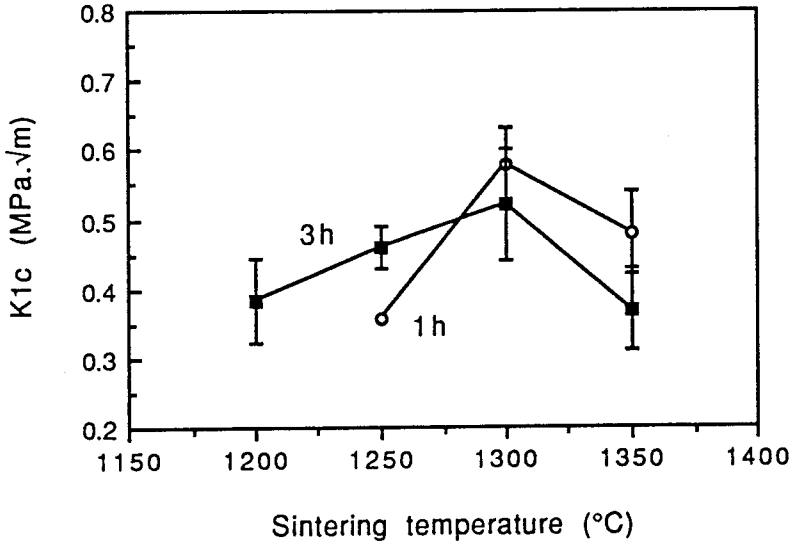

Figure VIII.17 Variation of K_{1c} with sintering temperature, using the indentation technique

Above that temperature, a marked decrease occurred, specially for samples sintered for 3h. Samples sintered at 1300 and 1350°C for 1h showed higher K_{1c} values than those sintered for 3h. The highest K_{1c} recorded was 0.6 MPa $m^{1/2}$.

VIII.3.7.3.2 Strength-indentation

Fracture toughness results, using the indentation-strength process, are shown in Figure VIII.18.

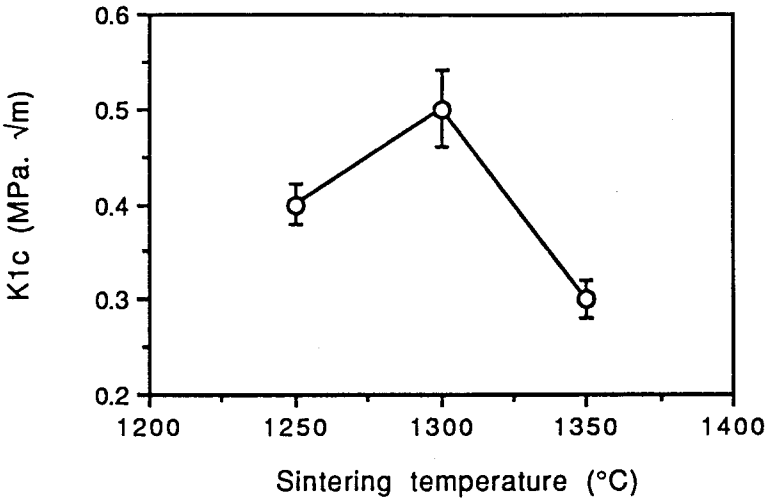

Figure VIII.18 Variation of K1c with sintering temperature, using the strength-indentation technique

The highest value attained was for samples sintered at 1300°C. A marked decrease was found for samples sintered at 1350°C. This behaviour was similar to that of the previous indentation method, although the results were slightly lower at all sintering temperatures. Strength values, for pre-cracked and uncracked samples, were compared, and a decrease of about 20-30% was found, which ensures that the precursor of the fracture for the pre-cracked samples was the Vickers indent.

VIII.3.7.3.3 Double torsion

A K_{1c}=0.7± 0.12 MPa $m^{1/2}$ value was obtained for samples sintered at 1300°C. This value is the averaged mean of 5 tests. However, some difficulties were found in performing the test. In some specimens, the crack followed a curved path although a groove had been made to ensure that the crack grew in a straight line. These results were not considered to calculate K_{1c}.

VIII.4 Hydroxyapatite-glass composites

VIII.4.1 Glass characterisation

In order to ensure a standard HA-glass composite fabrication process, chemical composition and particle size measurements of the glasses produced were performed. All chemical reactions for glass fabrication assumed a complete decomposition of reagents, therefore this fact should be assessed. Particle size measurement was also an important factor, as glasses were to be mixed with HA. Fine particles were then desirable to obtain a good glass dispersion in HA.

VIII.4.1.1 Particle size analysis

After 24h milling in a porcelain ball mill pot, particle size distribution was analysed for the 4 glasses. These results are shown in Figure VIII.19.

All particle size distribution showed an almost monomodal pattern. $D_{O.5}$ values varied between 6.08-9.92μm, although some large particles were also found with $D_{0.9}$=49.8-66.4μm. The HA powder used was much finer, as it was presented in Figure VIII.4, with $D_{0.5}$=1.58μm and $D_{0.9}$=6.50μm. However, the glasses were going to be wet-milled and mixed with HA powder for a further 24h, therefore a reduction in particle size was expected. Particle size analysis was then carried out, as will be presented afterwards. Ultimately, glass dispersion in the HA powder could only be examined by microstructural analysis after sintering.

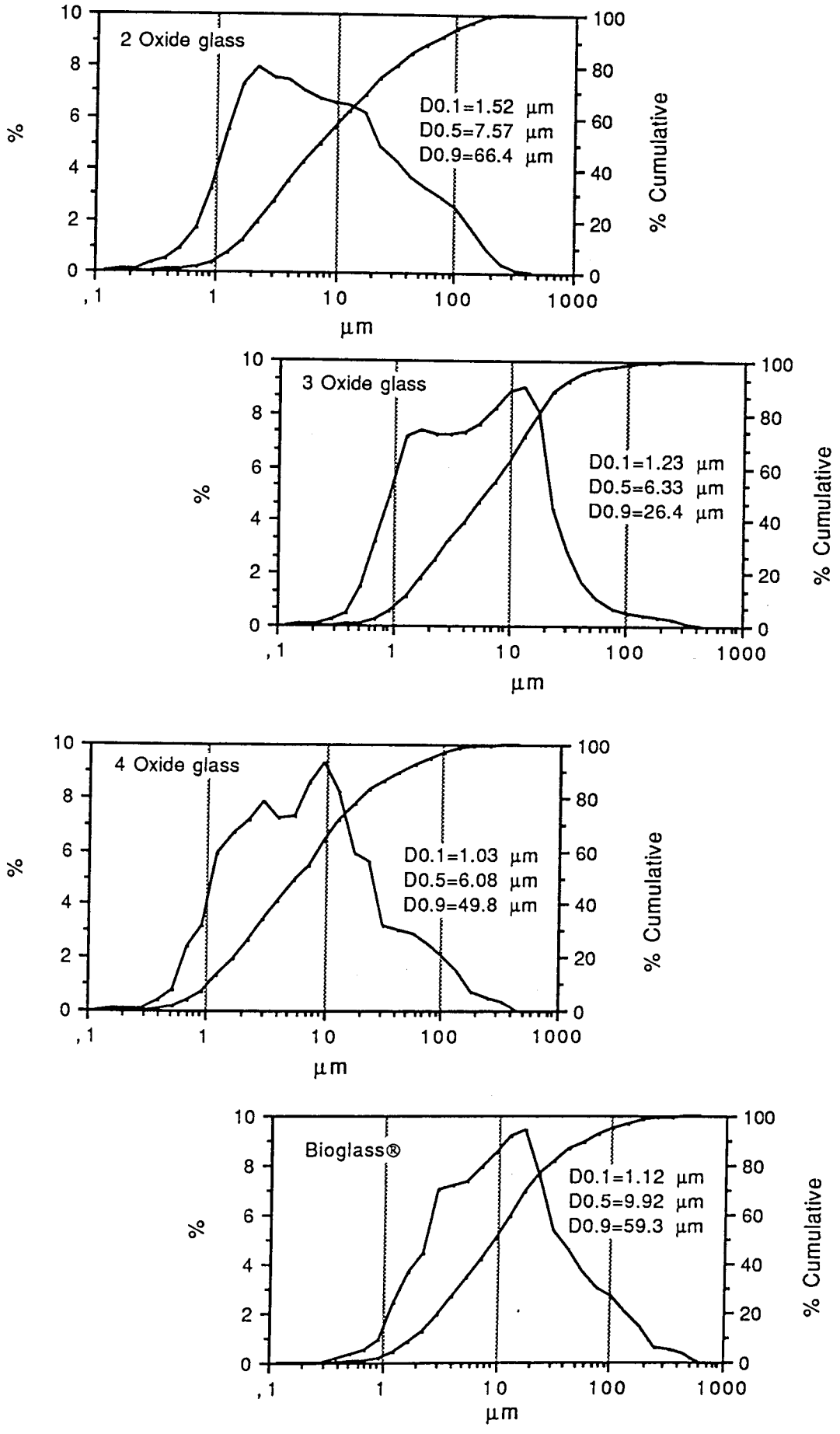

Figure VIII.18 Particle size distribution for the glasses after 24 milling

VIII.4.1.2 Chemical composition

Chemical composition, already converted to the oxide, of the phosphate based glasses are shown in Table VIII.6.

Table VIII.6 Chemical composition of phosphate based glasses (mol%)

Material	CaO	P_2O_5	Na_2O	Al_2O_3
2 Oxide gl.	54.53	45.47	-	-
3 Oxide gl	28.21	44.77	27.02	-
4 Oxide gl.	10.14	62.86	10.06	16.94

The 45S5-Bioglass® was also analysed and its chemical composition compared with its standard values, in wt%: SiO_2=45.02 (44.97), Na_2O=24.37 (24.55), P_2O_5=6.2 (5.99) CaO=24.41 (24.49), with standard values in brackets. All phosphate based glasses showed a lower percentage of P_2O_5 than the values theoretically calculated, probably due to the lost during degassing.

VIII.4.2 Composite characterisation

VIII.4.2.1 Particle size analysis

Before drying and pressing operations, particle size analysis was performed on HA-glass powders after being wet-mixed in methanol for 24h and sieved to -75μm. The HA batch was also analysed in terms of its particle size distribution. Figure VIII.20 shows the particle size profiles obtained for HA-2 Oxide glass powder for 5% addition. All powders showed identical particle size distribution profiles and therefore the results were not included.

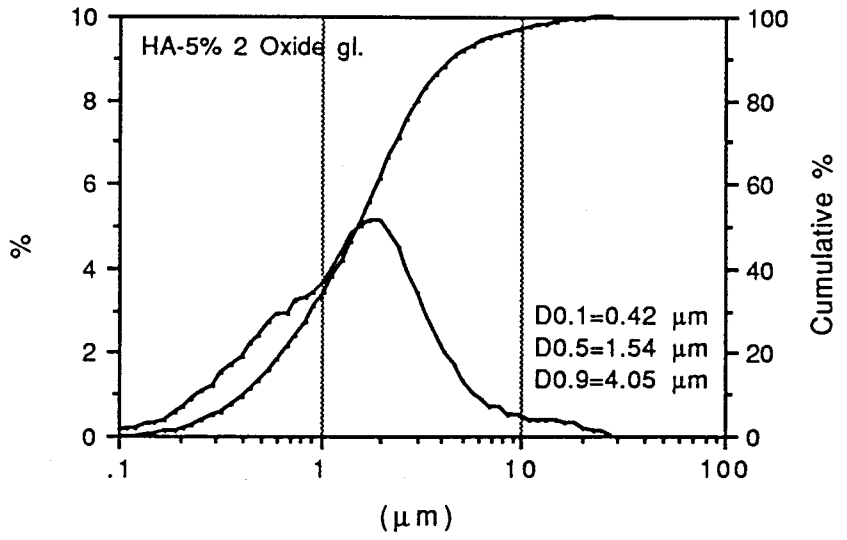

Figure VIII.20 Particle size distribution for HA-2 Oxide glass powder

Comparing this particle size pattern with that for HA, one verifies that the distribution is now monomodal and the larger particles disappeared leading to a decrease in $D_{0.9}$ value from 6.5 to 4.05µm. $D_{0.1}$ and $D_{0.5}$ values remained almost unchanged (0.41 to 0.42µm and 1.58 to 1.54µm). A further reduction in glass particle size seemed to have also occurred.

VIII.4.2.2 Density

Figures VIII.21-22 show the density results for HA-glass composites.

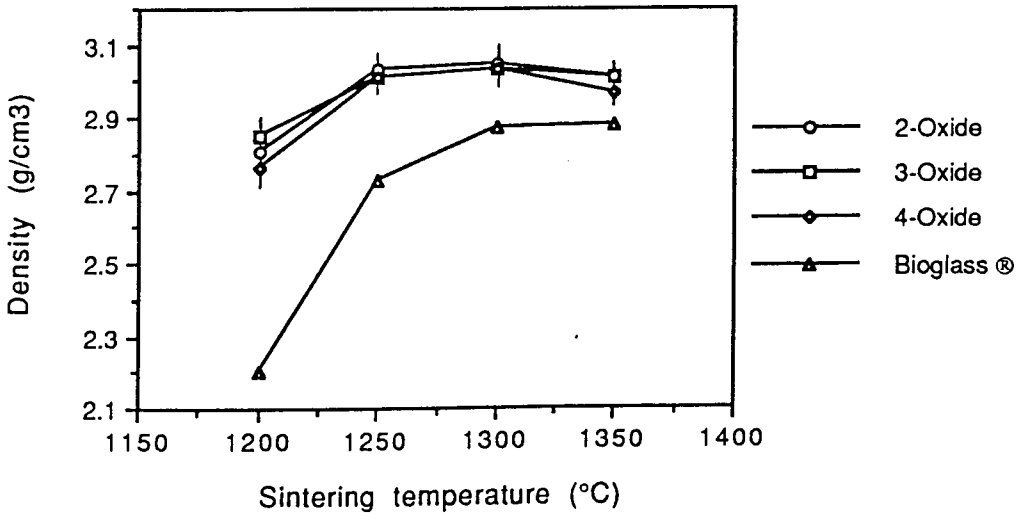

Figure VIII.21 Density results for HA-2.5 wt% glass composites

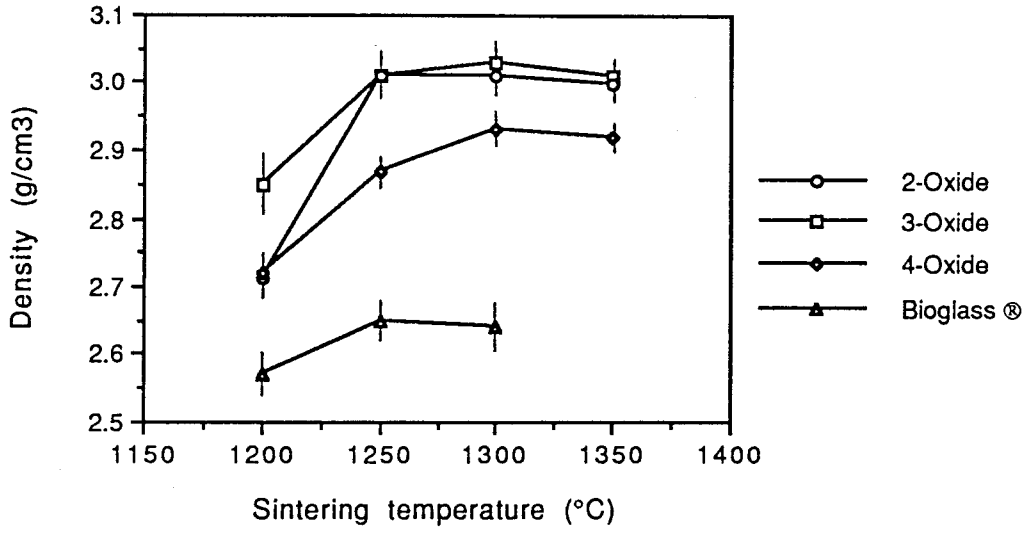

Figure VIII.22 Density results for HA-5 wt% glass composites

The densification process for the HA-phosphate glass composites seems to follow the same general behaviour of that for HA, at the same sintering conditions. Highly dense composites could be obtained above 1250°C. These results could be confirmed by light and scanning electron microscopy, where virtually no residual porosity was found. According to the X-ray analysis results which will be presented in the next section, the incorporation of a glassy phase during the sintering process of HA led to the formation of some β and α-TCP phases in the microstructures of HA-glass composites. Both have lower theoretical densities than HA, 3.07 (JCPDS 9-169) and 2.87 (JCPDS 9-348), respectively.

HA-Bioglass® composites showed significantly lower density than the HA-phosphate based glasses at all sintering temperatures. Some HA-5wt% 4 Oxide and all HA-5wt% Bioglass® samples sintered at 1350°C fractured during cooling.

VIII.4.2.3 X-ray diffraction

Figure VIII.23 shows the x-ray diffraction results for the HA-2 Oxide glass for 2.5% addition. Below 1250°C only β-TCP could be detected besides the HA matrix, and above 1300°C α-TCP is the main TCP phase present in the microstructure. At 1350°C, the proportions of HA and β-TCP are quite similar. This tendency was followed by all other HA-2.5% phosphate glass composites, although relatively smaller quantities of HA remained, particularly for samples sintered above 1250°C. Table VIII.7 shows relative phase amounts for HA-2.5% phosphate glass composites.

Table VIII.7 Phase contents in HA-2.5% phosphate glass composites

	1250°C	1300°C	1350°C
	HA/β-TCP/α-TCP	HA/β-TCP/α-TCP	HA/β-TCP/α-TCP
HA-2 Oxide	65/35/0	55/20/25	45/10/45
HA-3 Oxide	65/35/0	45/15/40	35/0/65
HA-4 Oxide	65/35/0	40/15/45	15/15/70

With 5% glass addition, the HA-2 Oxide glass composite showed the same trend previously reported in terms of phase transformations, although higher proportions of TCP were found at each sintering temperature. At 1250°C, a small amount of α-TCP was already detected. For the HA-3 Oxide glass and HA-4 Oxide glass composites, HA became much less stable and relatively higher proportions of β-TCP and α-TCP were found in the microstructure. Figure VIII.24 shows the x-ray diffraction analysis for HA-2 Oxide and HA-3 Oxide sintered at 1250°C.

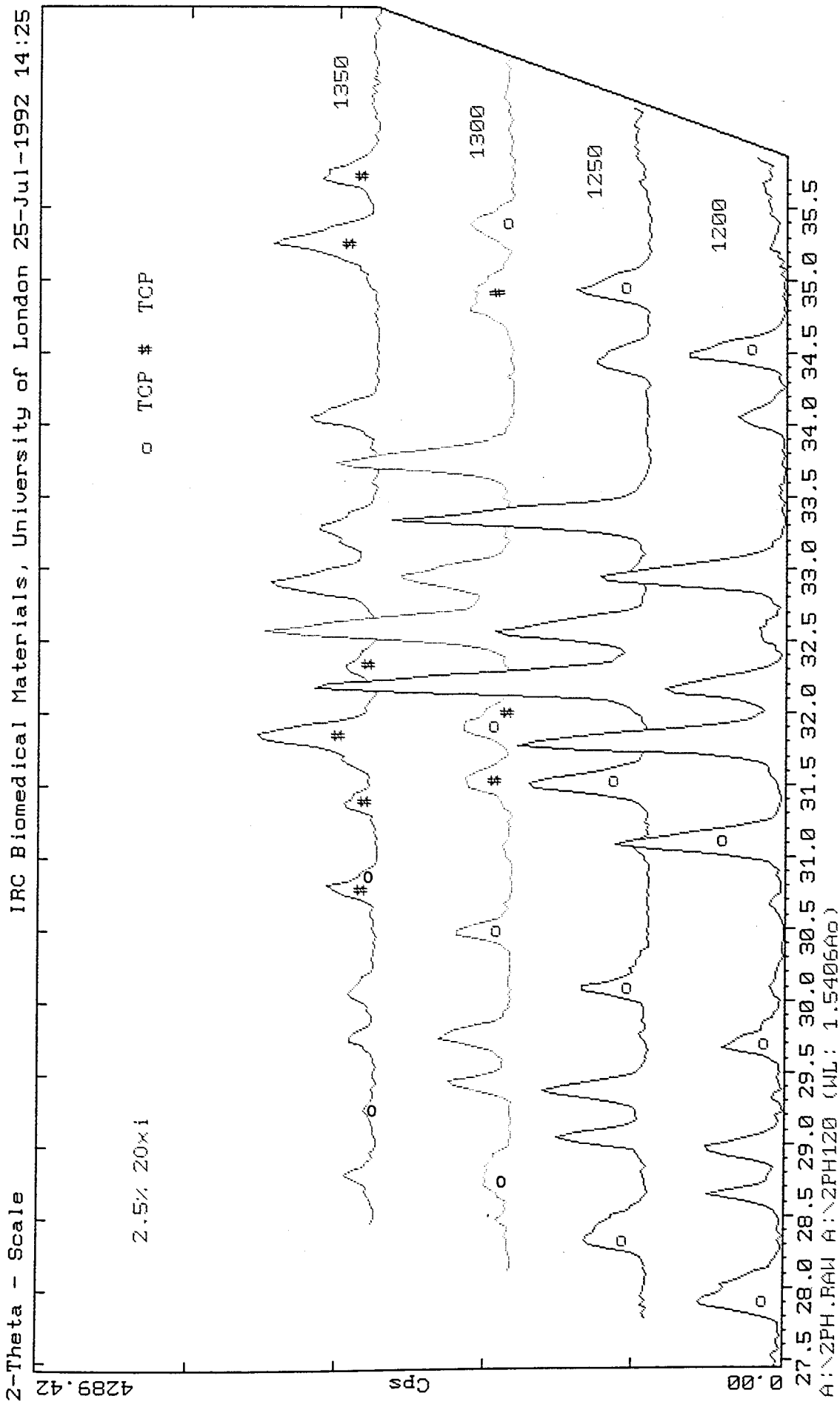

Figure VIII.23 X-ray diffraction analysis for HA-2.5 %wt 2 Oxide glass composites

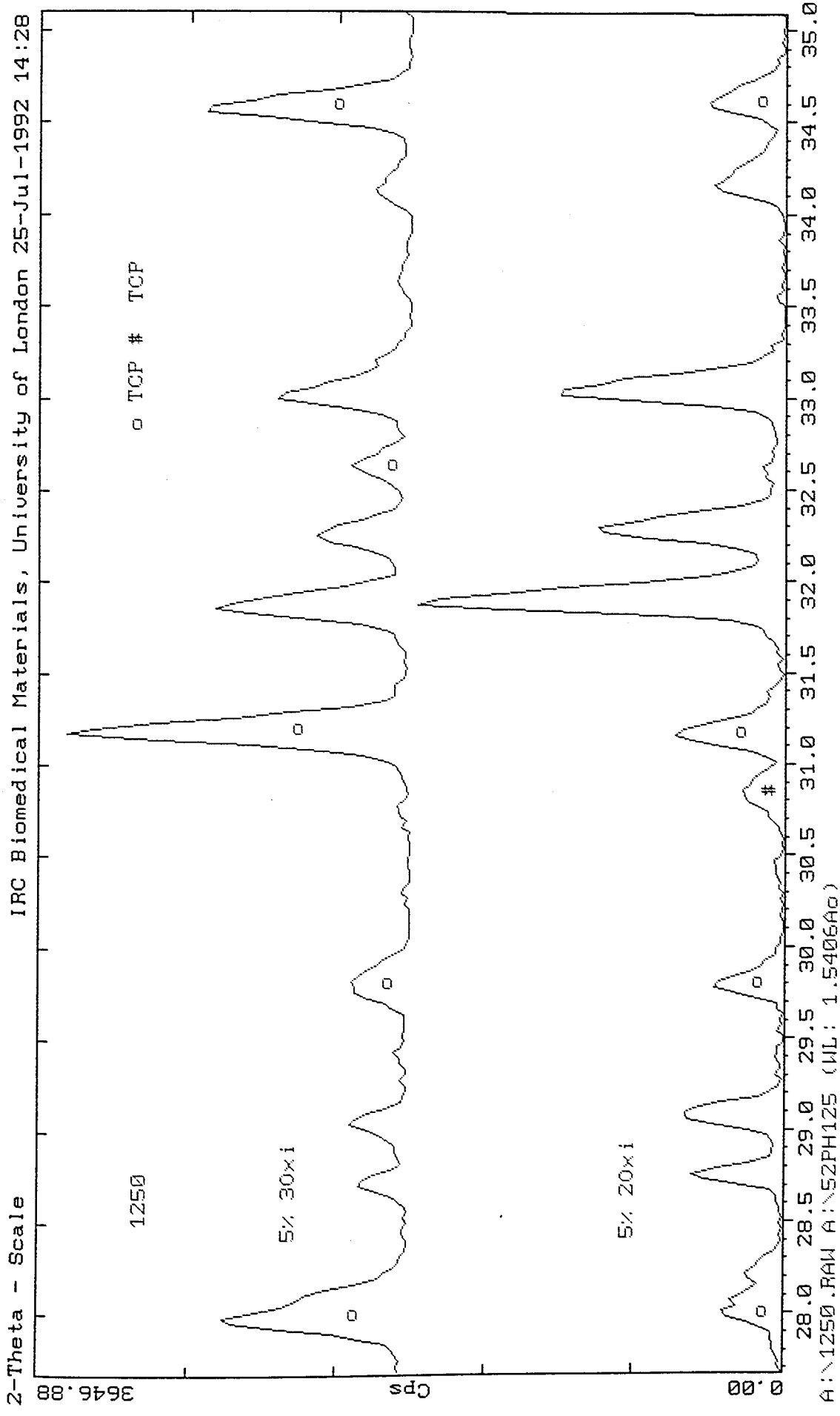

Figure VIII.24 X-ray diffraction analysis for HA-5 %wt 2 Oxide glass and 5 %wt 3 Oxide glass composites, sintered at 1250 °C

For HA-Bioglass® composites, calcium phosphate-silicate, $Ca_5(PO_4)2SiO_4$, was found at all sintering temperatures, besides β and α-TCP. The calcium phosphate silicate increased with the sintering temperature and the amount of glass added. Above 1300°C, only α-TCP was detected, for both 2.5 and 5% additions. For 5 wt% glass addition, considerable transformation to calcium phosphate silicate and α-TCP occurred at 1350°C, as may be seen in Figure VIII.25.

VIII.4.2.4 Microstructure

Samples were analysed using light microscopy and scanning electron microscopy after chemical etching with acetic acid. A good glass dispersion (second phase) in the HA matrix was achieved for all phosphate glasses, particularly for samples sintered above 1200°C. A strong chemical bond seems to exist as no gaps between phases were detected. Virtually no porosity was found in the composites sintered above 1250°C. The amount of second phase present in the microstructure increased with sintering temperatures and with the quantity of glass added. Figure VIII.26 shows the microstructure of these composites, using 2.5 wt% addition. For HA-Bioglass® composites residual porosity was found.

Phase identification was performed using scanning electron microscopy equipped with energy dispersive spectroscopy, after chemical etching. Ca/P ratios were qualitatively determined for HA 3 Oxide glass, as it is shown in the spectrum of Figure VIII.27. Na ions kept concentrated in the TCP phase and were not found in the HA matrix spectrum. The same occurred for Al and Na ions in the HA-4 Oxide glass composite.

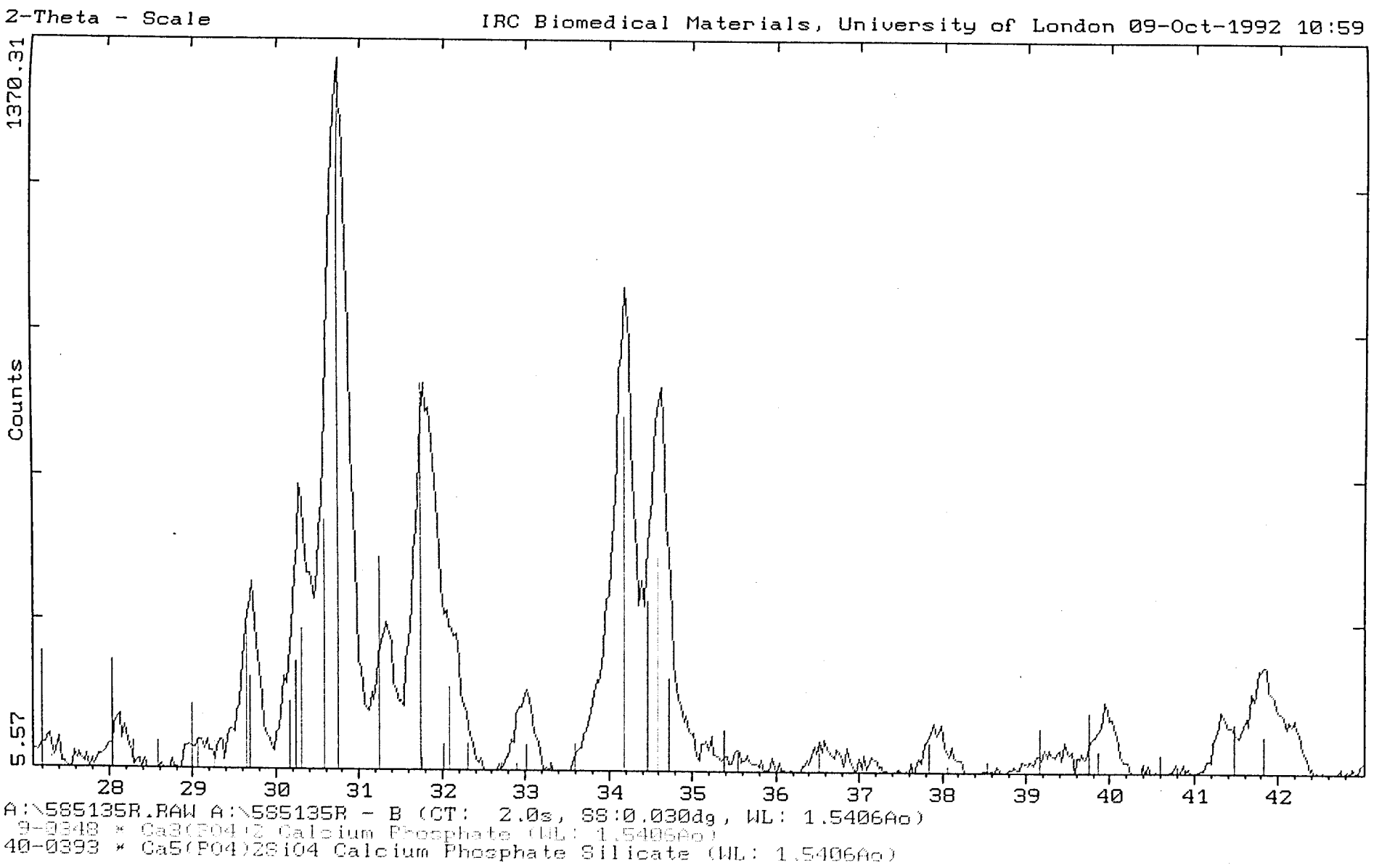

Figure VIII.25 X-ray diffraction analysis for HA-5 %wt Bioglass® composites, sintered at 1350 °C

HA-2 Oxide glass

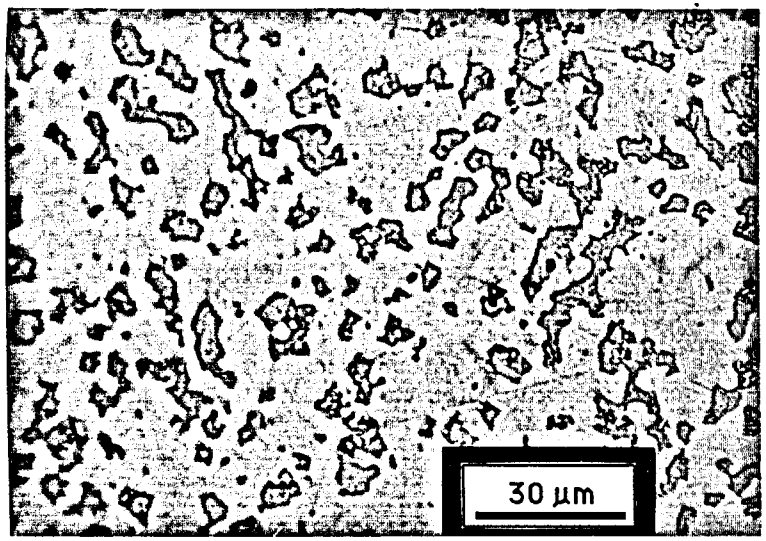

HA-3 Oxide glass

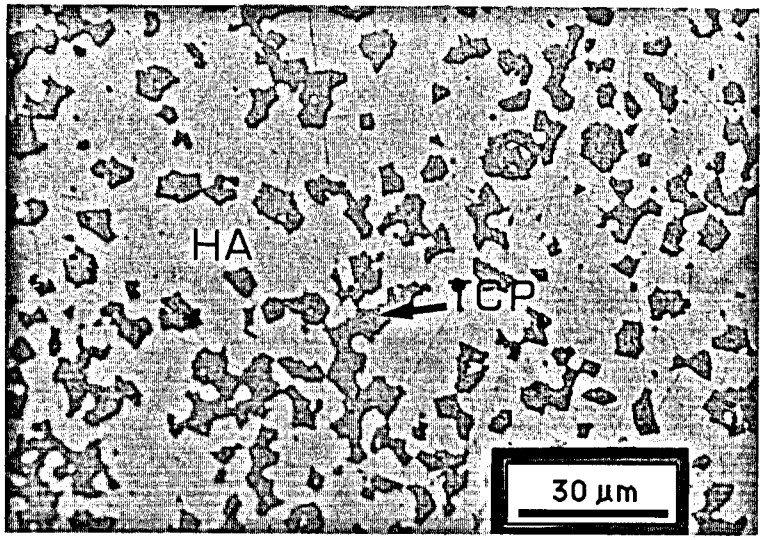

HA-4 Oxide glass

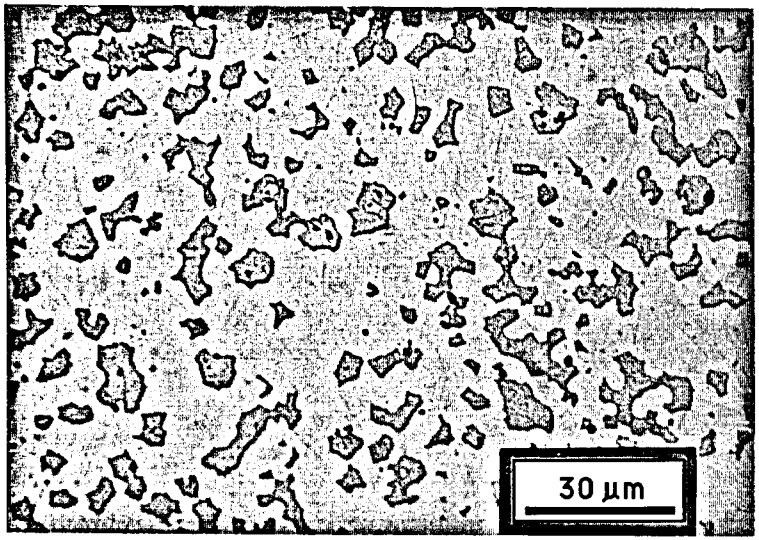

HA-Bioglass®

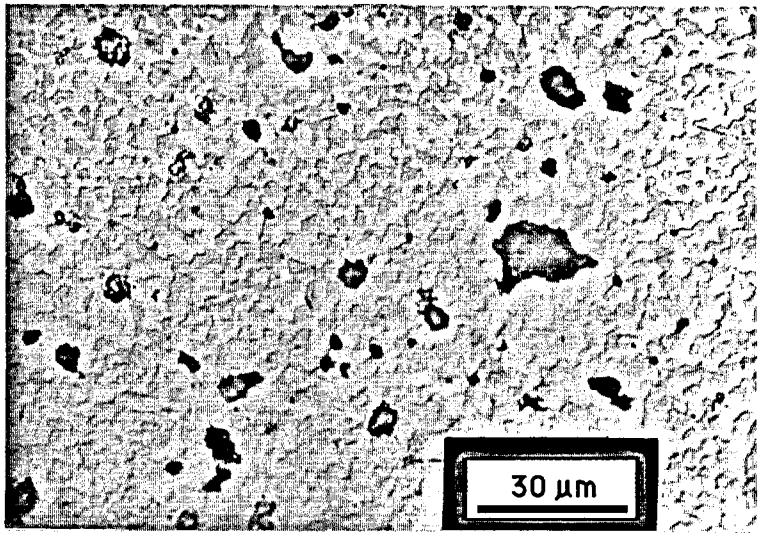

Figure VIII.26 Microstructure of HA-2.5% wt composites sintered at 1250 °C. As indicated, dark areas correspond to TCP and white ones to HA. Pores were observed for HA-Bioglass® composite

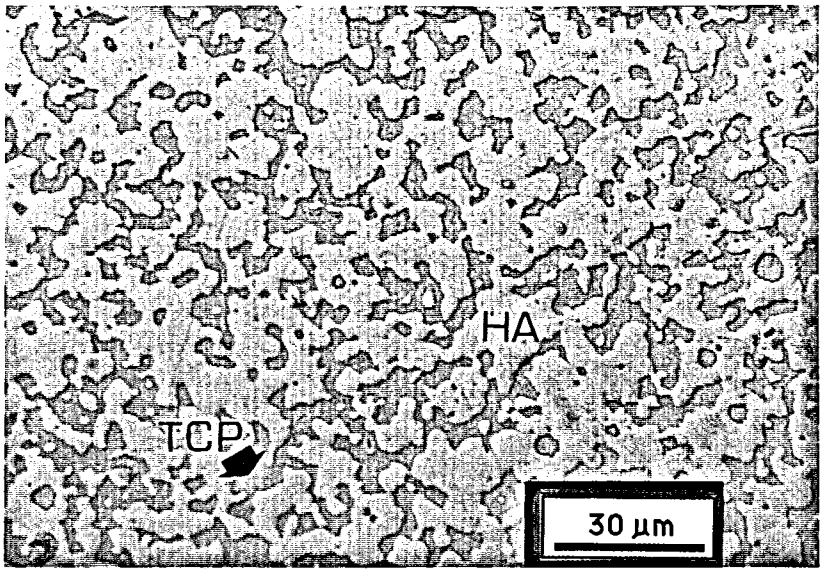

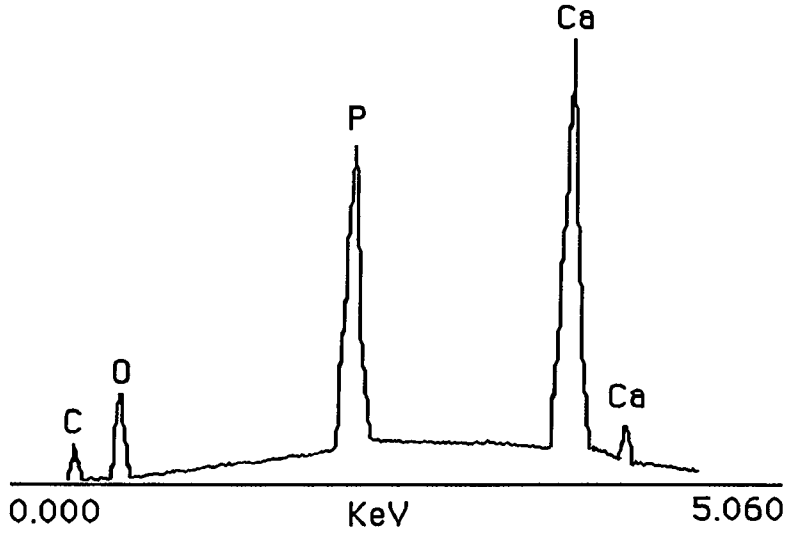

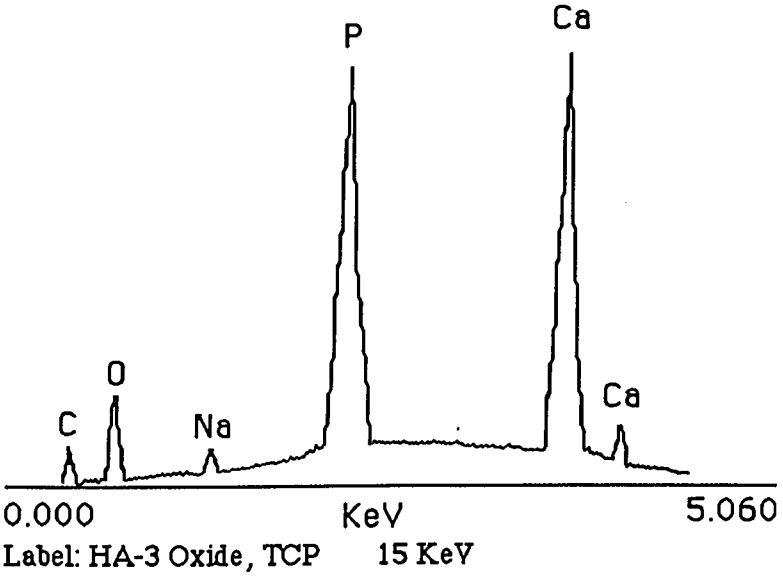

Figure VIII.27 Microstructure of HA-2.5% wt 3 Oxide composite sintered at 1300°C. Energy dispersive spectroscopy from selected HA and TCP areas indicated that Na kept concentrated on the TCP phase

For 5% wt phosphate glass additions, no discontinuities between phases were also detected and higher proportions of TCP were found in the microstructure. As indicated in the previous section, the amount of TCP depended on the glass composition. The 3 and 4 Oxide glasses had a larger detrimental effect on the stability of HA when compared to 2 Oxide glass, leading to higher proportions of TCP. Figure VIII.28 presents the microstructure of HA-2 Oxide glass and HA-3 Oxide glass sintered at 1250 °C for 5% wt addition.

For HA-5% wt Bioglass® composites, significant residual porosity was detected, comparing to what was observed for the HA-phosphate based glasses, which is in accordance with the density results. Cracking occurred for samples sintered above 1250°C. Calcium phosphate silicate was found next to pores by using energy spectroscopy microscopy, suggesting that it was the precursor for cracking developement. Figure VIII.29 shows the microstructure of HA-Bioglass® sintered at 1350°C.

In order to carry out grain size measurements, samples were chemically etched with a 10% citric acid solution for 3-4 min at room temperature to reveal grain boundaries. This etching solution dissolved the major part of the TCP structures, specially α–TCP. Measurements were made using the method described in V.3.6. Grain size increased slightly up to 1300°C, but above this temperature a much steeper increase rate was found, as may be seen in Figures VIII.30-31. This trend was also detected for HA sintered compacts (see Figure VIII.14). Comparing both values, HA-glass composites exhibit much lower grain size values than HA at the same sintering conditions.

HA-2 Oxide glass

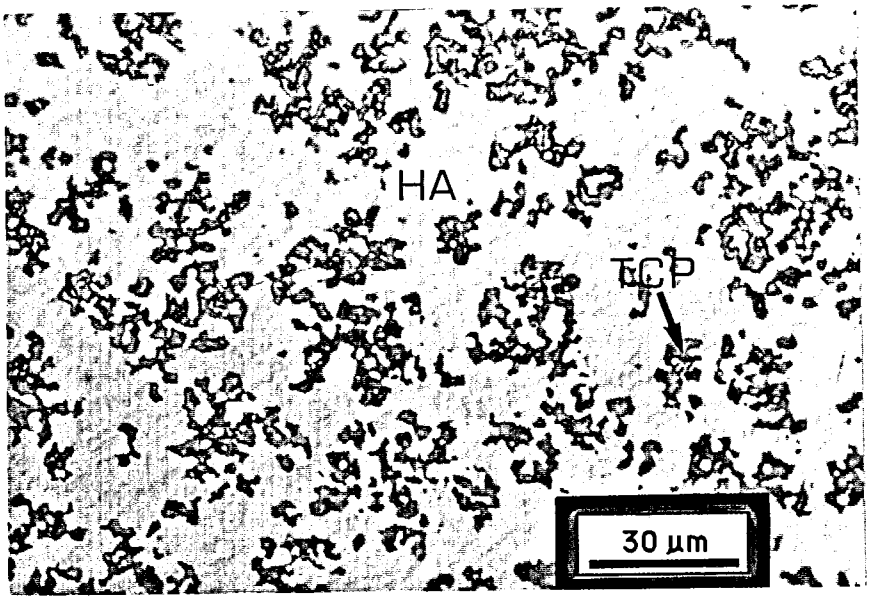

HA-3 Oxide glass

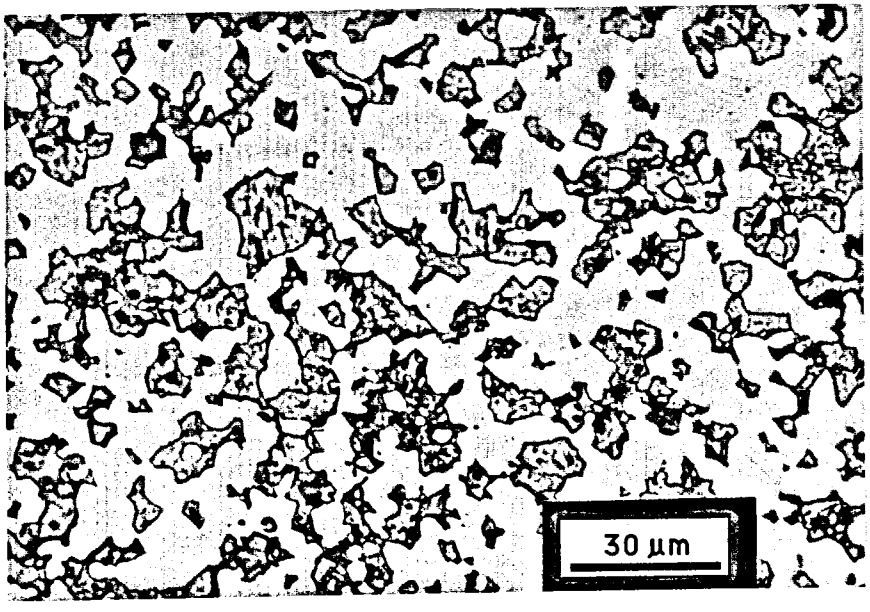

Figure VIII.28 Higher proportion of TCP was found in the microstructure of HA-3 Oxide glass than in HA-3 Oxide glass composite (5% wt addition). Samples were sintered at 1250°C

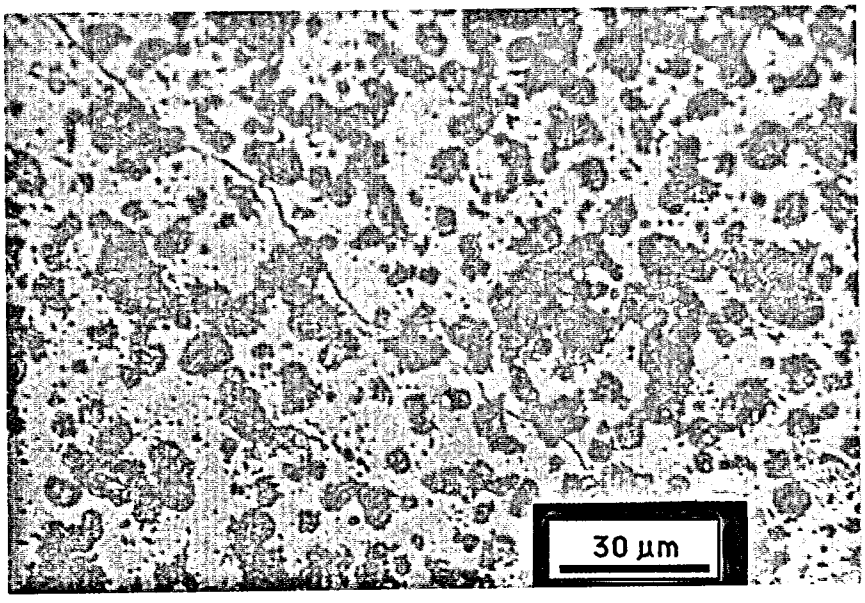

Figure VIII.29 High porosity and cracking in the microstructure of HA-5% wt Bioglass® composites sintered at 1350°C

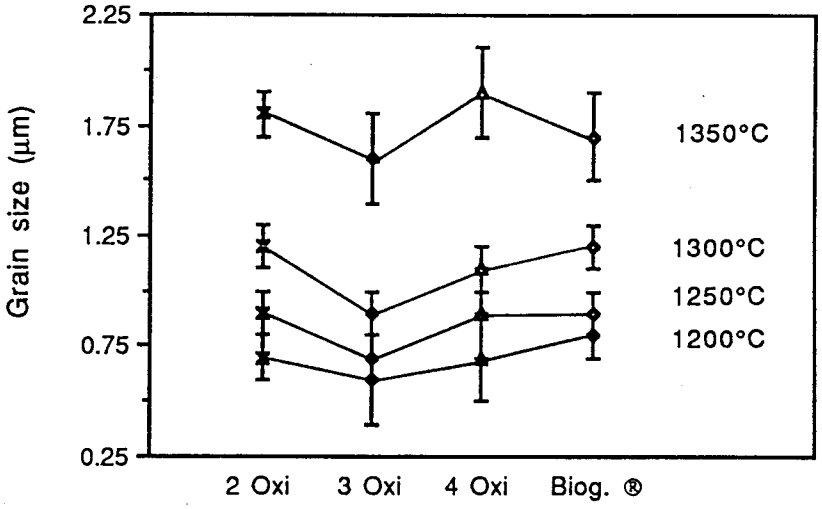

Figure VIII.30 Variation of grain size with sintering temperature for HA-2.5wt% glass composites

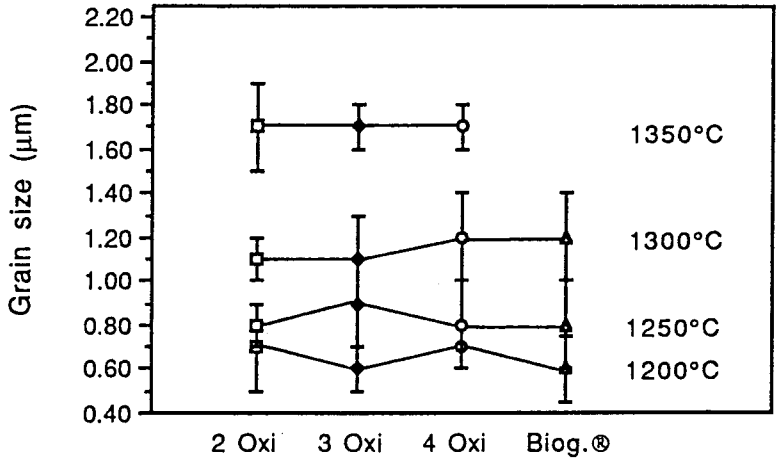

Figure VIII.31 Variation of grain size with sintering temperature for HA-5wt% glass composites

VIII.4.2.5 Mechanical properties

VIII.4.2.5.1 Biaxial bending strength

Biaxial bending strength and Young's modulus results are shown in Table VIII.8 and VIII.9, respectively.

Table VIII.8 Biaxial bending strength for HA-glass composites

		Biaxial bending Strength (MPa)			
	Material	1200°	1250°	1300°	1350°
2.5 %	2-Oxide glass	27±6	54±13	73±13	66±17
	3-Oxide glass	36±10	38±7	55±18	49±14
	4-Oxide glass	30±6	51±10	58±17	56±15
	Bioglass ®	30±5	50±10	60±11	60±9
5 %	2-Oxide glass	27±8	61±23	85±20	96±17
	3-Oxide glass	29±8	54±16	69±21	61±18
	4-Oxide glass	37±9	74±15	74±11	33±5
	Bioglass ®	23±5	40±6	27±7	*

* The samples fractured during cooling

Table VIII.9 Young's Modulus for HA and HA-glass composites

		Young's Modulus (GPa)			
	Material	1200°	1250°	1300°	1350°
2.5 %	2-Oxide glass	66±7	117±15	121±15	122±10
	3-Oxide glass	95±7	87±9	113±15	100±15
	4-Oxide glass	79±8	103±14	105±11	108±12
	Bioglass ®	89±10	99±14	109±13	109±9
5 %	2-Oxide glass	75±14	120±12	120±14	134±9
	3-Oxide glass	86±6	106±12	122±15	122±10
	4-Oxide glass	83±12	113±13	110±11	75±10
	Bioglass ®	72±9.0	85±7	74±8	-

Biaxial bending strength results for HA-phosphate glass composites showed a tendency to increase with sintering temperature up to 1300°C. Above that temperature a decrease seemed to have occurred, although the values were situated inside the standard deviation. For

5% addition, a slightly increase could be detected when compared with 2.5 % addition, except for HA-5% 4 Oxide glass sintered at 1350°C where a marked decrease was found.

HA-2.5% Bioglass® composites also showed an increase of biaxial strength with sintering temperature. For 5% addition, there was an increase from 1200°C to 1250°C but at 1300°C a sharp decrease was detected, and at 1350°C all samples fractured.

Comparing these values with those for HA, there has been a significant improvement in the biaxial bending strength for HA-phosphate based glass composites at the same sintering temperatures. HA-Bioglass® composites also showed an increase in biaxial strength for 2.5% addition, comparatively to HA. For 5% addition there was no significant improvement.

Young's modulus values followed the same general tendency of biaxial strength results. A proportional relationship seemed to exist between strength and Young' s modulus: the greater the former, the higher the later.

HA sintered compacts, produced from the milled batch, did not show any biaxial bending strength improvement, within the standard deviation, comparing with the previous ones.

No significant variation was found for HA-5% wt glass composites relative to 2.5% addition, and therefore those results were not considered. The Weibull modulus changed within the same range as for HA, indicating a large variation in strength. Figure VIII.32 shows the Weibull modulus results for HA-2.5 %wt glass composites.

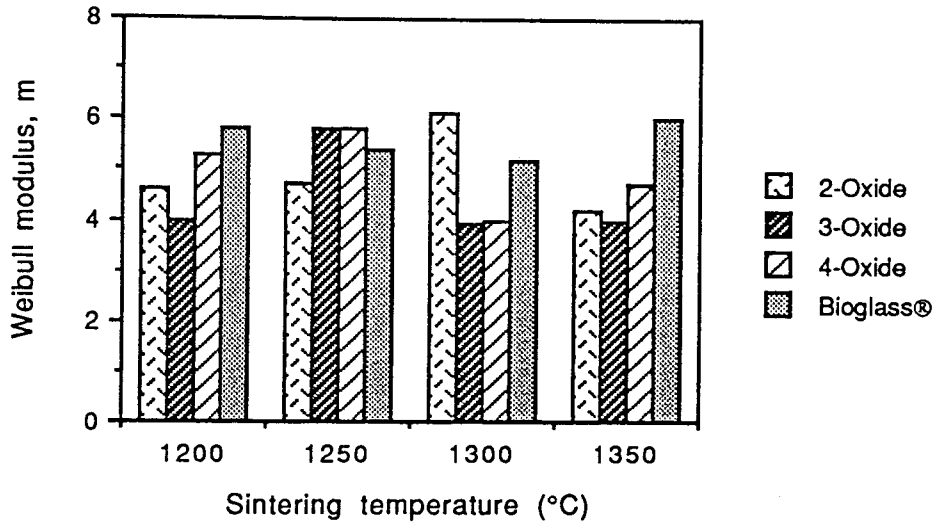

Figure VIII.32 Weibull modulus for HA-2.5% glass composites

VIII.4.2.5.2 Fracture toughness

VIII.4.2.5.2.1 Indentation

HA-glass composites showed higher fracture toughness when compared with HA sintered compacts, as it is presented in Table VIII.10.

Table VIII.10. K_{1c} results using the indentation method

		K_{1c} (MPa $m^{1/2}$)		
	Material	1250°	1300°	1350°
2.5 %	2-Oxide glass	1.5±0.2	1.6±0.3	1.3±0.2
	3-Oxide glass	1.2±0.2	1.5±0.2	1.1±0.2
	4-Oxide glass	1.4±0.3	1.7±0.4	1.5±0.3
	Bioglass ®	1.5±0.2	1.7±0.3	1.3±0.3
5 %	2-Oxide glass	1.5±0.1	1.6±0.2	1.4±0.2
	3-Oxide glass	1.3±0.2	1.5±0.2	1.2±0.2
	4-Oxide glass	1.4±0.1	1.6±0.2	1.3±0.1
	Bioglass ®	0.9±0.1	-	-

Fracture toughness increased from 1250°C to 1300°C but decreased after this sintering temperature. A similar behaviour was reported for HA sintered compacts. HA-5% Bioglass® samples sintered above 1250°C were not considered because they showed microcracks.

VIII.4.2.5.2.2 Strength-Indentation

Fracture toughness results, using a strength-indentation method, are presented in Figure VIII.32.

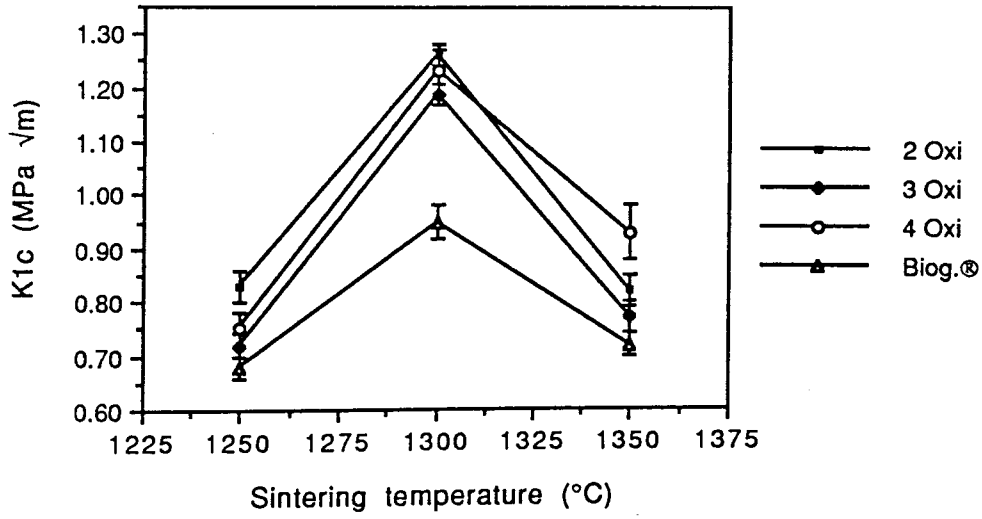

Figure VIII.32 K_{1c} results vs sintering temperature using the strength-indentation method.

A similar tendency was observed when comparing these values with the previous ones, with the highest peaks found for samples sintered at 1300°C, followed by a decrease above that temperature. However, HA-4 oxide glass samples showed significantly lower values than those determined by the indentation method. Although the general trend was the same, the indentation-strength test gave lower K_{1c} values than the indentation technique.

VIII.5 In vitro tests

VIII.5.1 Weight loss

No sample weight loss was detected after all immersion periods (4, 28, 56 and 84 days) in de-ionised water and physiological solution, within the accuracy used, ±0.0001g. In some cases, there was even a small weight increase for samples immersed in physiological solution, which had been due to some NaCl crystals precipitated on their surface caused by an incomplete surface cleaning after drying. No dimensional change was found within the accuracy used, ±0.01mm.

VIII.5.2 Chemical analysis

Chemical analysis of the physiological solution revealed that it had the following composition in terms of the ions analysed: Ca-0.5 ppm, Na-3100 ppm and P-718 ppm. Its initial pH value was 7.4. Stationary concentrations of Ca and P were reached after 28 days' immersion and no variation was detected after 84 days. Table VIII.11 shows the Ca and P concentration in de-ionised water and physiological solution after 28 days.

Table VIII.11 Ca and P concentrations in de-ionised water and physiological solution (*)

Material	Ca [ppm]	P [ppm]
HA	9.2/9.4*	5.2
HA-2 Oxide	10.1/10.0*	5.4
HA-3 Oxide	10.9/10.1*	5.6
HA-4 Oxide	10.7/10.1*	5.4
HA-Bioglass®	10.6/10.6*	5.8

P and Na leached out from samples immersed in physiological solution were not determined, because its initial P and Na contents were already 718 ppm and 3100 ppm respectively, and no accurate values could be determined with such high initial concentration. Si and Na contents in de-ionised water after 24 and 84 days' immersion were both less than 1 ppm, which is the lower limit for atomic absorption analysis.

VIII.5.3 Biaxial bending strength

Biaxial bending strength results for HA and HA-glass composites after 84 days' immersion in physiological saline solution and de-ionised water are shown in Table VIII.12. Similar values (within the standard deviation) were found for samples immersed during 24 days, therefore results were not presented.

Table VIII.12 Biaxial bending strength results after 84 days' immersion

Material	Water	Phys. solution
HA	26±6	29±7
HA-2 Oxide	75±15	69±13
HA-3 Oxide	63±15	65±17
HA-4 Oxide	66±14	59±18
HA-Bioglass®	58±16	61±14

Comparing these results with those of HA and HA-glass composites, no significant change in biaxial bending strength occurred after immersion in de-ionised water and physiological solution.

IX DISCUSSION

IX.1 HA-glass composites for bone replacement

It is well-known that for a bioactive ceramic implant to obtain full clinical success it will require many different and simultaneous achievements, of which a stable and sound interface with the host tissue and mechanical compatibility of the implant with the tissue to be replaced are an absolute requests. Due to its bioactivity and biocompatibility, HA has been extensively used in biomaterials. However, HA shows much lower mechanical strength than bone, and therefore its use should be limited to low load applications. A careful control of its synthesis and sintering process has not shown significant improvements in terms of its mechanical properties which continue to be far behind those reported for bone. On the other hand, there is a great need for producing biomaterials whose bioactivity might be higher than that of HA, which is a fairly inert material when compared to Bioglasses, for example, and to adjust the degradation rate of the implant to the self-repairing rate of body tissues. Therefore, it is of great interest to match the chemical composition of the implant with a particular host tissue, although preserving a HA structure, which is the basic bone mineral constituent. These demands were the basis to carry out this research.

Recently, glass-ceramics have been produced by controlled crystallisation of glass which have met considerable success. Their microstructure basically comprises an apatite structure, crystals of

a second crystalline phase and a residual glassy phase. Different types of glass-ceramics have been prepared, although the best well-known are: the A-W glass ceramic (159,160,161,163,164,165), which is based on the SiO_2-P_2O_5-CaO-MgO system and usually with some Na_2O additions, and Bioverit (155,166) obtained by crystallisation of the Na_2O-K_2O-MgO-Al_2O_3-SiO_2-CaO-P_2O_5-F system. Apart from the crystalline apatite, there is wollastonite in the case of the A-W glass-ceramic, and mica or aluminium phosphate for Bioverit. These second crystalline phases are usually mentioned as responsible for the improvement in mechanical properties. However, many authors observed that a Ca-P rich layer was formed 'in vivo' at the interface between bone and glass-ceramic. This layer has been characterised as having an apatite structure, and considered as an essential requirement for bone bonding to occur (92,157,158,164,167). Hench (21) also indicated the following essential requirements for bioactive glasses which contain SiO_2, Na_2O, CaO and P_2O_5: less than 60 mol% SiO_2, high Na_2O and CaO contents and high CaO/P_2O_5 ratio. Ducheyne (20) indicated that above 60mol% of SiO_2 tissue bonding no longer occurs. Increasing amounts of SiO_2 in SiO_2-Na_2O-CaO-P_2O_5.glass led to very high mortality in mice (96).

In this work, only Ca-P phases were found for HA-phosphate glasses as no SiO_2 was added to the glass formulation. Apart from Al_2O_3, which is considered as a bioinert material, all ions added to the glass formulation were chosen taking into account the mineral composition of bone. Glasses made from calcium-sodium-phosphate system have been considered as having enormous potential as biomaterials, because their chemical composition is analogous to the inorganic constituent of bone. The first study aiming biomedical applications

was due to Burnie (2). Cell and animal studies have been used to assess their biocompatibility specially for dental and maxillofacial applications. Their high bioactivity makes phosphate glasses very useful as temporary space fillers. Animal studies shown that new bone had filled the gap left by the dissolution of the glass (2,23).

Mineral constituent of hard tissues not only contains HA but also small amounts of Na^+, Mg^{2+}, CO_3^{-2} (see Table I.1). The amounts of these elements differ from one bone to another. For example, higher Na^+ contents are found in more active tissues (19,66). In this work, we started from a simple 2 Oxide phosphate glass, $54.5CaO\text{-}45.5P_2O_5$, then a 3 oxide glass was fabricated, $28CaO\text{-}45.5P_2O_5\text{-}27Na_2O$, aiming the introduction of Na^+ ions and finally Al_2O_3 was added by using a 4 oxide glass, $10.1CaO\text{-}62.9P_2O_5\text{-}10.1Na_2O\text{-}Al_2O_3$. Using these glasses it was also possible to introduce ions commonly found in body tissues joining a HA structure and to significantly improve the mechanical properties of HA.

The commercial HA powder, supplied by Plasma Biotal, was initially characterised using a wide range of techniques. Mineralogical transformation and the loss of OH^- occurring during the sintering process were followed, and its sintering regime established in order to produce sintered compacts. After this study, HA-glass composites were fabricated and their properties compared with those of HA compacts.

IX.2 Hydroxyapatite powder

X-ray diffraction analysis showed that the starting powder was crystalline and its mineralogical composition corresponded to HA,

without TCP phases. This HA powder was however non-stoichiometric as its Ca/P ratio was higher than 1.67, according to the different chemical analysis methods used. The higher Ca/P ratio and the presence of CO_3^{-2} in the structure detected by infra-red analysis, seem to indicate that the HA powder was a B-type carbonated HA (19,40,41,168), where CO_3^{-2} substitutes PO_4^{-3}. The carbonated HA has a chemical composition between HA and $Ca_8{\cdot}2(PO_4)_4(CO_3)_2{\cdot}2$, with vacancy formation at Ca^{2+} and OH^- positions. The symbol · represents a vacancy in the structure of HA. Generally, one has $Ca_{10-x}(PO_4)_{6-y}(CO_3)_y(OH)_{2-z}$ where $0<x<2$, $0<z<2$ and $2x=y+z$ (41). In carbonated HA the Ca/P ratio is always higher than 1.67.

Carbonated hydroxyapatite has been shown to be chemically more reactive than pure HA. Therefore, development of sintered carbonated apatite is of great interest (49,66). The mineral constituent of hard tissues also contains CO_3^{-2} (19,49), and the higher its percentage, the higher its metabolic activity. For example, dental enamel contains 2-5% wt and bone has almost twice, being in the 6-8 %wt range (19). The former is an almost inert material and the latter is a much more active tissue.

The CO_3^{-2} content present in HA structure shown to be easily detected by infra-red analysis, although some authors (10,41) refer the possibility of using x-ray diffraction, specially when its content is relatively high (>3% wt). In this case, CO_3^{-2} is indirectly detected by the presence of CaO, after thermal treatment. More controversially, CO_3^{-2} can also be detected by lattice parameters changes of the crystal structure. According to Raemdonck (19), the presence of increasing amounts of CO_3^{-2} produces a contraction of 'a'

lattice parameter at a rate of 0.006Å/wt% CO_3^{-2}. This effect could be confirmed, as parameter 'a' was 1.3% higher than its standard value for HA. However, one should remember that the HA powders synthesised by precipitation reactions always contain impurities. These elements cause substitutions in the HA crystal structure, altering its lattice parameters (19,40,49). Therefore, it is always very difficult to isolate the effect of one single element or compound on the HA lattice, especially for additions of the order of ppm.

Besides the presence of CO_3^{-2}, infra-red analysis also clearly showed the presence of OH^- and PO_4^{3-}. Hydration water could be detected, as well. Part of this water might have come from the KBr used in sample preparation, as it sometimes occurs in this analysis (145).

FWHM and IW values indicated a relative trace enlargement for the starting powder. This was due not only to an instrumental error contribution (slight misalignment of the specimen with respect to the position of the detector, for example), but also to the low crystallinity of the HA powder (10). The absence of any thermal treatment after the precipitation process can lead to this effect, as it seemed to have occurred for this HA powder. The presence of CO_3^{-2} also confirmed this hypothesis. Powders obtained by solid state reaction at high temperatures are more crystalline (8,28).

HA particles size and morphology seems to depend on the synthesis process (28,35,39). Several authors suggested that HA powders had agglomerates which could be resolved into smaller particles, as it was found for the powder used in this work. Kijima (32) detected crystallites of 0.02-0.03μm in size, Bigi (50) estimated a value of 0.03μm, Jarcho (31) 0.002μm, and Lopes (169) 0.077μm. Best (10),

analysing a Plasma Biotal powder, indicated a 0.1μm value using scanning electron microscopy, which agrees with the observations made in this work. Particle size analysis determined a $D_{0.5}$=1.58μm which is within the mean particle size of primary particles found by scanning electron microscopy, 1-3μm. Laser diffraction analysis and surface area results showed that the HA powder was fine, as 90% of its particles were ≤6.5μm and its surface area was 16.9 m^2/g. The large agglomerates detected by scanning electron microscopy were also found by laser diffraction and should correspond to particles bigger than 10μm situated in the second part of the distribution. However, the particle size distribution pattern did not seem to be ideal for the sintering process as it showed a bimodal distribution (45).

Table IX.1 compares the HA powder with other commercial and laboratory-prepared powders.

Table IX.1 Impurities in the HA powders

Concentration (ppm)								
Fe	Al	Zn	Si	Cu	Mg	Cr	Ni	Ref
240	200	10	1200	10	2000			thiswork
100-1000	100-1000	-	100-1000	1-10	>1000	-	-	(115) ♠
33.5	-	40	-	<1	42.6	<1	<1	(34) *
1000	600	-	500	1	2000	-	-	(35) ♠
40	400	-	20	1	50	-	-	(35) *

* Laboratory-prepared ♠ Commercial

The impurity content of the HA powder used in this work, seems to be similar to that of the others commercial powders, which tend to exhibit a much higher impurity level than laboratory-prepared HA by solutions contact with steel containers. Heavy metals can be extremely harmful to health, under certain circumstances (170,171).

IX.2.1 Thermal behaviour

The HA powder exhibited high thermal stability as it did not transform into TCP structures, even after being sintered at 1350°C for 3h, as was shown by x-ray diffraction. The thermal stability of HA compacts seems to be related to the Ca/P ratio of the initial powder. According to Jarcho (31) and With (115), the initial Ca/P ratio <1.67, i.e. calcium-deficient crystals, tended to lead to some amount of TCP structures in the sintered compacts. These crystals would act as precursors to the development of TCP structures. According to Jarcho (31), powders with Ca/P=1.55 and 1.57 led to only 23% and 39% HA structure in the sintered compacts, respectively. Powders with Ca/P ratio 1.65-1.72 led to 100% HA structures. More recently, Rey (41) indicated that Ca/P=1.5-1.67 forms β-TCP and stoichiometric HA mixtures. When Ca/P ratio is much higher than 1.67, the final microstructure of the sintered compacts will be composed of some amount of CaO. The HA powder, supplied by Plasma Biotal, had a Ca/P=1.689 but CaO was not found in the microstructure of the sintered compacts because the amount was probably too low to be detected. Infra-red analysis also indicated a HA structure in all sintered compacts, exhibiting the OH^- peak between 3590-3650cm^{-1}, although from this analysis it cannot be concluded that the structure of the sintered compacts was 100% HA.

However, some modifications seemed to occur in the HA structure during heating and cooling cycles. Thermogravimetric analysis showed that HA powder lost its hydration water, on heating between 100 and 400°C. Above 850°C, another weight loss was detected which was likely due to CO_3^{-2} liberation and probably some dehydroxylation, according to the reaction II.7. This reaction is reversible and it is possible that the slight weight increase detected during cooling by thermogravimetric analysis may have been the result of a reincorporation of some OH^- from H_2O present in the atmosphere of the furnace. Similarly, the loss of some OH^- also seemed to be confirmed by infra-red spectroscopy, as the small OH^- peak at $630cm^{-1}$ disappeared from the spectrum after heating above 1200°C. The same behaviour was found by Kijima (32), where the OH^- peak intensity decreased sharply with increasing sintering temperatures, and for samples sintered at 1300°C the OH^- peak was hardly detected. Identical results were found by Yamashita (172), where partial dehydroxylation was also detected when HA was sintered in air. Rootare (48) indicated that water vapour in the sintering atmosphere replenished hydroxyl deficient areas. Therefore, it is possible that the final structure after sintering was partially oxyhydroxyapatite.

The loss of hydration water has been extensively referred in the literature (39,50,169,173), but dehydroxylation is rarely mentioned. Kijima (32) indicated that, when HA loses OH^- the main HA structure is basically retained but there is a decrease in the 'a' lattice parameter and an increase in 'c' parameter. Figure IX.1 compares the results obtained in this work with Kijima's, for the lattice parameter 'a'.

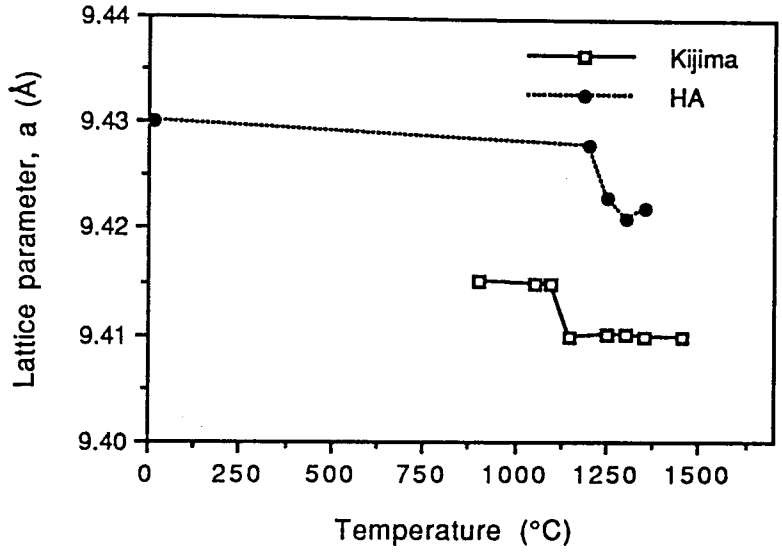

Figure IX.1 Variation of 'a' parameter with sintering temperature

The results show a comparable evolution tendency, although some discrepancies can be observed for two consecutive temperatures. Results for parameter 'c' from this work were not included because no general trend was observed. Lattice parameters evolution for HA are always difficult to follow as other phenomena may occur during heating, such as CO_3^{-2} loss and impurities solubilisation, for example, which may influence lattice parameters values (49). As it was previously mentioned, the presence of increasing amounts of CO_3^{-2} produces a contraction of 'a' lattice parameter at a rate of 0.006Å/wt% CO_3^{-2}. Since sintering at high temperatures removed the CO_3^{-2} from the lattice, an increase in the 'a' parameter would have been expected, i. e., an opposite effect to that caused by the loss of OH^-.

FWHM and IW results showed decreasing values up to 1250°C and increasing values above that temperature. A decrease in FWHM values is usually mentioned in the literature when HA is heated at a given sintering temperature within the 1000-1300°C range (10,31,48,169),

but their systematic evolution had not been followed, yet. The decrease in FWHM and IW is usually associated with a decrease in lattice strain, and therefore an increase in crystallinity, as the powder did not receive any prior heat treatment before sintering. In order to obtain a better clarification of the phenomenon, further analyses were conducted on this HA, using Fourier Transform Raman spectroscopy (174). Powder HA samples were heated at the various temperatures within the 1200-1300°C range. The analysis indicated a marked change in the OH^- region of the spectra, after heating at 1250°C which led to a small, broad and flat band. Therefore, it is possible that the loss of OH^- caused some distortion in the structure of HA which led to an increase in the FWHM values.

The blue coloration of HA sintered compacts seems to be related to trace element impurities, as it was indicated by Jarcho (31), Lopes (169) and Best (10). Best suggested Mn as being responsible for the blue coloration of HA. Yellow-coloured HA could also be obtained by Fe incorporation using $Fe(NO_3).9H_2O$ in the synthesis process, without any mineralogical change. This yellow-coloured HA is used as inlays in biomedical applications (175). These facts indicate that HA has a very 'open' structure where many substitutions are possible 19,40). Although Mn ion content was not determined in this HA, Best (10) determined 87 ppm using a commercial powder from Plasma Biotal.

IX.3 Sintered hydroxyapatite and HA-glass composites

IX.3.1 Densification

Although die pressing and isostatic pressing were initially used, the later process was abandoned because no specific implant was

intended to be fabricated. Die uniaxial pressing is suitable for producing simple and reproducible shapes (bars and discs) for mechanical testing, which was the aim of this work.

A sharp densification rate occurred up to 1300°C, followed by no further densification above that temperature, for both dwell times. The compacts sintered at 1300°C showed a relative theoretical density of 97%. Residual porosity is usually attributed to a wide range of variables (46,56,60), where inhomogeneity of the green compact plays an important role, as it was mentioned in chapter II. The densification behaviour of these HA sintered compacts appeared to match well, for the same range of temperatures, with that of the powders used by Denissen (35), Akao (110) and With (115), as it is represented in Figure IX.2.

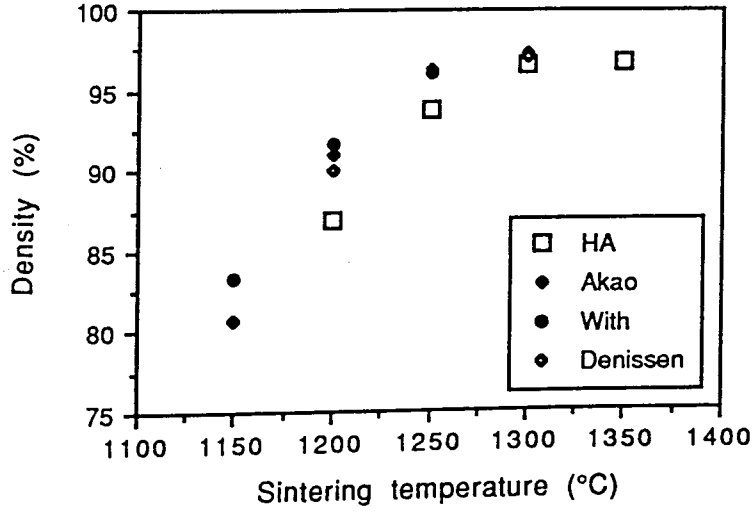

Figure IX.2 Densification behaviour for different HA

Up to 1300°C the great increase in density was followed by a relative small increase in grain size. Above 1300°C, a marked increase in grain size occurred without any significant increase in the density of the compacts (see Figure VIII.7 and VIII.12-13). Therefore, it was

possible to conclude that this HA powder exhibited abnormal grain growth above 1300°C.

Similar behaviour was also mentioned in the works above reported, where equivalent grain size values were also determined, within the same sintering temperatures range used for this work. Abnormal grain growth also occurred above 1300°C without any significant increase in the densification process. Best (10) also reported abnormal grain growth above 1300°C for HA supplied by Plasma Biotal.

Different densification behaviour is also referred in the literature. For example, Jarcho (31) reported density over 99% after sintering at 1150°C. However, the starting HA powder was much finer. Similar behaviour was indicated by Hirayama (176), combining a fine starting powder with hot isostatic pressing.

Density measurements and scanning electron microscopy showed that the densification of HA could be significantly enhanced by the presence of a liquid phosphate phase chemically related to its composition, during its sintering process. Initially, a great care had to be taken to adjust the particle size of the glass and HA powders, in order to obtain good glass dispersion in HA. The glass particle size had to be reduced to the same order of magnitude of that of HA powder. A strong particle size reduction occurred after 24h milling, although some big particles were also found, within the 100-400μm range. After a further 24h milling in methanol, the glass seemed to have been well-dispersed in the HA powder and, at the same time, the big particles disappeared (see Figure VIII.20). The HA powder did not seem to suffer any significant particle size reduction after this

mixing process, as its $D_{0.1}$ and $D_{0.5}$ remained almost unchanged. The agglomerates detected in the previous analysis of HA (particles between 20-50μm), were broken up after 24h milling. The same effect may have occurred when the powder was pressed. This hypothesis seems to be supported by the fact that no further improvement in biaxial bending strength was detected.

The HA-phosphate glass composites also exhibited a high densification rate up to 1250-1300°C, followed by no further densification improvement after 1300°C. This behaviour is common in liquid phase sintering. Rapid densification occurs by liquid formation and spreading (stage I) immediately followed by diffusion and shape accommodation mechanisms (stage II). These overlapping phenomena seemed to occur until 1250°C-1300°C with the densification rate sharply decreasing towards this sintering temperature. Highly dense samples were then obtained. Above 1300°C microstructural grain coarsening took place. Abnormal grain growth was also detected for HA samples sintered at 1350°C. According to the literature the last stage is referred to as a 'solid state controlled sintering' and solid state sintering is of major significance. Liquid phase mechanism is very complex as many variables are involved (solubility of the solid in the liquid, wetting properties, segregation effects, processing conditions, etc.). It was not the aim of this work to produce any model for the sintering mechanism, and further studies should be carried out in order to a better characterisation of this HA-phosphate glass sintering mechanism.

Due to the chemical similarity between HA and phosphate glasses, residual porosity was reduced to a very low level and eventually theoretical density values could be achieved. A strong bond developed between HA and the phosphate glasses and no discontinuities were also found. The liquid phosphate phase acted on the solid HA particles to reduce interfacial energy and eliminate porosity.

Generally, the following mechanism reaction is proposed :

$$\text{Hydroxyapatite} + \text{Glass} \rightarrow \text{Tricalcium phosphate} + OH^- \uparrow \quad \text{(IX.1)}$$

Ca^{2+} ions appeared to play an important role, as TCP was formed which has a Ca/P ratio=1.5 comparing to the 1.67 for stoichiometric HA. It should de noted that the phosphate glasses used had a lower Ca/P ratio. Schematically, it may be shown as:

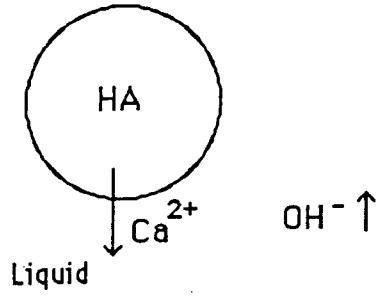

Figure IX.2 Probable mechanism that occurred at high temperatures

For each phosphate glass composition used, the transformation reported in (IX.1) was enhanced by increasing sintering temperatures, by amount of glass added and possibly by its composition, according to x-ray diffraction results.

The presence of a solid HA skeleton (favouring heterogeneous nucleation), the tendency of HA to be transformed into TCP and the slow cooling rate used after sintering, led to the development of

crystalline TCP structures. The general transformation tendency was observed, HA⇒β-TCP⇒α-TCP. This is also the decomposition trend of HA with increasing sintering temperatures when the starting powder has a deficient Ca/P ratio, or when sintering occurs under vacuum. Both TCP structures are widely used in biomedical applications and their biocompatibility is well-known (177,178,179,180,181,182). They show different bioactivities from HA, and a suitable combination with HA may offer a wide range of biomedical applications. α-TCP is usually classified as 'resorsable material' and designed to gradually degrade over a period of time and be replaced by natural host tissue (21,22,65).

Because of the high temperature used for sintering, apparently no significant differences in the flow characteristics among phosphate glasses were found particularly above 1250°C, where good glass dispersion on HA was obtained after sintering. The liquidus temperature of phosphate based glasses depend on their metal oxide contents (2,93,183). All glasses were liquid at the sintering temperature range used. The 2 Oxide glass has a liquidus temperature very close to 1180°C (183), and Na_2O addition significantly decrease the liquidus temperature of these glasses (2). The earlier presence of a glassy phase in the sintering process of HA seemed to lead to higher proportions of HA transformed into TCP phases. Physical and chemical characteristics of phosphate glasses may be found in Burnie's work (2) and Parker (184). Energy dispersive spectroscopy results showed that Na^+ ions from the phosphate glass, kept concentrated on TCP phase, without being detected in the HA matrix, although some Na^+ diffusion cannot be ruled out, as Na^+ can easily be incorporated in HA structure at Ca^{2+} positions (40).

The SiO_2 based glass did not develop a strong bond with HA, when compared with phosphate glasses, probably due to the mismatch in chemical compositions. The structure of HA seemed to have been destroyed and, apart form TCP structures, calcium phosphate silicate was formed making the reinforcement process useless. High level of porosity was also detected in microstructures. These detrimental effects tended to be enhanced by increasing sintering temperature and higher amount of glass added, 5 wt%. It is likely that, for 2.5wt% addition, the lower amount of SiO_2 added and therefore the lower amount of calcium phosphate silicate formed, led to a less detrimental effect on the densification of HA.

Kasgasniemi (1) also tried to sinter HA, at 800-1000°C, in the presence of a liquid bioglass phase within the SiO_2-Na_2O-CaO-P_2O_5 system. A much higher wt% glass/HA ratio was used, between 1:1 to 7:3. After sintering, the microstructure of the composites consisted of calcium silicate, a residual Si-glassy phase and $CaNaPO_4$. Large pore formation occurred which was also corroborated by a more recent work (93). Using different amounts of Na^+ ions in the glass composition, that author concluded that Na^+ diffused into the HA lattice and promoted the transformation of HA. Similarly, Al_2O_3 additions to the glass also caused HA to transform into TCP phases. No HA was left using these sintering conditions. Recent work (185) demonstrated that Al_2O_3 partially decomposed HA into α-TCP and calcium aluminates. Stresses were generated in the microstructure, and cracks detected. HA-5% 4 Oxide composite fired at 1350°C showed an β-TCP and α-TCP structure, with all HA transformed. It is possible that the presence of Al_2O_3 associated with the complete

vanishing of the HA skeleton may have led to cracking of the samples found after sintering.

Other elements or compounds are also mentioned in the literature as having accelerated the transformation of HA into TCP structures during its sintering process namely, lithium phosphate (186), zirconia (187,188), and titania (189). These compounds were added to HA aiming to either enhance its sintering process or increase its mechanical properties. Therefore, HA seems to be easily transformed into TCP by a wide range of additions, which seems to substantiate its lower stability when Na, Al, and Si were used in the glass formulation, besides Ca and P.

IX.3.2 Mechanical properties

Hardness values increased with sample densification, indicating a good correlation between these properties. Similar values can be found in the literature, usually in the 450-680 HV range. (31,32,35,114,169). According to Evans (15) the hardness of bone can differ substantially, depending on its mineral/organic proportion. For a 0.26 mineral fraction its hardness is about 16 HV, but for a 0.46 proportion its hardness increases to 74.9 HV. Therefore, sintered HA has a much higher hardness than bone.

In this work, Young's modulus of HA varied between 59-89 GPa. Bone has a Young's modulus in the 11.5-24 GPa range (11,12,13), once again indicating that bone is much softer than HA, which is a brittle ceramic. The high hardness and Young's modulus values have probably led to the development of HA-polymer composites (190,191,192), as a means to reduce stiffness. The brittle nature of HA was also

indicated by the low Weibull modulus found. Similar results were referred by Best (10) and Puajindanetr (36).

Table IX.2 summarises and compares some bending strength results presented in the literature with those determined in this work.

Table IX.2 Bending strength for HA

σ_r (MPa)	Technique	Ref
113±12	3P-B	(110)
111,7±11,0	3P-B	(31)
100	3P-B	(193)
115	3P-B	(115)
38-56	4P-B	(114)
45-65	4P-B	(194)
84,1±17,2	4P-B	(31)
28	Biaxial bend.	this work

Undoubtedly, 3-point bending tests give lower strength values than 4-point bending, because in this case a much larger area is submitted to maximum bending momentum. Likewise, in an equibiaxial stress field more flaws are highly stressed than in the uniaxial case, where only those flaws nearly transverse to the uniaxial stress are highly stressed. Thus, the probability of a more severe flaw being highly stressed is greater under biaxial than uniaxial bending, which should cause reduction on the values obtained (117,121,123). In conventional bending tests, there are additional flaws generated by particular shaping process, which may even dominate the failure behaviour of the specimen. Biaxial bending was created to eliminate these effects, and this is now being tried to be introduced as the standard technique to test the strength of bioceramics (117,118). Other variables are

also important to compare strength results such as, material volume really subjected to maximum strength (loading-span), grain size, cross-head speed, etc. but unfortunately all these values are not usually quoted in literature, which makes discussion very difficult.

According to the literature, the bending strength of polycrystalline ceramics depends on density and grain size (98,135,176). For this sintered HA, a 17% increase in strength (24 to 28 MPa) was obtained when density increased 10% (87-97%), and apparently these results seem to match well with those previously reported. Akao (110) and Best (114) detected 9% and 11% strength increase with 7% and 11% density increase within the same density range, respectively. Best (114) quoted those values using a HA powder supplied by Plasma Biotal. In the present work, no strength variation with grain size was detected, for samples sintered above 1300°C which seems to contradict the general behaviour of ceramics. However, similar values were found by Aoki (8), where strength was almost insensitive to changes in grain size, and therefore not consistent with Petch equation (195).

The peak in toughness for samples sintered at 1300°C may be attributed to the combination of good densification and small grain size. Fracture toughness may be considered in terms of the ability of a material to resist to crack propagation. Grain boundaries serve to increase toughness of a material (97,131). The HA sintered at 1350°C showed abnormal grain growth and therefore a marked decrease in k_{1c} occurred. This behaviour was found using both techniques, i.e. indentation and strength-indentation, for samples sintered for 1h. The former technique gave higher results than the later, which is in

accordance with the fact that the lateral cracks produced by Vickers indentation were not taken into account by the formulation, and therefore over-estimated results were obtained (136,137,140). Best (10), using the same indentation technique, determined K_{1c}=0.5-0.9 $MPam^{1/2}$ for a HA powder supplied by Merck, on samples sintered in the 1220-1280°C range. Double-torsion test showed many difficulties to be implemented as HA is very fragile and difficult to pre-crack and therefore was abandoned.

Biaxial bending strength and fracture toughness of HA were largely improved by the presence of a liquid calcium-phosphate phase during sintering. The following facts seem to have contributed to this improvement: a) the liquid phase promoted atomic diffusion among HA particles, developing a strong bonding b) this greater atomic diffusion and the possible solubility of the solid HA in the liquid, enhanced the densification process and led to highly dense structures, approaching theoretical density c) precipitation of TCP structures which have improved mechanical properties over HA, namely bending strength and fracture toughness, usually 10-15% higher for bending strength (8,177) and 15-20% higher for fracture toughness (8,196) d) a significant decrease in grain size, whose growth was prevented by the liquid phase. These are common features that increase mechanical properties of ceramics (97,110,131,176). In the case of HA, grain size seemed to have been particularly important in terms of the enhancement of fracture toughness as it markedly decreased when abnormal grain growth occurred at 1350°C.

Mechanical properties of HA-glass composites are comparable to those quoted for glass-ceramics, namely (89,165,197,198,199):

bending strength, 2-2.5 times higher than that of HA, fracture toughness in the 1.2-2.0 MPa.$m^{1/2}$ range and Young's modulus, 120-130 GPa. It should be emphasised that the Young's modulus determined in this work tended to be over-estimated because the calculation of the deflection at mid-span did not take into account the deflection of the loading system itself. A much better accuracy for the calculation of the Young's modulus is obtained using vibrational methods (115,200,201,202).

Although the improvement in bending strength and fracture toughness of HA-glass composites were very promising features, as an approximation to the mechanical properties of bone has been achieved, it should be underlined that these materials have a much higher Young's modulus than bone. In the case of implantation, a deformation mismatch between them and bone will occur for a given applied load, which may cause problems at the interface. Young's modulus values seem to increase with increasing values of strength for ceramics, and the seek of high strength values usually widens the gap to the Young's modulus of bone. Fracture toughness of these composites is still far behind the values determined for bone, and further progress should be attained.

IX.4 In vitro tests

No weight and dimensional variations were found for HA and HA-glass composites immersed in physiological solution or de-ionised water, within the accuracy used in the measurements, i.e. ±0.0001g and ±0.01mm, respectively. Bagambisa (203) carried out similar tests on sintered macro-porous blocks, using a physiological solution and no

weight loss was detected after 4 weeks immersion at 70°C, within $\pm 10^{6-}$ g accuracy. Aoki (8) estimated, for sintered HA, a 1μm/year dissolution rate in destilled water.

Low levels of [Ca] and [P] leached out from HA samples were found. Similar results are extensively referred in the literature (8,43,203,204,205,206). For example, Aoki (8) found [Ca]=4 ppm after 10 days and [Ca]=5 ppm after 300 days, for sintered HA samples immersed in destilled water, and Bagambisa (203) detected [Ca]=13.812 ppm and [P]=11.290 ppm in physiological solution. HA-glass composites showed a slightly higher [Ca] and [P] in solution than sintered HA which may be attributed to the presence of TCP structures. It is well-known that TCP structures have higher degradation rate than HA, showing the following biological activity tendency α-TCP>β–TCP, as it is extensively exposed in literature (21,63,204,205,206,207).

However, some authors refer that (35,43) TCP is unstable in water and an HA layer is formed on its surface, according to the following reaction:

$$2H_2O + 4Ca_3(PO_4)_2 \rightarrow Ca_{10}(PO_4)_6(OH)_2 + 2Ca^{2+} + 2HPO_4^{-2} \quad (IX.2)$$

and no difference should exist in terms of interfacial behaviour. Nonetheless, this layer should not be complete and further dissolution seems to be allowed as it was suggested by Driessens (206).

Two reasons may have contributed to the stoppage of the dissolution after 24 days' immersion: 1) an equilibrium at the saturation point

preventing any further dissolution or 2) the existence of a layer an the surface of HA as suggested by Driessens (206).

The Ca/P ratio determined in de-ionised water was lower than the theoretical value for HA, which indicates an incongruent dissolution. Identical results are also described in the literature (8,203,208). This fact does seem to be clearly understood (205,206), although some authors referred the re-precipitation of Ca crystals, initially released, on the surface of HA (203,209).

No strength variation was detected using biaxial bending strength after immersion in de-ionised water and physiological solution. Thomas (210) found similar results using sintered HA immersed in destilled water and physiological solution, after 8 weeks immersion. No variation in fracture strength was detected. These results seem to agree with the low level of ions leached out from samples.

X CONCLUSIONS & SUGGESTIONS FOR FUTURE WORK

X.1 Conclusions

HA maintained its mineral structure after sintering at 1200-1350°C for 3h, without being transformed into TCP. However, some loss of OH^- occurred, leading probably to oxyhydroxyapatite. The loss of OH^- seemed to be particularly significant above 1200°C. Some of the OH^- lost during heating, seems to have been reincorporated in the HA structure, according to thermogravimetric analysis.

CO_3^{-2} was completely liberated from HA structure at least at 1200°C. Carbonated HA is more bioactive than stoichiometric HA (similarly to tissues with higher CO_3^{-2} content) and the presence of some amount of CO_3^{-2} could be beneficial for biomedical applications.

The commercial HA powder showed some metallic impurities in its composition which were probably responsible for the blue coloration after sintering.

Highly dense compacts could be easily achieved, applying relatively low compacting pressures and using short sintering times. However, sintered HA showed to have inadequate mechanical properties for substituting cortical bone. Its hardness and Young's modulus were much higher than those quoted for cortical bone, indicating that HA is a much more fragile material.

By choosing phosphate glass compositions containing ions commonly found in the physiological environment (Ca, P, Na, etc.) it was

possible to fabricate composites with only Ca-P structures, and incorporate inorganic elements commonly found in the mineral part of bone.

HA could be reinforced by the incorporation of phosphate based glasses during its sintering process. By choosing glasses chemically related to HA, atomic diffusion was enhanced and a strong bonding was developed between phases. The presence of this liquid phase reduced the residual porosity to a very low level and theoretical density could be approached.

The liquid phosphate glassy phase promoted the transformation of HA into TCP structures, following the tendency: HA $\Rightarrow\beta$–TCP $\Rightarrow$ α–TCP. The transformation was enhanced by a low liquidus temperature of the glass. It was also probable that Na_2O and Al_2O_3 additions play some detrimental role in the stability of the HA structure.

The presence of a liquid phase during the sintering process of HA inhibited its grain growth, leading to structures of much smaller grain size for each sintering temperature.

The highly density achieved, the strong bonding between phases, the small grain size of the microstructure and the precipitation of a crystalline phase with higher mechanical strength, seemed to be important factors in the improvement observed in mechanical properties. However, the increase in the Young's modulus can be a disadvantage for these materials.

The silicate network forming structure of Bioglass®, based on SiO_2, led to the formation of calcium phosphate silicate, which seemed to have impaired the sintering process of HA. The higher the amount of

Bioglass® added to HA, the higher the proportion of calcium phosphate silicate formed.

Low levels of [Ca] and [P] leached out from samples were detected after immersion in destilled water and physiological saline solution, either due to saturation of the solutions or to the formation of a layer on the surface of HA. No variation in biaxial bending strength was observed.

X.2 Suggestions for future work

- A wide range of tests are already underway to characterise the bioactivity of these composites, using 'simulated body fluid' which are almost equal to human blood plasma. These solutions are already extensively used for this purpose (260,263,241).

- *'In vitro'* and *'in vivo'* tests should be carried out to assess biocompatibility and *'in vivo '* response of these composites.

- The use of hot-isostatic pressing seems to be a very promising process to be implemented, as it would allow pressure and sintering to be performed simultaneously, promoting the densification process.

- Other phosphate based glasses compositions may prove to be important, namely with K_2O and MgO additions, as K and Mg are usually found in the mineral constituent of bone.

- HA has been extensively applied as a coating on metallic substrates (Ti alloys) by a plasma spraying process. During the spraying process, HA particles partially fuse and bond together. The

use of a biocompatible glass which easily melts may help to strengthen the structure of the coating and improve its mechanical properties.

REFERENCES

1 Kangasniemi, I.; De Groot, K., *J. Mater. Sci.: Materials in Medicine*, **2**, 1991, 133-137

2 Burnie, J., *Controlled Release Glass-A New Biomaterial*, PhD. Thesis, University of Glasgow, 1982

3 Behiri, J., *Compact Bone-Structure and Properties*, Short Course, IRC-in Biomedical Materials, University of London, 1990

4 Bloom and Fawcett, *A Textbook of Hystology*, Chp. 8 and 24, 11th Edition, W. S. Sanders Company, 1986

5 Ganong, W. F., *Review of Medical Physiology*, Chp. 21, 9th Edition, Lange Medical Publications, 1979

6 Netter, F. H., *The CIBA Collection of Medical Illustrations*, Vol. 8, CIBA-GEIGY Corporation, 1989

7 Junqueira, C., *Histologia Básica*, 2ª Edição, Chp. 8 and 16, Guanabara Koogan, 1971

8 Aoki, H., *Science and Medical Applications of Hydroxyapatite*, JAAS, 1991

9 Harper, H. A.; Rodwell, V. W.; Mayes, P. A., *Review of Physiological Chemistry*, 16th Edition, Lange Medical Publications, 1977

10 Best, S., *Characterisation, Sintering and Mechanical Properties of Hydroxyapatite Ceramics*, Ph. D. Thesis, Queen Mary & Westfield College, University of London, 1990

11 Grenoble, D. E.; Katz, J. L., *J. Biomed. Mater. Res.*, **6**, 1972, 221-233

12 Reilly, D. T.; Burstein, A. H., *J. Biomechanics*, **4**, 1975, 393-405

13 Bonfield, W.; Datta, P. K., *J. Biomechanics*, **9**, 1976, 131-134

14 Bonfield, W.; Tully, A. E., *J. Biomed. Engng.*, **4**,1982, 23-27

15 Evans, G. P.; Bonfield, W., *J. Mater. Sci.: Materials in Medicine*, **1**, 1990, 38-43

16 Hobatho, M. C.; Ashman, R. B., *J. Biomechanics*, **22**, 1989, 895-900

17 Charalambides, B., *Fracture Toughness of Cortical Bone-The Effect of Specimen Geometry*, Ph. D. Thesis, Queen Mary & Westfield College, University of London, 1984

18 Evans, G. P., *Bones, Joints and Implants*, Short Course, IRC-in Biomedical Materials, University of London, 1990

19 Raemdonck, W.Van; Duckeyne,P.; Meester, P. De, *Metal and Ceramic Biomaterials*, CRC Press, Chp.6, 1984, 143-146

20 Ducheyne, P., *J. Biomed. Mater. Res.: Applied Biomaterials*, **21**, A2, 1987, 219-236

21 Hench, L. L., *J. Am. Ceram. Soc.*, **7**, 1991, 1487-1510

22 Heimke, G., *Euro-Ceramics*, Vol. 13, Elsevier, 1989, 3.1-3.10

23 Pernot, F.; Baldet, P., *Ceramics in Surgery*, Elsevier, 1983, 177-186

24 Hench, L. L.; Andersson, O. H.; Latorre, J. P., *Bioceramics 4*, Butterworth Heinemann Ltd., London, U. K., 1991, 155-162

25 Jarcho, M., *Bioceramics 1*, Ishiyaku EuroAmerica, Inc., Kyoto, Japan, 1989, 57-61

26 Hench, L. L., *J. Biomed. Mater. Res.*, **23**, 1989, 685-703

27 Hastings, G. W., *Advances in Biomaterials*, Short Course, IRC-in Biomedical Materials, University of London, 1990

28 Kanazawa, T., *Inorganic Phosphate Materials*, Elsevier, 1989

29 Collin, R. L., *J. Am. Chem. Soc.*, **81**, 1959, 5275-5279

30 Newsley, H., *Inorg. Chem.*, **95**, 1963, 270-274

31 Jarcho, M; Bolen, C. H.; Thomas, M. B.; Bobick, J., *J. Mater. Sci.*, **11**, 1976, 2027-2035

32 Kijima, T.; Tsutsumi, M., *J. Am. Ceram. Soc.*, **62**, 1979, 455-460

33 Hirano, M.; Takeuchi, H.; Ono, M., *Ceramic Developments*, Materials Science Forum Vol.34, Trans. Tech. Publications Ltd., 1988, 1338-1343

34 Xingdong, Z.; Jiyong C.; Jiming, Z.; Jianqing, F.; Cheguei, L., *Clinical Materials*, **4**, 1989, 319-327

35 Denissen, H.; Mangano, C.; Venini, G., *Hydroxyapatite Implants*, Piccin Nuova Libraria, Padua, 1985

36 Puajindanetr, S.; Best, S.; Lorprayoon, C.; Bonfield, W., *Bioceramics 4*, Butterworth Heinemann Ltd., London, UK, 1991, 373-374

37 Rao, W. R.; Boehm, R. F., *J. Dent. Res.*, Nov-Dec, 1974, 1351-1354

38 Ioku, K.; Yoshimura, M.; Somiya, S., *Mat. Res. Soc. Symp. Proc.*, **110**, 1989, 445-450

39 Somiya, S.; Ioku, K.; Yoshimura, *Ceramic Developments*, Materials Science Forum Volumes, Vol. 34, Trans. Tech. Publications Ltd., 1988, 371-378

40 Heughbaert, J. C.; Bonel, G., *Biological and Biomechanical Performance of Biomaterials*, Elsevier, 1986, 9-14

41 Rey, C; Fréche, M., *Bioceramics 4*, Butterworth Heinemann Ltd., London, U. K., 1991, 57-64

42 McConnell, D., *Archs. Oral Biol.*, **10**, 1965, 421-427

43 De Groot, K., *Biomaterials 1*, Butterworth Heinemann Ltd., Kyoto, Japan, 1989, 47-50

44 Reed, J., *Introduction of Principles of Ceramic Processing*, John Wiley & Sons, 1988

45 Barringer, E.; Jubb, N., *Ultrastructure Processing of Ceramics and Glasses*, J. Wiley & Sons, 1984

46 Coble, R. L.; Burke, J. E., *Progress in Ceramics Science*, Vol. 3, Pergamon Press, 1963

47 Best, S.; Bonfield, W.; Doyle, C., *Bioceramics 1*, Ishiyaku EuroAmerica, Inc., kyoto, Japan, 1989, 68-72

48 Rootare, H.; Craig R. G., *J. Oral Rehabil.*, **5**, 1978, 293-307

49 Ellies, L. G.; Nelson, D. G. A.; Featherstone, J. D. B., *J. Biomed. Mater. Res.*, **22**, 1988, 541-553

50 Bigi, A.; Incerti, A.; Rovieri, N.; Ravaglioli, A., *Biomaterials*, **1**, 1980, 140-144

51 Simões, L. P.; Correia, R. N., *Bioceramics 4*, Butterworth Heinemann Ltd., London, U. K., 1991, 91-97

52 Galassi, C.; Roncari, E.; Ravaglioli, A.; Martinetti, R., *Euro-Ceramics*, Vol.13, Elsevier, 1989, 3.43-3.47

53 Smith, W. F., *Principles of Materials Science and Engineering*, McGraw-Hill Inc., 1986

54 Askeland, D. R., *The Science and Engineering of Materials*, Van Nostrand Reinhold International Co. Ltd., 1988

55 Andersson, J. C.; Leaver, K. D.; Rawlings, R. D.; Alexander, J. M., *Materials Science*, 4th Edt, Chapman and Hall, 1988

56 Kellett, B.; Lange, F. F., *J. Am. Ceram. Soc.*, **5**, 1989, 725-734

57 Vieira, J. M., *Introdução aos Modelos de Sinterização*, Internal Publication, University of Aveiro, 1983

58 Shaw, N. J.; Brook, R. J., *J. Am. Ceram. Soc.*, **69**, 107-110, 1986

59 Cahoon, H. P.; Christensen, C. J. , *J. Am. Ceram. Soc.*, **39**, 1956, 337-344

60 Coble, R. L., *J. of Applied Physics*, **32**, 5, 1961, 787-792

61 Coble, R. L., *J. of Applied Physics*, **32**, 5, 1961, 793-799

62 German, R. M., *Liquid Phase Sintering*, Plenum Press, 1985

63 Monteiro, R., *Sinterização em Presença de Fase Líquida*, Mestrado em Engª de Materiais, University of Nova de Lisboa, 1991

64 Assolant, D. B., *Improvements in Bioceramic Technology Biomaterials-Hard Tissue Repair and Replacement*, Elsevier, 1990

65 Oonoshi, H., *Biomaterials*, **12,** March, 1991, 171-178

66 Cavalheiro, J. R., *Quintessência*, **1**, 1990, 69-75

67 Hastings, G. W.; Daily, D., *Bioceramics 1*, Ishiyaku EuroAmerica, Inc., Kyoto, Japan, 1989, 355-358

68 Daculsi, G.; Passuti, N., *Bioceramics 1*, Ishiyaku EuroAmerica, Inc., Kyoto, Japan, 1989, 375-381

69 Hasegawa, S.; Furuya, K., *Bioceramics 1*, Ishiyaku EuroAmerica, Inc., Kyoto, Japan, 1989, 382-387

70 Osborn, J. F., *Biomedizinische Technik*, **7-8**, 1987, 177-183

71 De Groot, K., *High. Tech. Ceram.*, Elsevier, 1987, 381-386

72 Nishihara, K.; Akagawa, T., *Bioceramics 4*, Butterworth Heinemann Ltd., London, U. K., 1991, 223-230

73 Rivero, D. P.; Fox, J., *J. Biomed. Mater. Res.*, **22**, 1988, 191-201

74 Thomas, K. A.; Kay, J. F., *J. Biomed. Mater. Res.*, **21**, 1987, 1305-1414

75 De Groot, K.; Geesink, R., *J. Biomed. Mater. Res.*, **21**, 1987, 1375-1381

76 Geesink, R.; De Groot, K., *Chemical Implant Fixation*, **225**, 1987, 147-170

77 Dhert, W. J. A.; Klein, C. P. A. T., *J. Biomed. Mater. Res.*, **25**, 1991, 1183-1200

78 Filiaggi, M. J.; Coombs, N. A., *J. Biomed. Mater. Res.*, **25**, 1991, 1211-1229

79 Ducheyne, P.; Healy, K., *Bioceramics 1*, Ishiyaku EuroAmerica, Inc., Kyoto, Japan, 1989, 359-364

80 Ducheyne, P.; Radin, S., *Bioceramics 1*, Ishiyaku EuroAmerica, Inc., Kyoto, Japan, 1989, 365-374

81 Van Vlack, L. H., *Elements of Materials Science and Engineering*, 5th Edition, Addison-Wesley Publishing Company, 1985

82 Rizkalla, A.; Jones, D. W., *Br. Ceram. Trans. J.*, **91**, 1992, 12-15

83 Hench, L. L.; Stanley, H. R., *Bioceramics 4*, Butterworth Heinemann Ltd., London, U. K., 1991

84 Hench, L. L.; Latorre, J. P., *Bioceramics 5*, Kobunshi Kankokai, Kyoto, Japan, 1992, 67-74

85 Moroni, A.; Giannini, S., *Bioceramics 2*, Heidelberg, Germany, 1989, 125-131

86 Andersson, O. H.; Guizhi, L., *J. Mater. Sci.: Materials in Medicine*, **1**, 1990, 219-227

87 Andersson, O. H.; Kangasniemi, I., *J. Biomed. Mater. Res.*, **25**, 1991, 1019-1030

88 Ebisawa, Y.; Kokubo, T., *J. Mater. Sci.: Materials in Medicine*, **1**, 1990, 239-244

89 Rawlings, R. D.; Rogers, P. S., *Ceramics in Clinical Applications*, Elsevier, 1987, 73-82

90 Kitsugi, T.; Yamamuro, T., *J. Biomed. Mater. Res.*, **21**, 1987, 1109-1123

91 Amir, D.; Gross, U., *Biomaterials*, **10**, 1989, 585-589

92 Kitsugi, T.; Yamamuro, T., *J. Biomed. Mater. Res.*, **23**, 1989, 631-648

93 Wolf, M. B., *Glass and Science Technology*, Vol. 7, Elsevier, 1984, 208

94 Burnie, J.; Gilchrist, T. G., *Ceramics in Surgery*, Elsevier, 1983, 169-176

95 William, Y. N.; Lee, E., *J. Am. Ceram. Soc.*, **75**, 1992, 1641-47

96 Nagase, M.; Abe, Y., *Biomaterials*, **13**, 1992, 172-175

97 Davidge, R. W., *Mechanical Properties of Ceramics*, Cambridge University Press, 1980

98 Lawn, B. R.; Wilshaw, T.R.,*Fracture of Brittle Solids*, Cambridge University Press, 1975

99 Andersson, T. L., *Fracture Mechanics-Fundamentals and Applications*, Cambridge University Press, 1990

100 Ashby, M. F.; Jones, D. R., *Engineering Materials 1-An Introduction to their Properties and Applications,* Pergamon Press, 1986

101 Ewalds, H. L., *Fracture Mechanics*, Chapman and Hall Inc., 1989

102 Davidge, R. W., *Contemp. Phys.*, **10**, 2, 1969, 105-124

103 Griffith, A. A., *Philos. Trans. R. Soc. Lond.*, A221, 1920, 163-180

104 Kirchner, H. P., *Strengthening of Ceramics. Treatments, Test and Design Applications*, Marcel Decker Inc., 1979

105 Rosa, L. G.; Fernandes, J. J.; Silva, C. P., *Algumas Considerações sobre os Ensaios Usados na Caracterização do Comportamento Mecânico de Cerâmicos*, Internal Publication, Departamento de Tecnologia de Materiais, LNETI, 1989

106 Duckworth, W. H., *J. Am. Ceram. Soc.*, **34**, 1951, 1-9

107 Sedlacek, R.; Haldeen, A., *The Review of Scientific Instruments*, **33**, 2, 1962, 298-300

108 Ashby, M. F.; Jones, D. R., *Engineering Materials 2-An Introduction to Microstructures, Processing and Design*, Pergamon Press, 1986

109 Rootare, M. H.; Powers, J. M., *J. Dent. Res.*, July-Aug., 1978, 777-783

110 Akao, M.; Aoki, H.; Kato, K., *J. Mater. Sci.*, **16**, 1981, 809-812

111 Stanley, P., *Mechanical Strength Testing of Compacted Powders*, Internal Publication, Queen Mary & Westfield College, University of London, 1991

112 *Standard Test Methods for Flexural Properties of Unreinforced and Reinforced Plastics and Electrical Insulating Materials*, ASTM, D 790 M-82

113 *Standard Methods of Bend Testing of metallic Flat Materials for Spring Applications*, ASTM, E 855-84

114 Best, S.; Bonfield, W., *Bioceramics 2*, Heidelberg, Germany, 1989, 57-64

115 With, G. De; Van Dijk, H. J. A.; Hattu, N., *J. Mater. Sci.*, **16**, 1981, 1592-1598

116 Kirstein, A. F.; Woolley, R. M., *Journal of Research of the National Bureau of Standards* , 71C, **1**, Jan-Mar, 1967

117 Soltesz, U.; Ritcher, H.; Kienzler, R., *Ceramics in Clinical Applications*, Elsevier, 1987, 149-158

118 Fricker, D. C., *Ceramics in Clinical Applications*, Elsevier, 1987, 139-148

119 Watchtman, J. B.; Capps, W.; Mandel, J., *J. of Materials*, **7**, 2, 1972, 188-194

120 Godfrey, D. J., *British Ceramic Proceedings*, **39**, 1987, 133-140

121 Giovan, M. N.; Sines, G., *J. Am. Ceram. Soc.*, **62**, 9-10, 1989, 510-515

122 Marshall, D. B., *Ceram. Bull.*, **59**, 5, 1980, 551-554

123 Shetty, K.; Rosenfield, A. R.; Bansal, G. K., *Ceram. Bull.*, **59**, 12, 1980, 1193-1197

124 Weibull, W., *J. Applied Mechanics*, Sept., 1951, 293-297

125 Braiden, P. M., *An Introduction to Weibull Statistics*, Internal Publication, Harwell U. K. Company, 1975

126 Davies, D. G. S., *British Ceramic Society*, **22**, 1973, 429-487

127 Evans, A. G., *J. Mater. Sci.*, **7**, 1972, 1137-1146

128 Almond, E. A.; Roebuck, B., *Metal and Materials*, Feb., 1986, 76-82

129 Braiden, P. M., *Fracture Mechanics of High Temperature Ceramics*, Internal Publication, Department of Ceramics, Staffordshire University, 1990

130 *Standard Method for Plane-Strain Fracture Toughness of Metallic Materials*, ASTM, E 399-83

131 Orange, G; Liang, K. M., *Science of Ceramics*, **14**, Elsevier, 1988, 709-714

132 Ritcher, H.; Seidelmann, U., *Evaluation of Biomaterials*, John Wiley & Sons Ltd., 228-232

133 Singh, D.; Shetty, D. K., *J. Am. Ceram. Soc.*, **72**, 1989, 78-84

134 Sano, O., *J. Mater. Sci.*, **23**, 1988, 2505-2511

135 Bradt, R. C.; Lange, F. F., *Fracture Mechanics*, Plenum Press, New York, 1973

136 Lawn, B. R.; Swain, M. V., *J. Mater. Sci.*, **10**, 1975, 113-122

137 Lawn, B. R., *J. Mater. Sci. Letters*, **11**, 1976, 573-575

138 Laugier, M. T., *J. Mater. Sci. Letters*, **6**, 1987, 355-356

139 Ponton, C. B.; Rawlings, R. D., *Br. Ceram. Trans. J.*, **88**, 83-90, 1989

140 Mestral, F. de; Drew, R. A. L., *J. European Ceram. Soc.*, **5**, 1987, 47-53

141 Chantikul, P.; Anstis, G. R.; Lawn, B. R.; Marshall, D. B., *J. Am. Ceram. Soc.*, **64**, 9, 1981, 539-543

142 Neuerburg, G. J., *J. Res. U. S. Geol. Sur.*, **3**, 1975, 377-378

143 Sotera, J. J.; Stux, R. L., *Standard Operations for Flame Operations*, Vol. 1, Instrumental Laboratory Inc., 1977

144 *Standard Metods for the examination of Water and Wastewater*, American Public health association, Inc., 15th edition, 1980

145 Dudley, H. W.; Fleming, I., *Spectroscopy Methods in Organic Chemistry*, McGraw-Hill Book Company, 1980

146 Fowler, B. O., *Inorg. Chemistry*, **13**, 1, 194-207, 1974

147 Smith, R. *Infrared Studies on Calcium Hydroxyapatite*, Internal Communication, IRC-in Biomedical Materials, University of London, 1990

148 Allen, T., *Particle Size Measurements*, Chapman and Hall, 1981

149 Haertlein, J., *Characteristics, Testing and Applications of Metal Powders*, John Wiley & Sons, 1974

150 Allen, W., *Malvern Mastersizer Principles of Operation* , IM 100, Issue 3, Malvern Company Ltd, U. K., 1989

151 Soltesz, U.; Ritcher H., *Metal and Ceramic Biomaterials*, Chp. 2, CRC Press, 1984, 23-61

152 *Testing Method for Flexural Strength (Modulus of Rupture) of High Perfomance Ceramics*, JIS R 1601, 1981

153 Urry, S. A.; Turner, P. J., *Solution of Problems in Strength of Materials and Mechanics of Solids*, Pitman Publishing Ltd.,1976

154 Feodosiev, V. I., *Resistencia de Materiales*, Editorial Mir, URSS 1980

155 Holand, W.; Vogel, W, *Bioceramics 2*, Heidelberg, Germany, 1989, 97-104

156 Abe, Y.; Hosono, H., *Bioceramics 1*, Ishiyaku EuroAmerica, Inc., Kyoto, Japan, 1989, 181-186

157 Kotani, S.; Yamamura, T., *Bioceramics 2*, Heidelberg, Germany, 1989, 105-122

158 Kokubo, T.; Kushita, H., *Bioceramics 1*, Ishiyaku EuroAmerica, Inc., Kyoto, Japan, 1989, 157-162

159 Kokubo, T., *Biomaterials*, **12**, 1991, 155-163

160 Shimizu, K.; Iwasaki, R.; Matsushita, M, *Bioceramics 5*, Kobunshi Kankokai, Kyoto, Japan, 1992, 435-441

161 Yoshii, S.; Kakutani, Y., *J. Biomed. Mater. Res.: Applied Biomaterials*, **22**, Nº A3, 1988, 327-338

162 Kangasniemi, J. M. O.; De Groot, K., *J. Biomed. Mater. Res.*, **26**, 1992, 664-674

163 Kitsugi, T.; Yamamuro, T., *J. Biomed. Mater. Res.*, **24**, 1990, 259-273

164 Ohtsuki, C.; Aoki, Y., *Bioceramics 5*, Kokunshi Kankokai, Kyoto, Japan, 1992, 87-94

165 Sedel, L.; Fumery, P., *Bioceramics 5*, Kokunshi Kankokai, Kyoto, Japan, 1992, 427-434

166 Holand, W.; Volksch, *Bioceramics 4*, Butterworth Heinemann Ltd., London, U. K., 1991, 171-178

167 Kitsugi, T.; Yamamuro, T., *Bioceramics 1*, Ishiyaku EuroAmerica, Inc., Kyoto, Japan, 1989, 169-174

168 Hodgskinson, R. A.; Bonfield, W., *Advances in Biomaterials*, Vol. 8, Elsevier,1988, 233-237

169 Lopes, A. B.; Correia, R. N.; Fonseca, A. T., *Bioeng 90*, Aveiro, Portugal, 1990, 141-146

170 Harrison's, *Principles of Internal Medicine*, 9th Edition, McGraw-Hill Book Company, 1980

171 Fabre, R.; Thuhaut R., *Toxicologia*, Fundação Calouste Gulbenkian, Lisboa, 1971.

172 Yamashita, K.; kitagaki, K.; Umegaki, T.; Kanazawa, T., *J. Mater. Sci. Letters*, **9**, 1990, 4-6

173 Marraha, M.;Heughbaert, J. C.; Bonel, G., *Biomaterials and Biomechanics*, Elsevier,1983, 445-450

174 Tudor, A. M.; Davies, M. C.; Santos, J. D.; Hastings, G. W.; Barbosa, M. A., The Analysis of Biomedical Hydroxyapatite Powders and Hydroxyapatite Coatings on Metallic Medical Implants by Near-Infrared FT-Raman Spectroscopy, accepted for publication in *Spectrochimica Acta*

175 Hornung, R.; Engel, A., Preparation and Characterisation of Ivory Coloured Hydroxyapatite, accepted for publication in *J. Mater. Sci.*

176 Hirayama, Y.; Ikata, H.; Akyyama, H., *Ceramic Developments*, Materials Science Forum Vol.34, Trans. Tech. Publications Ltd., 1988, 1332-1337

177 Akao, M.; kato, A., *J. Mater. Sci.*, **17**, 1982, 343-346

178 Krajewski, A.; Ravaglioli, A., *J. Biomed. Mater. Res.*, **22**, 1988, 445-457

179 Hon, M.; Lin, F. H., *High Tech. Ceramics*, Elsevier, 1987, 43-51

180 Rey, C., *Biomaterials*, **11**, 1989, 13-15

181 Klein, P. A. T. C.; De Groot, K., *J. Biomed. Mater. Res.*, **25**, 1991, 53-65

182 Oonishi, H.; Aoki, H., *Bioceramics 2*, Heidelberg, Germany, 1989, 57-64

183 Levin E. M.; Rabbins, C. R.; Mcmurdie, H. F., *Phase Diagrams for Ceramists*, Vol. 4, American Ceramic Society, 1981, 88-177

184 Parker, B., *A Feasibility Study into the Drawing of Phosphate Fibres*, Research report, Pilkington Technology Centre, 1989

185 Ji, Huaxia; Marquis, P. M., *Biomaterials*, **13**, 11, 1992, 744-748

186 Goto, T.; Wakamatsu, N.; Kamemizu, H., *J. Mater. Sci.: Materials in Medicine*, **2**, 1991, 149-152

187 Yamashita, K.; Kobayashi, *Ceramics in Surgery*, Elsevier, 1983, 1320-1325

188 Ioku, K.; Yoshimura, M.; Somiya, S., *Biomaterials*, **11**, 1990, 57-61

189 Forberg, J. L.; Hermansson, L., *Biomaterials*, **12**, 1991, 438-440

190 Downes, R. N.; Vardy, S., *Bioceramics 4*, Butterworth Heinemann Ltd., London, UK, 1991

191 Smith, *Polymeric Materials*, Short Course, IRC-in Biomedical Materials, University of London, 1990

192 Deb, S., *Degradable Polymers*, Short Course, IRC-in Biomedical Materials, University of London, 1990

193 De Groot, K, *Ceramics in Surgery*, Elsevier, 1983, 90-98

194 Puajindanetr, S.; Best, S; Bonfield, W., *Bioceramics 5*, Kokunshi Kankokai, Kyoto, Japan, 1992, 23-28

195 Petch, N. J. *Cleavage Strength of Polycrystals*, Iron and Steel Inst., London, 1974

196 Akao, M.; Miura, N.; Aoki, H., *Yogyo-Kyokai-Shi*, **11**, 1984, 78-81

197 Kokubo, T.; Ito, S.; Yamamuro, T., *J. Mater. Sci.*, **20**, 1985, 2001-2004

198 Manabe, T.; Shigematsu, M., *High Tech. Ceramics*, Elsevier, 1987, 63-72

199 Ono, K.; Yamamuro, T., *J. Biomed. Mater. Res.*, **24**, 1990, 47-63

200 *Standard Test method for Sonic Velocity in Manufactured Carbon and Graphite Materials for Use in Obtaining Young's Modulus*, ASTM, C 769-80

201 Gilmore, B. S.; Katz, J. L., *J. Mater. Sci.*, **17**, 1982, 1131-1141

202 Schreiber, E.; Anderson, O. L., *Elastic Constants and their Measurement*, Chp. 10, McGraw-Hill, 1989

203 Bagambisa, F. B., *J. Mater. Sci.*, **25**, 1990, 5091-5095

204 De Groot, K., *Ceramics in Surgery*, Elsevier, 1983, 79-90

205 Osborn, J. F., *Biomaterials*, **1**, 1980, 108-111

206 Driessens, F. C., *Euro-Ceramics*, Vol.13, Elsevier, 1989, 3.48-3.52

207 Hyakuna, K.; Yamamuro, T., *J Biomed. Mater. Res.*, **24**, 1990, 471-488

208 Ribeiro, C. C.; Barbosa, M. A., *Bioceramics 4*, Butterworth Heinemann Ltd., London, U. K., 1991, 145-153

209 Hyakuna, K.; Yamamuro, T., *J. Biomed. Mater. Res.*, **24**, 1990, 471-488

210 Thomas, M. B.; Doremus, R. H., *J. Mater. Sci.*, **15**, 1980, 891-894

=APENDICES=

Appendix 1

Weibull statistics

This Appendix describes the application of Weibull statistics for samples sintered at 1300°C. The same process was used for all other HA samples and HA-glass composites.

Table 1 Application of Weibull statistics to samples sintered at 1300°C

P_{si}	Strength MPa	$\ln\left\{\ln\left(\frac{1}{Ps}\right)\right\} = y$	$\ln\left(\frac{\sigma}{\sigma_o}\right) = x$
0.93	18.7	-2.623	-0.521
0.84	21.4	-1.746	-0.386
0.74	22.7	-1.200	0.327
0.64	24.5	-0.806	-0.250
0.55	26.8	-0.514	-0.161
0.45	30.3	-0.225	-0.038
0.36	32.0	0.021	0.016
0.26	33.6	0.297	0.065
0.16	34.9	0.605	0.103
0.07	36.0	0.980	0.134

P_{si} values were calculated from equation (III.18). σ_o value was determined by a fitting procedure, considering two points below and above the point correspondent to σ_o:

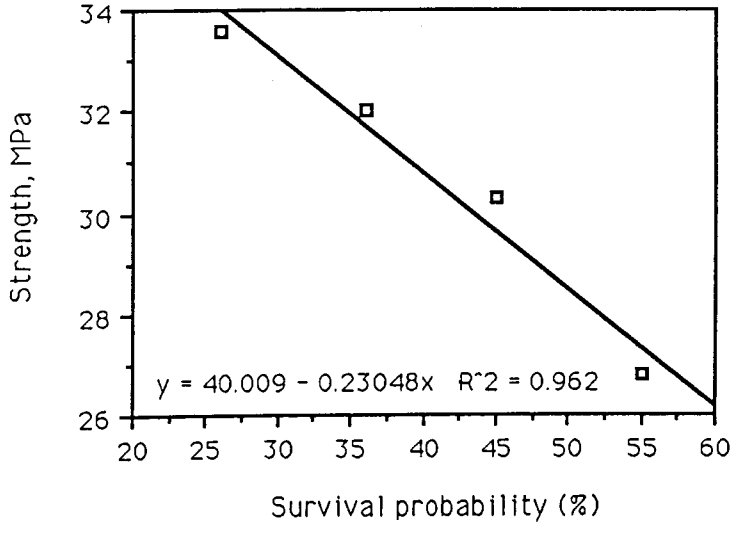

Figure 1 Calculation of σ_o value

It follows, from the graph: σ_o=31.48. Weibull's modulus was finally determined by the following procedure:

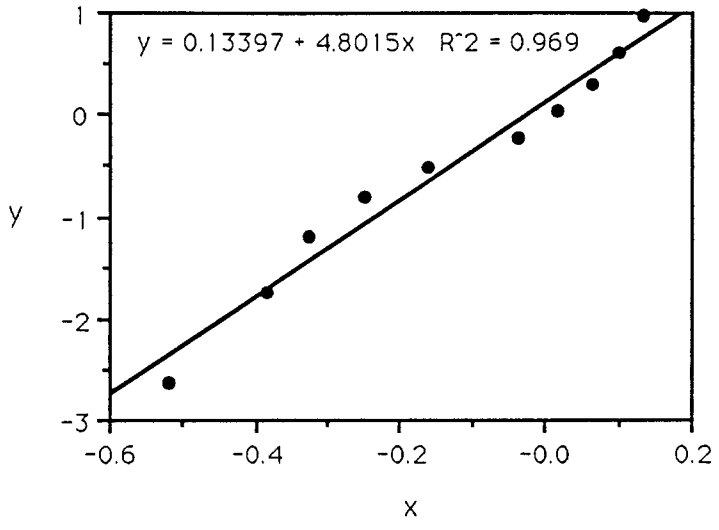

Figure 2 Calculation of Weibull modulus

Appendix 2

Estimation of phase proportions

In order to estimate the phase proportions in the microstruture of HA-2.5wt% phosphate glass composites, three HA/β–TCP and three HA/α-TCP powder mixtures were used to establish the calibration curve, with 90/10, 70/30 and 50/50 relative wt%, respectively. The powders were weighed with an accuracy of ±0.0001g, and mixed in a ball mill pot for 24 h before x-ray analysis. The peak height ratios between the three main peaks of HA and TCP were used for the calculation, using the fitting procedure in the Phillips P-1877 software. Table 1 presents the calculated ratios for the HA/β–TCP.

Table 1 Peak height ratios between HA and β-TCP

Mixture HA/β–TCP	1st peak HA/β–TCP	2th peak HA/β–TCP	3th peak HA/β–TCP	Mean ratio
90/10	9.10	9.32	8.71	9.04±0.31
70/30	2.42	2.71	2.19	2.44±0.26
50/50	0.98	1.32	0.91	1.07±0.22

Based on these results, a calibration curve was established as may be seen in Figure 1.

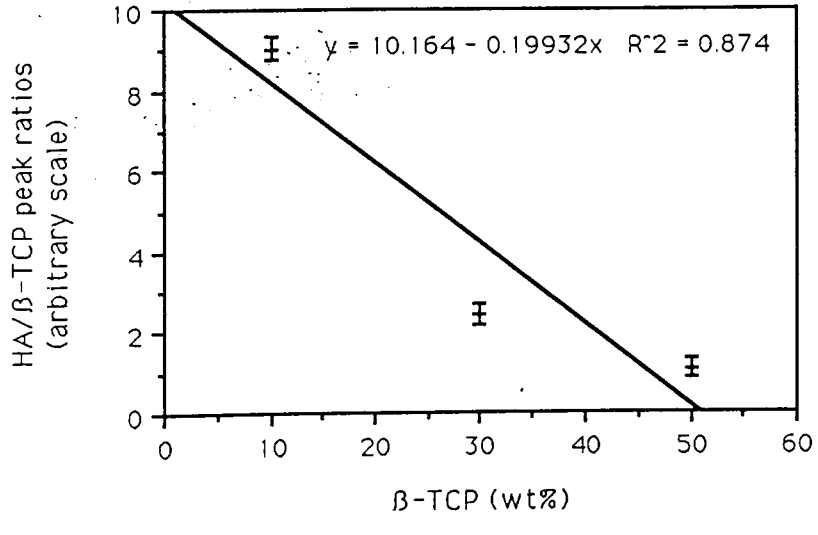

Figure 1 Calibration curve for HA/β–TCP mixtures

Using this calibration curve, phase proportions were estimated for samples fired at 1250°C, where only HA/β–TCP were present. Similarly, another calibration curve was also established for the HA/α-TCP mixtures, as is shown in Figure 2.

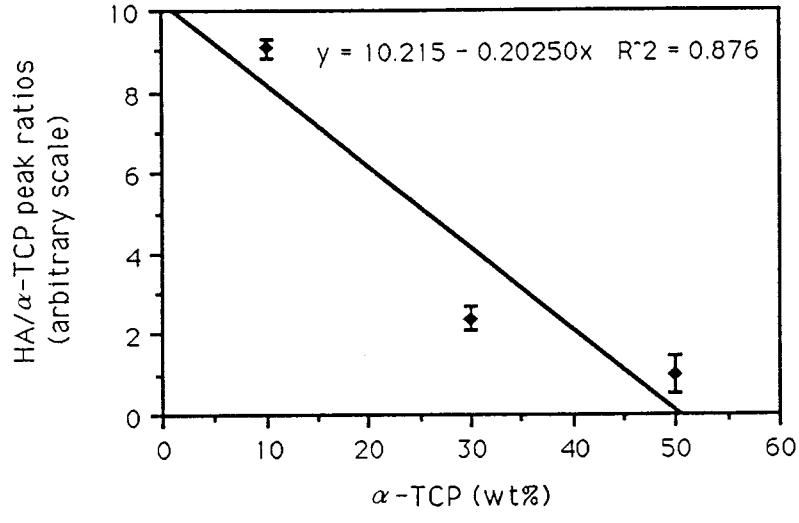

Figure 2 Calibration curve for HA/α–TCP mixtures

For microstructures presenting the three phases i.e., samples sintered above 1250°C, a calibration curve based on the HA/β–TCP/α-TCP mixtures would have been required. However, when the proportions of the three phases are significant, the calculation of the ratios between height peaks is difficult to perform, as they are mostly present in a tight 2θ interval between 31 and 35° approximately, and strong overlapping effects occur. This effect was also found for the HA-5wt% composites, where much higher proportions of β–TCP and α–TCP than those for 2.5wt% additions were found, and therefore this calculation method was abandoned. In these cases software to deconvolute the peaks is required.

As the peak height ratios between HA/β–TCP and HA/α–TCP phases were basically the same as the mixtures wt% ratios, as seen in Table 1 and Figures 1 and 2, it was decided to estimate the phase proportions based only on the relative peak height ratios of the x-ray diffraction spectra. It should be emphasised that a similar process was also used by kokubo (197) to estimate the phase proportions of an apatite phase, wollastonite and β–TCP, in A-W glass ceramics, without using any calibration curve.

Appendix 3

The HA-glass composites developed on this work are covered by the British Patent **'Densified Hydroxyapatite'**, Nº 9213774.4, filed on 29/06/92, by the authors: *J. D. Santos*, J. C. Knowles, G. W. Hastings and W. Bonfield.

Based on this work, the following publications were written:

- *Santos, J. D.*; Morrey, S.; Hastings, G. W.; Monteiro, F. J., **'The Production and Characterisation of a Hydroxyapatite Ceramic Material'**, Bioceramics 4, Butterworth-Heinemann Ltd, London, U.K., 1991, 71-78

- *Santos, J. D.*; Knowles, J. C.; Morrey, S.; Monteiro, F. J.; Hastings, G. W., **'Development of a Glass Reinforced Hydroxyapatite with Enhanced Mechanical Properties: Physical characterisation and 'in vitro' studies'**, Bioceramics 5, Kobunshi Kankodai, Kyoto, Japan, 1992, 35-41

- *Santos, J. D.*; Knowles, J. C.; Reis, R. L.; Monteiro, F. J.; Hastings, G. W, **'Microstructural Characterisation of Glass Reinforced Hydroxyapatite Composites'**, Submitted for publication in 'Biomaterials'

Complementary work has been carried out on HA and HA-glass composites, which led to other publications:

-Tudor, M. C.; Davies, M. C.; Hastings, G. W.; *Santos, J. D.;* Monteiro, F. J.; Barbosa, M.; Morrey, S., **'The Analysis of Biomedical Hydroxyapatite powders and Hydroxyapatite coatings on Metallic Medical**

implants by Near-Infrared FT-Raman Spectroscopy', Accepted for publication in 'Spectrochimica Acta'

- Reis, R. L; *Santos, J. D.*; Monteiro, F. J., **'Influência da Temperatura de sinterização na Composição fásica de Compósitos de Hydroxyapatite Reforçada'**, Accepted for presentation at the 4th Conference of SPM, Materiais-93

- Leadley S. R.; Davies, M. C.; Johnson, D.; *Santos, J. D.*; Monteiro, F. J.; Hastings, G.W.; Barbosa, **'The Surface analysis of Biomedical hydroxyapatite powders and Hydroxyapatite coatings on Metallic Implants by Secondary Ion Mass spectroscopy & SIMS Imaging'**, Submitted for publication in 'Biomaterials'

- Cavalheiro, J.; Reis, R. L.; Santos, J. D.; Branco, R., Carvalho, B., **In Vitro Apatite Layer Formation on Hydroxyapatite, Synthetic Sintered Bone, HA-Bioglass Composites and HA-Plasma Sprayed Coatings**, Submitted to 'Biointeractions-93'

U.K. PATENT APPLICATION

Number _____

Filing Date 29th June, 1992

Applicant(s) QUEEN MARY AND WESTFIELD COLLEGE

Inventor(s) J.C. Knowles
J.D. Santos
G.W. Hastings
W. Bonfield

Priority Claimed -

Case "Densified Hydroxyapatite"

BOULT, WADE & TENNANT

CLAIMS

1. A sintered enhanced hydroxyapatite which comprises hydroxyapatite, $Ca_{10}(PO_4)_6(OH)_2$, and a biocompatible glass based upon CaO and P_2O_5.

2. A material as claimed in claim 1 wherein the biocompatible glass is contained in an amount of less than 10% by weight based on the weight of hydroxyapatite.

3. A material as claimed in claim 2 wherein the biocompatible glass is contained in an amount of from 2.5% to 5.0% by weight based on the weight of hydroxyapatite.

4. A material as claimed in any one of the preceding claims wherein the biocompatible glass is a two oxide $CaO-P_2O_5$ glass.

5. A material as claimed in any one of claims 1 to 3 wherein the biocompatible glass is a three oxide $CaO-P_2O_5-Na_2O$ glass.

6. A material as claimed in any one of claims 1 to 3 wherein the biocompatible glass is a four oxide $CaO-P_2O_5-Na_2O-Al_2O_3$ glass, or Bioglass.

7. A method for the preparation of a material as claimed in claim 1 which comprises sintering a mixture of hydroxyapatite, $Ca_{10}(PO_4)_6(OH)_2$, and a biocompatible glass based upon CaO and P_2O_5 at a temperature of above 1200°C.

8. A method as claimed in claim 7 wherein the sintering is carried out at a temperature in the

range of from 1250° to 1350°C.

9. A method as claimed in claim 7 or claim 8 wherein the mixture of hydroxyapatite and biocompatible glass has a particle of less than 75 micrometres.

10. A method as claimed in any one of claims 7 to 9 wherein the biocompatible glass is contained in an amount of less than 10% by weight based on the weight of hydroxyapatite.

11. A method as claimed in claim 5 wherein the biocompatible glass is contained in an amount of from 2.5% to 5.0% by weight based on the weight of hydroxyapatite.

12. A method as claimed in any one of claims 7 to 11 wherein the biocompatible glass is a two oxide $CaO-P_2O_5$ glass.

13. A method as claimed in any one of claims 7 to 11 wherein the biocompatible glass is a three oxide $CaO-P_2O_5-Na_2O$ glass.

14. A method as claimed in any one of claims 7 to 11 wherein the biocompatible glass is a four oxide $CaO-P_2O_5-Na_2O-Al_2O_3$ glass, or Bioglass.

15. A bone implant or bone filler which comprises an enhanced hydroxyapatite as claimed in any one of claims 1 to 6.

16. An artificial joint which comprises a coating of an enhanced hydroxyapatite as claimed in any one of claims 1 to 6 on at least a part of a

metal or alloy joint.

17. A composition which comprises an enhanced hydroxyapatite as claimed in any one of claims 1 to 6 together with a pharmaceutically acceptable diluent or carrier.

18. A composition as claimed in claim 17 which is a bone cement or a dental cement.

Bioceramics, Volume 4 Edited by W. Bonfield, G. W. Hastings and K. E. Tanner
(*Proceedings of the 4th International Symposium on Ceramics in Medicine, London, UK, September 1991*)

The Production and Characterisation of a Hydroxyapatite Ceramic Material

J.D. Santos, S. Morrey, G.W. Hastings and F.J. Monteiro*

IRC in Biomedical Materials, Queen Mary and Westfield College, Mile End Road, London, E1 4NS, U.K. and
*Department of Engineering Metallury, Faculty of Engineering, University of Porto, Rua dos Bragas, 4099 Porto, PORTUGAL.

ABSTRACT

The chemical and physical properties of a commercial available hydroxyapatite, $Ca_{10}(PO_4)_6(OH)_2$, powder were determined. Sintering of the powder, to produce a ceramic, was examined using range firing curves. Properties including density, hardness, fracture toughness and microstructure were used to characterize the ceramic. Mineralogical and chemical changes with sintering were measured by X-Ray Diffraction (XRD) and Infra-Red (IR) analysis.

EXPERIMENTAL PROCEDURE

The mineral composition of the starting HAp powder P-120 was analysed by XRD and IR. The XRD was performed in a Philips PW-1710 diffractometer using Cu-Kα radiation at 35 mA and 50 KV. The IR analysis was made from a compressed HAp-KBr disc in a Perkin Elmer 1600 Series FTIR. The Ca/P ratio was measured by Gravimetric Analysis, Photocolourimetric Analysis and Atomic Absorption Spectroscopy (AAS). The trace elements were also determined by AAS. Particle size distribution was obtained by Laser Diffraction using a Malvern Mastersizer MS-20. The surface area was measured using a Rapid Surface Area Analyser by BET method. The thermal behaviour was studied by thermogravimetric analysis using a Stanton Redcroft apparatus. The heating rate was at 6 °C/min followed by natural cooling inside the furnace.

Disc samples of 30 mm diameter x 2 mm height were produced using a single action die lubrificated with silicone oil aerosol in a uniaxial CAM press at 19 MPa. Wet-bag Isostatic pressing at 100 MPa was employed to prepare cylinders of 25 mm diameter x 25 mm height. The samples were sintered at

1200 °C, 1250 °C, 1300 °C and 1350 °C using a heating rate of 4 °C/min, dwell times of 1h and 3h followed by natural cooling inside the furnace.

The density of sintered compacts was measured using Archimedes principle by mercury and the percentage densification calculated assuming the theoretical density of 3.156 g/cm^3. The average grain size was calculated using the linear intercept method[2] from SEM micrographs. The grain bondaries were revealed by etching the samples with a 10 % citric acid solution for 4 min at room temperature. XRD and IR analysis were made to verify any mineralogical transformations occuring during sintering.

The hardness of each sample was tested using a Schimadzu microhardness machine with a 9.8 N load. To obtain a given hardness value at each sintering condition 30 indents were measured. The fracture toughness was calculated by an indentation method according to the following equation formulated by Laugier[1]:

$$K_C = K^p \ (c\text{-}a/a)^{-1/2} \ (E/H)^{2/3} \ P/c^{3/2} \qquad (1)$$

where: **k^p**-Calibration constant **E**-Young's modulus **P**-Load **c**-Crack length **H**-hardness **2a**-Indent diagonal

RESULTS

The mineral composition of the powder P-120 was in agreement with the HAp standard peaks as shown in Figure 1.

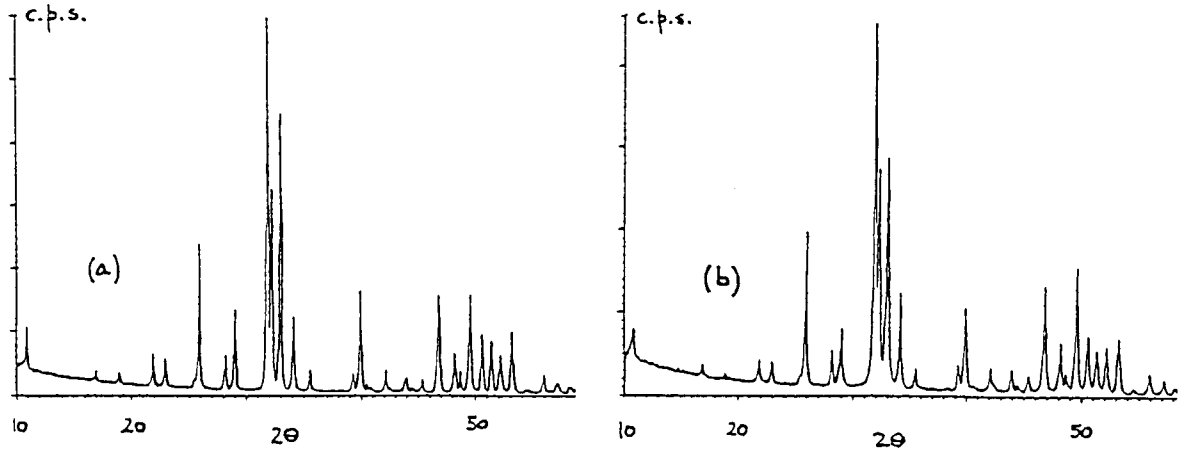

Figure 1-XRD traces of HAp. (a) Powder P-120 (b) After firing at 1350 °C

The IR spectrum shows the presence of PO_4, OH and hydration H_2O (Figure 2).

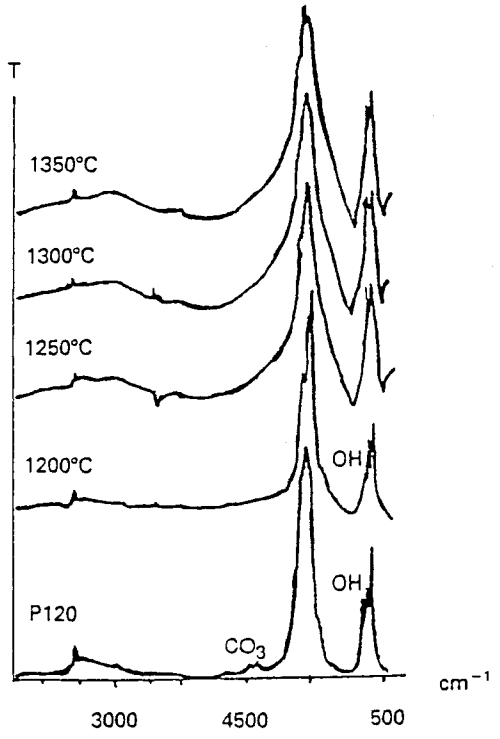

Figure 2-IR trace showing loss of CO_3 and OH during sintering

The Ca/P ratio was 1.687±0.002. A good agreement was obained with the techniques used. The concentration in trace elements were (ppm): Fe-240, Al-200, Si-1200, Cu-10 and Mg-2000. The surface area was 16.9 m^2/g. The particle size distribution profile is shown in Figure 3. The values of the median particle size ($D_{0.5}$) and the particle diameter at 10% and 90% ($D_{0.1}$ and $D_{0.9}$) were also recorded.

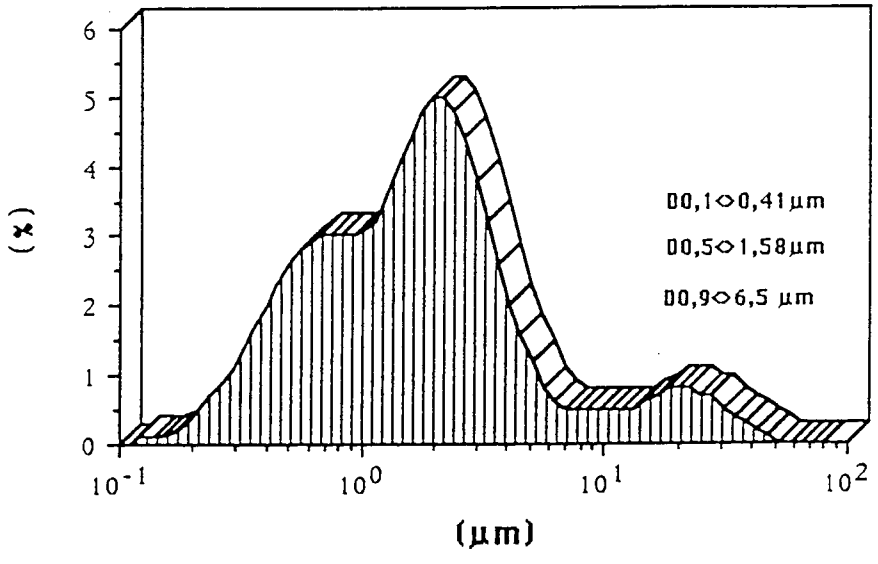

Figure 3-Particle size distribution of powder P-120

The thermogravimetric analysis is shown in Figure 4.

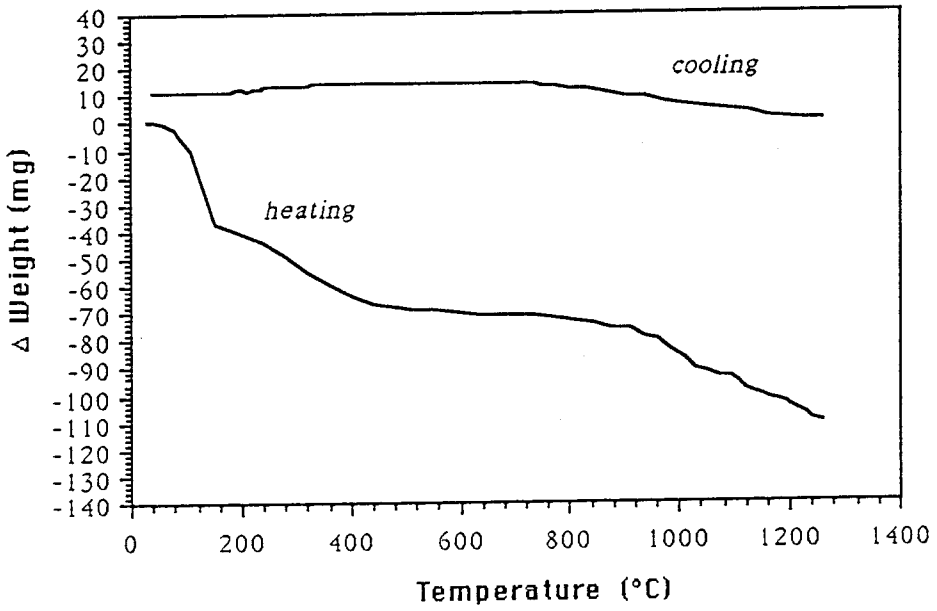

Figure 4-Thermogravimetric analysis

The densification of the HAp for sintering conditions studied is shown in Figure 5 and 6. High density could be achieved by sintering at temperatures above 1250 °C for both 1h and 3h dwell time.

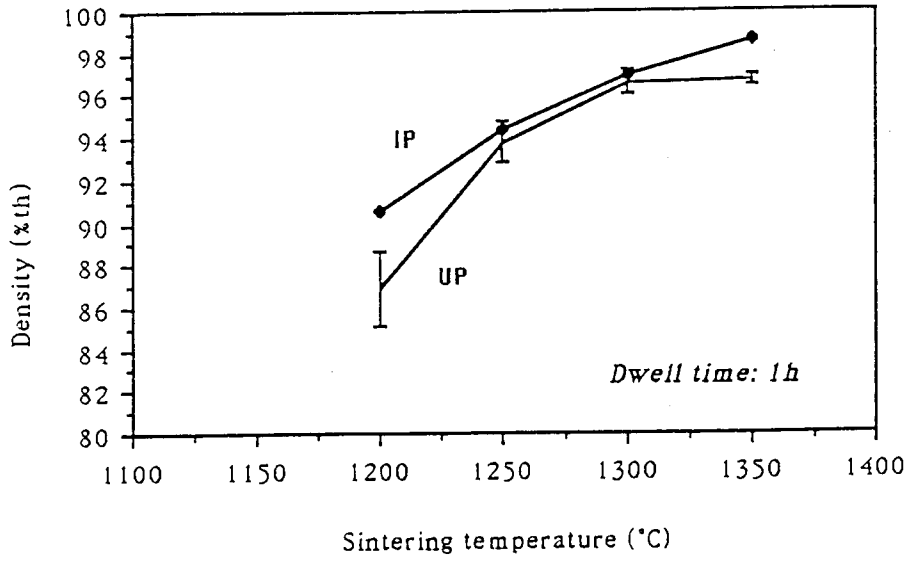

Figure 5- Density versus temperature curves for HAp ceramic

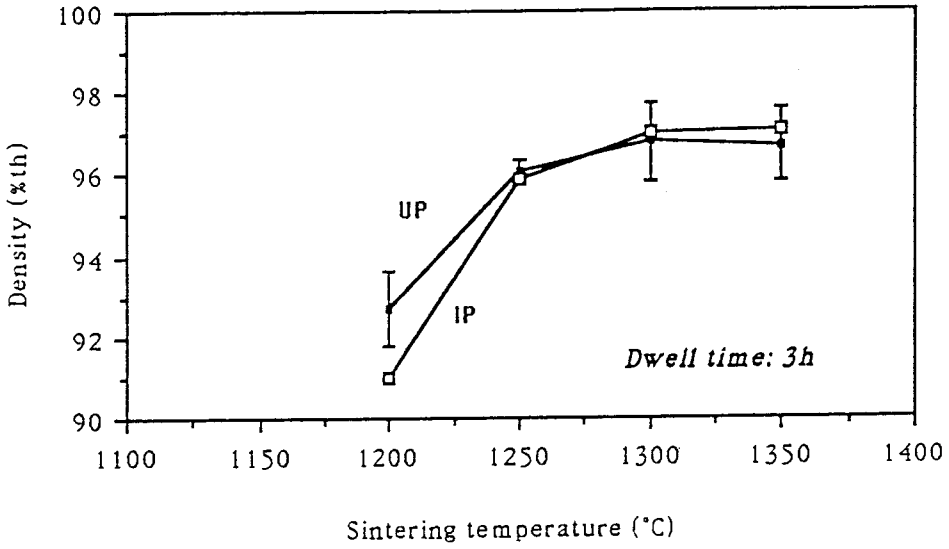

Figure 6-Density versus temperature curves for HAp ceramic

The densification of the HAp was acccompanied of grain growth as indicated in Figure 7.

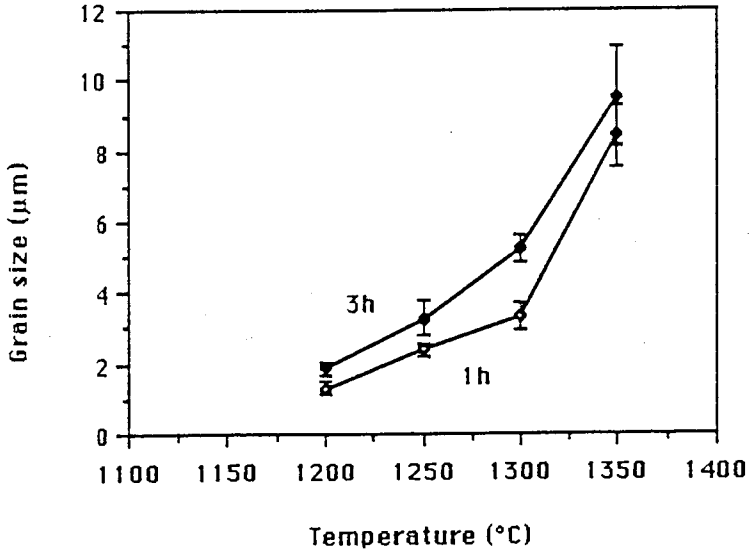

Figure 7-Grain size versus temperature curve for HAp ceramic

The powder P-120 has a high thermal stability since no mineralogical transformation was detected by XRD and IR even when sintered at 1350 °C for 3h (Figure 1b). However, CO_3 was lost when the HAp was heated at high temperatures. Similarly, the OH found at 630 cm^{-1} in IR spectrum disappeared when the HAp was heated above 1200 °C (Figure 2).
The increase in density is followed by an increase in hardness (Figure 8).

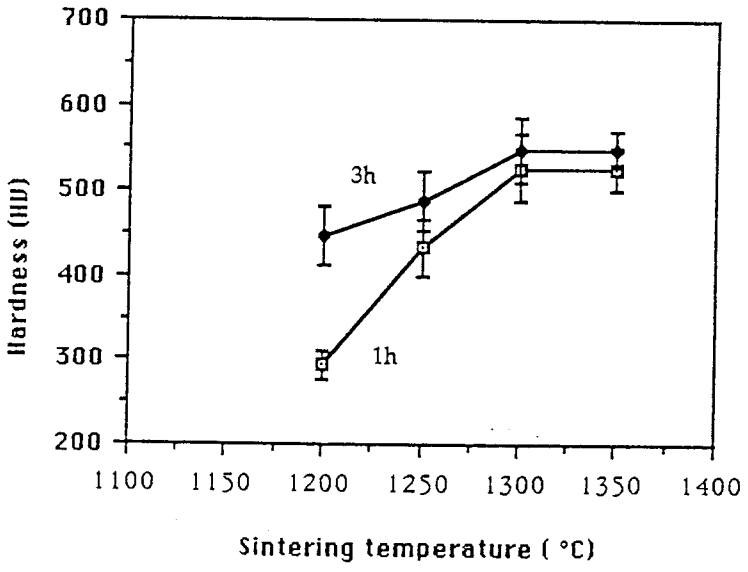

Figure 8-Hardness versus temperature curve for HAp ceramic

The fracture toughness results show an increase of the toughness of the HAp for samples sintered until 1300 °C. Above that temperature a marked decrease occured as can be seen in Figure 9.

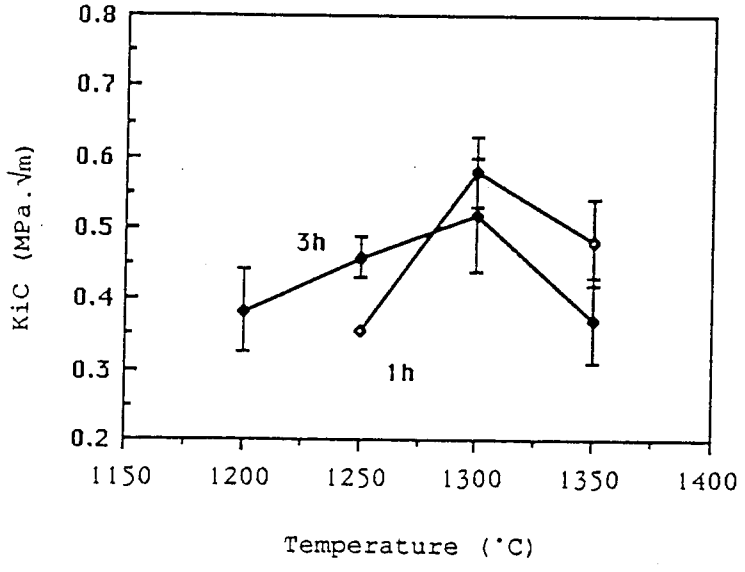

Figure 9-Fracture toughness for HAp ceramic

DISCUSSION/CONCLUSIONS

The higher Ca/P ratio of the powder P-120 as compared to the stoichiometric HAp and the presence of CO_3 seem to indicate that the powder is a type B carbonated HAp where CO_3 substitutes PO_4 in the structure[3,4]. The Laser Diffraction and BET showed that the powder is a finely dispersed HAp, 90% of

the particle size distribution is not ideal for sintering if a high density and uniform texture are required[5].

In the thermogravimetric analysis curve it is possible to see two different zones where the rate of weight loss is high: between 100-400 °C and above 850 °C approximatelly. The weight loss detected at low temperatures is most likely due to the liberation of adsorbed water on HAp surface. The weight loss at higher temperatures than 850 °C is usually attributed to the dehydroxylation of HAp in accordance with the reaction[4]:

$$Ca_{10}(PO4)_6(OH)_2 \leftrightarrow Ca_{10}(PO4)_6(OH)_{2-2x}\ \square_x O_x + xH_2O$$

The symbol $\square$ means a position of vacancy in the HAp structure and x<1. The end product is oxyhydroxyapatite. As the powder contained CO_3 the weight loss detected at high temperatures may also be due to its liberation. The above reaction is reversible. It is possible that the slight increase of weight detected during cooling may be a result of a reincorporation of H_2O present in the furnace's atmosphere. The OH losses during heating seem to be confirmed with IR analysis. The OH peak at 630 cm^{-1} disappeared when the temperature was increased above 1200 °C. A broad band can be seen in the spectrum for powder P-120. These results are in agreement with those reported by Kijima[6]. The densification of the powder P-120 match well with those reported by Akao[7] and DeWith[8]. At temperatures above 1250 °C there is no difference in the density of ceramics shaped by uniaxial or isostatic pressing. The XRD results showed a very stable and crystalline powder. These factors are usually related to stoichiometry of the HAp[2]. The grain size increases rapidly with increasing temperature indicated during sintering of HAp grain growth occurs as in other ceramics.

Fracture toughness results increases in line with density up to 1300 °C. Beyond 1300 °C density remains constant while fracture toughness decreases. This occurs at the same time as the rate of grain growth increases. The decrease in fracture toughness may be related to the increased grain size. The fracture toughness results are in a range of 0.35-0.6 MPa $m^{1/2}$. They are similar to the values reported by Best[9] for a range of powders. Hirayama[10] obtained higher values on hot isostatically pressed HAp of a higher density. In each case fracture toughness was measured by similar technique. Hirayama[10] used a different calculation to obtain fracture toughness. It is likely that all the results overestimate fracture toughness because no account is taken of subsurface lateral cracks[11] Further tests will be conducted to examine these results. When the ceramic is fully characterized hydroxyapatite composites will be produced in an attempt to improve toughness.

REFERENCES

1 Laugier, M.T. J. Mat. Sci 1987, 6, 355-356

2 Jarcho, M. and Bolen, C. H. J. Mat. Sci. 1976, 11, 2027-2035

3 Heughbaert, J. C. In: Biological and Biomechanical Performance of Biomaterials Elsevier Science Publishers, Amsterdam, 1986, 9-14

Development of a Glass Reinforced Hydroxyapatite with Enhanced Mechanical Properties: Physical Characterization and *'in vivo'* Studies

J. D. Santos, J. C. Knowles, S. Morrey, F. J. Monteiro and G. W. Hastings

IRC in Biomedical Materials, Queen Mary & Westfield College, Mile End Road, London E1 4NS U.K.

ABSTRACT

Using 2.5 and 5wt% additions to hydroxyapatite (HA) of phosphate based glasses, the mechanical properties were investigated with respect to firing temperature. All mechanical properties (flexural bend strength, Young's Modulus and K1c) showed a substantial increase, ie for K1c an increase from 0.7MPam$^{1/2}$ at 1300°C sintering temperature, to 1.6MPam$^{1/2}$ for a 2 Oxide glass. These values are approaching the fracture toughness for cortical bone. Phase analysis of the composites showed that at high glass additions (5%) and high firing temperatures (1350°C), certain glasses produced phase changes with consequent detrimental effect on the mechanical properties. *In Vitro* after 1 month immersion, no change in mechanical properties were observed.
The work presented in this paper is covered by a patent filed on 29/6/92.

INTRODUCTION

HA is currently of much interest in the biomedical field, due to its well established bioactivity. The material is however limited to low load applications due to its inadequate mechanical properties (1). Enhancement of the mechanical properties of HA has centred around development of compaction methods and also choice/control of grain size. Whilst optimising the fabrication process of the HA, they do not give significant increases in the properties (2,3). More recently glass-ceramic materials have been developed which show higher mechanical properties (4,5,6) but have a different microstruture and thus a difference in biological behaviour should be expected.

In this work a classical sintering process was chosen, namely using a liquid phase mechanism. this method is used from low grade pottery to highly specialise materials such as SiC. The reinforcement of HA by inclusion of a glassy phase have met with some success but they are hampered by detrimental phase changes that can occur such as transformation to tricalcium phosphate (7). These phase changes were related not only to the composition of the glass but also to the high percentage of glass added. Glasses closely related to HA, ie soluble phosphate based glasses and Bioglass® were added to HA at very low

percentages, 2.5 and 5wt%, to avoid problems of altered bioactivity and minimise phase changes.

MATERIALS AND METHODS

The phosphate based glasses were produced from reagent grade chemicals heated at 1300°C in an Al_2O_3 crucible for 1h. The following compositions were prepared (mol%): 54.5CaO-45.5P_2O_5 (2-Oxide glass), 28CaO-45P_2O_5-27Na_2O (3-Oxide glass) and 10.1CaO-62.9P_2O_5-10.1Na_2O-16.9Al_2O_3 (4-Oxide glass). The Bioglass® was obtained from the Bioglass® Research Centre, University of Florida.

Once the glass was poured, it was coarsely reduced to a sand type particle and milled in a porcelain ball mill pot for 24h. After milling its particle size was smaller than 100 μm and with median particle size, $D_{0.5}$=6-9 μm according to Laser Diffraction analysis using a Malvern Mastersizer Ms-20. Having milled the glass, HA and methanol was added (350 ml of methanol/200 g of material) to wet mill the powders together for a further 24hrs. Following the milling process, the slip was poured and oven dried. The dried powder was then auto sieved to -75 μm. Particle size distribution profiles were carried out after milling.

Discs were uniaxilly pressed at 20 MPa and fired at 4°C/min heating rate with 1hour soak at 1200 to 1350°C followed by natural cooling inside the furnace. The density of the sintered compacts was measured by mercury using Archimedes principle.

Bending strength and Young's Modulus were obtained from 4-point biaxial bending test in a concentric ring jig with 20 mm supporting span and 10 mm loading span at cross head speed of 5 mm/min on 10 specimens. The concentric ring test eliminates many problems associated with the fracture induced by the edges of the samples although it gives lower results when compared with the usual bending tests (8,9). Fracture toughness measurements were performed using an indentation technique proposed by Laugier (10) using a 9.8 N load.

The materials were characterised by X-Ray Diffraction (XRD) (Siemens D5000 diffractometer) and their microstruture analysed using SEM. *In Vitro* tests were carried out in a phosphate buffered saline solution and samples were bending strength tested after 1 month.

RESULTS

A representative particle size distribution profile for the HA/glass powders after being milled is shown in Figure 1.

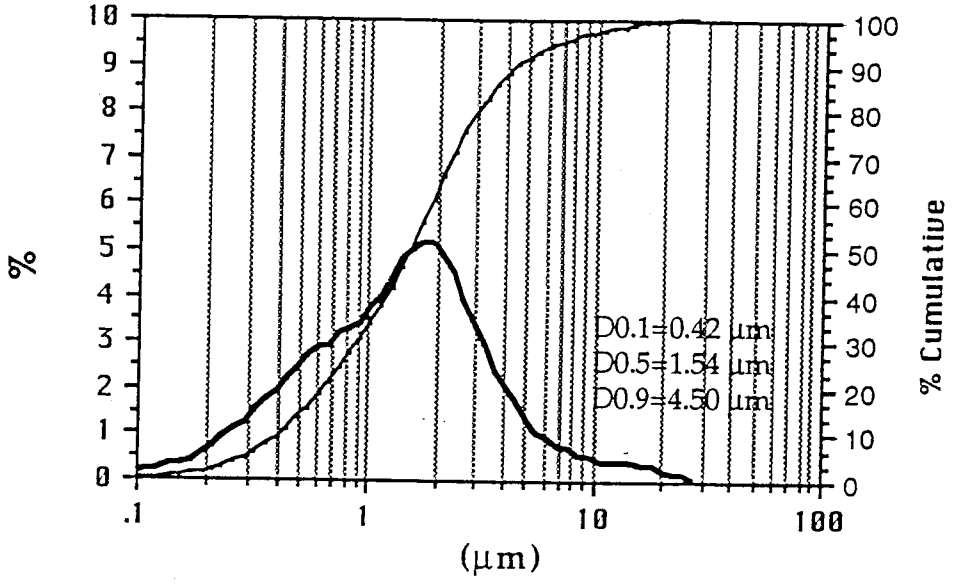

Figure 1 Particle size distribution profile for HA/glass powder

The densification process of the HA/glass composites is similar to that for the HA in the sintering conditions studied. Due to the close chemical relationship between the glass and the HA, difficulties were found with etching the glass for microscopical analysis. using acetic acid, good contrast was obtained between the grain boundary phase and the HA. The glasses were seen to be well dispersed which also reduced the porosity to very low levels, ie the materials were approaching theoretical density.

There are some differences in density at 1200 °C between the various composites, which are not perfectly clear at this stage but they may be due to the different viscosities of the glass additives affecting the sintering process. SEM analysis showed that the HA/ phosphate based glasses were very dense when sintered above 1250°C. The flexural strength and Young's Modulus results are shown in Table 1-2.

Examination of the mechanical properties, shows that for both the biaxial flexure strength and the Young's Modulus, there is a significant improvement in the mechanical properties at both the 2.5 and the 5% glass addition level.

Table 1. Biaxial Flexure for HA and HA/glass composites

		Biaxial Flexure (MPa)			
	Material	1200°	1250°	1300°	1350°
2.5 %	HA	24±4	24±5	28±7	28±7
	2-Oxide glass	27±6	54±13	73±13	66±17
	3-Oxide glass	36±10	38±7	55±18	49±14
	4-Oxide glass	30±6	51±10	58±17	56±15
	Bioglass ®	30±5	50±10	60±11	60±9
5 %	2-Oxide glass	27±8	61±23	85±20	96±17
	3-Oxide glass	29±8	54±16	69±21	61±18
	4-Oxide glass	37±9	74±15	74±11	33±5
	Bioglass ®	23±5	40±6	27±7	-

Table 2. Young's Modulus for HA and HA/glass composites

		Young's Modulus (GPa)			
	Material	1200°	1250°	1300°	1350°
2.5 %	HA	59±7	87±10	88±8	89±9
	2-Oxide glass	66±7	117±15	121±15	122±10
	3-Oxide glass	95±7	87±9	113±15	100±15
	4-Oxide glass	79±8	103±14	105±11	108±12
	Bioglass ®	89±10	99±14	109±13	109±9
5 %	2-Oxide glass	75±14	120±12	120±14	134±9
	3-Oxide glass	86±6	106±12	122±15	122±10
	4-Oxide glass	83±12	113±13	110±11	75±10
	Bioglass ®	72±9.0	85±7	74±8	-

As for HA, the optimal firing temperature can be seen to be 1300°C. At the higher glass addition of 5%, and at 1350°C for all the glasses, there can be seen to be changes occurring to the ceramic. For the 45S5 glass composite, at 2.5%, (Figure 2) all the characteristic peaks of HA may be detected, with the addition of two minor peaks assigned to a calcium silicate. At 5wt% and fired at 1350°C, virtual complete phase transformation of the HA occurred.

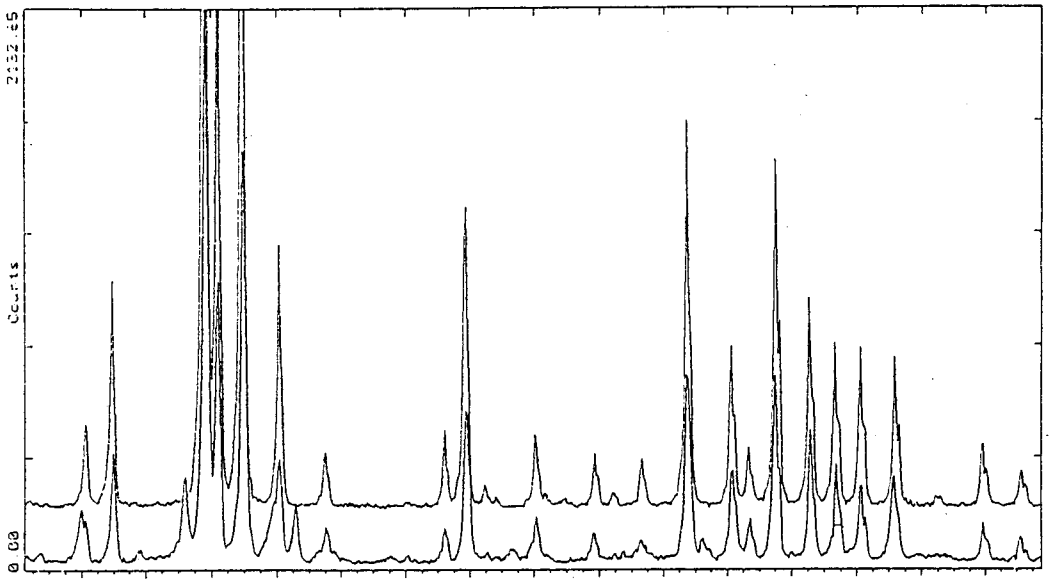

Figure 2. XRD traces for: Upper HA only, Lower HA+45S5glass

All HA/glass composites showed higher fracture toughness when compared with HA, but at the higher firing temperatures, again there is a reduction in mechanical properties for some glasses and this data is shown in Table 3:-

These values are also higher than the usual quoted for HA (1,2,3). A slight decrease in the fracture toughness was found for the materials fired at 1350°C. Grain boundaries are important microstrutural features to stop crack propagation. This particular HA exhibits abnormal grain growth above 1300°C as was reported previously (11).

Table 3. K1c for HA and HA/glass composites

		K1c (MPa $m^{1/2}$)		
	Material	1250°	1300°	1350°
2.5 %	HA	0.51±0.05	0.7±0.12	0.58±0.09
	2-Oxide glass	1.5±0.2	1.6±0.3	1.3±0.2
	3-Oxide glass	1.2±0.2	1.5±0.2	1.1±0.2
	4-Oxide glass	1.4±0.3	1.7±0.4	1.5±0.3
	Bioglass ®	1.5±0.2	1.7±0.3	1.3±0.3
5 %	2-Oxide glass	1.5±0.1	1.6±0.2	1.4±0.2
	3-Oxide glass	1.3±0.2	1.5±0.2	1.2±0.2
	4-Oxide glass	1.4±0.1	1.6±0.2	1.3±0.1
	Bioglass ®	0.9±0.1	-	-

A slight increase in the weight was detected for samples immersed in the saline after 1 month which was related to the precipitation of crystals on the surface of the materials. No changes were found in the flexural strength after 1 month. The results are in agreement with previous work conducted on HA (12).

DISCUSSION

The use of glass to reinforce ceramics has long been used and liquid phase sintering is also used for high tech ceramics. For HA, glasses have been used before, but significant phase changes have occurred, due to the high glass additions used. With this study, the minor additions of glass (2.5 and 5wt%) provide enough liquid along the grain boundaries to aid sintering, seen as a significant increase in mechanical properties, yet there is not enough to cause significant phase changes except at the higher firing temperatures, but this is as expected, the high temperature allowing the reactions to occur more easily. The most successful glass used was the 2-Oxide glass, this producing minimal phase changes throughout. Of significance were the changes brought about by the Bioglass ®. This glass caused major phase changes which as yet are not completely identified.

CONCLUSIONS

HA does not as yet possess adequate mechanical properties for use in either static or dynamic orthopaedic surgical problems (1). The use of a glass to liquid

phase sinter and to help it approach theoretical density has significantly increased the mechanical properties. The use of a phosphate based glass is an obvious one due to the close links in chemical composition with the HA. The low levels of addition of the glass ensures that little occurs in the way of phase transformations, whilst increasing the mechanical properties. Due to the soluble nature of the glass, the deterioration of these properties may have occurred, but *in vitro* degradation studies showed no change in mechanical properties. Further work is now underway to look at the materials in a dynamic system *in vitro*. We shall also be looking at cellular attachment onto the materials surface and any effects that the glass might produce.

REFERENCES

1 Aoki, H. In: Science and Medical applications of Hydroxyapatite JAAS, Japan, 1991

2 With, De G., Dijk, H. J. A. Van, Hattu, N., Prijs, K. J. Mater. Sci. 1981, 16, 1592-1598

3 Best, S. , Bonfield, W.and Doyle, C. In : Bioceramics 2 Butterworth, Heidelberg, Germany, 1989, 57-64

4 Kokubo, T.,Ito, S., Shigematsu, M., Sakka, S. and Yamamuro, T. J. Mater. Sci. 1985, 20, 2001-2004

5 Vincenzini, P. in: High Tech Ceramics Elsevier Science Publishers B. V., Netherlands ,1897, 73-82

6 Vincenzini, P. in: High Tech Ceramics Elsevier Science Publishers B. V., Netherlands ,1897, 63-72

7 Kangasniemi, I., Groot, K., Wolke, W., Luklinska, Z. and Yli-Urpo, A. J. Mater. Sci.: Mat. in Medicine 1991, 2, 133-137

8 Giovan, M. N. and Sines, G. J. Am. Ceram. Soc. , 1979, 62, 510-515

9 Vincenzini, P. in: High Tech Ceramics Elsevier Science Publishers B. V., Netherlands ,1897, 110-118

10 Laugier, M. T., J. Mater. Sci. , 1987, 6, 355-356

11 Santos, J. D., Morrey, S., Hastings, G. W., Monteiro, F. J. In:Bioceramics 4 Butterword, London, UK, 1991, 71-78

12 Thomas, M. B., Doremus, R. H., Jarcho, M., Salsbury, R. L. J. Mater. Sci. 1980, 15, 891-894.

4 Raedmonck, V. W. In: Metal and Ceramic Biomaterials Hastings, G. W. and Ducheyne, P. CRC Press, 1984, Ch. 6, 143-166

5 Barrinder, E. and Jubb, N. In: Ultrastructure Processing of Ceramics and Glasses Wiley, D. R., New York, 1984, Ch. 26.

7 Akao, M. and Aoki, H. J. Mat. Sci. 1981, 16, 809-812

8 Dewith, G. and Dick, V.J.A. J. Mat. Sci. 1981, 16, 1592-1598

9 Best, S. and Doyle, C. In: Bioceramics 2 Heidelberg, 1989, 57-64

10 Hirayama, Y. Bioceramics 2 Heidelberg, 1989, 1332-1339

11 Mestial, F. and Drew, R. A. L. J. European Cer. Soc. , 1989, 5, 47-53